# On Curve Reconstruction in Riemannian Manifolds

## Ordering Motion Frames

by

**Pratik Shah**

A Thesis Submitted in Partial Fulfilment of the Requirements for the Degree of

**Doctor of Philosophy**

in

Information and Communication Technology

to

Dhirubhai Ambani Institute of Information and Communication Technology


December, 2011

## Declaration

This is to certify that

1. the thesis comprises my original work towards the degree of Doctor of Philosophy in Information and Communication Technology at DA-IICT and has not been submitted elsewhere for a degree,
2. due acknowledgement has been made in the text to all other material used.

Pratik Shah

## Certificate

This is to certify that the thesis work entitled *On Curve Reconstruction in Riemannian Manifolds* has been carried out by *Pratik Shah* (200521002) for the degree of Doctor of Philosophy in Information and Communication Technology at this Institute under my supervision.

Prof. Samaresh Chatterji

# Acknowledgement

I have been waiting long for this moment to acknowledge all those who contributed in building this work. I am indebted to my advisor Prof. Samaresh Chatterji, without whose support this work would have never begun. I am grateful to Prof. V P Sinha who inspired me to travel the unknown territories with the search light of curiosity. I am also grateful to Prof. Gautam Dutta for the discussions and interactions we had during my stay at DAIICT.

I would like to acknowledge the Resource Center DAIICT and Dr. T S Kumbar for providing a wonderful study and research atmosphere. It will be difficult for me to find a substitute for the Resource Centre. At the same time I would also like to thank the director of the institute Prof. S C Sahasrabudhe for his continuous support.

My special thanks goes to Ratnik and Aditya for discussing thoughts and sharing all ups and downs with me during the course of this work. I am also thankful to Guneshwar and Asim for the wonderful sunset moments we shared together. I would also like to thank all my colleagues Purushottaman, Bhavesh, Sunil, Vikram, Zakir, Dileep, Nilesh and all my friends at DAIICT for wonderful moments we shared together.

Last but not the least I would like to thank my grand parents, my parents, my wife and my family members, who made me capable of reaching this point of life and for giving me their kind support and love. I dedicate my work to them.

Pratik Shah
DAIICT, Gandhinagar
December, 2011.

# Table of Contents

# Abstract

In this work we generalize the computational geometric curve reconstruction approach to curves embedded in Riemannian manifolds. We prove that the minimum spanning tree, given a sufficiently dense sample, correctly reconstructs smooth arcs which can be used to reconstruct simple closed curves in Riemannian manifolds. The proof is based on the behavior of a curve segment inside a tubular neighborhood of the curve. To take care of the local topological structure of the underlying manifold, a tubular neighborhood is constructed using the injectivity radius of the underlying Riemannian manifold. We also present examples of successfully reconstructed curves and apply curve reconstruction to ordering motion frames.

To give a specific example, think of a graphic game designer designing a game. To design a path of an object and the way the object moves along that path he must first create a sequence of orientations and displacements in the space. A typical method of animation is to begin with the first frame and the last frame. The graphic designer will create in between frames iteratively. For the movements along the path, he may create intermediate frames in an order which best suits his imagination. Now he provides these frames to an interpolator. At this stage he is also required to provide an ordering of the frames to the interpolator.

Results presented in this work provide a way to automate the process of ordering the frames created by a graphic designer. In this work we present a uniform sampling criterion, an ordering algorithm and an interpolation scheme that reconstructs an approximation to the original motion. In addition an attempt has been made here to generalize the computational geometric curve recon-

# Synopsis

*Connect the dots* is a classic puzzle, wherein for a given set of dots (sample points) in a plane we are supposed to connect the dots using a proximity criterion, to form a closed figure. The curve reconstruction problem can be thought of as that of connecting the dots. Reconstructing a curve from an arbitrary set of sample points is a non-trivial problem, since there may be a variety of ways to connect the points. A brief review of the work carried out in the area of curve reconstruction is presented in [14]. It discusses the reconstruction of curves embedded in $\mathbb{R}^n$ (endowed with the standard metric). The curve reconstruction problem falls in a subclass of the more general problem of manifold reconstruction. The focus in this field has been on the reconstruction of manifolds embedded in $\mathbb{R}^n$. Reconstruction of manifolds of co-dimension one is dealt with in [20].

For curves in a plane, in [13], the *Euclidean Minimal Spanning Tree* (EMST) is proposed for reconstruction. The approach is based on the combinatorial characterization of minimal spanning paths. The behavior of arcs inside the tubular neighborhood is a key ingredient of the approach. A limitation of EMST-based reconstruction is that it relies on a dense uniform sample. This limitation of uniform sampling has been overcome by a more intuitive sampling strategy based on the medial axis. In [4], the problem of reconstruction has been solved for curves in a plane with a non-uniform sampling criterion. It recommends more samples to be taken where the details are more, i.e. the sampling is based on the local feature size of the curve, measured as the least distance from the curve point to the medial axis of the curve. Reconstruction of curves in $\mathbb{R}^n$ is solved in [15]. The above mentioned approaches using non-uniform samples are based on the characterization of

Voronoi construction and in particular on the empty circle property [14]. They are combinatorial in nature. All the combinatorial curve reconstruction approaches based on the Voronoi construction have been unified and presented in [18]. They have been shown to be instances of what are known as restricted Delaunay complexes and differ only in the way the restriction is put on the simplicial complex.

In this work we extend the computational geometric curve reconstruction approach to curves embedded in curved spaces. As an example, take an object in space undergoing a rigid body motion. Suppose we have captured some frames of this motion, but these frames are jumbled up (the ordering is lost). We want to reconstruct the original motion from this sample set (of frames). If this motion is represented by a curve in the special euclidean group then the problem is of reconstructing a curve in a Riemannian manifold. We pose the problem of curve reconstruction in the Riemannian manifolds as follows. Let $\mathcal{C}$ be a smooth, closed and simple curve in a Riemannian manifold $\mathcal{M}$ . Given a *finite sample*, $\mathcal{S} \subset \mathcal{C}$, reconstruct $\mathcal{C}$. The first step towards the solution of the problem of curve reconstruction requires to define a criterion for an appropriate sample $\mathcal{S}$. Next it demands to suggest an algorithm to introduce an order on the sample. And the final step involves suggesting a suitable interpolation scheme for the ordered sample set.

To the best of our knowledge, no results have so far been reported in this direction, where the curve to be reconstructed is embedded in a curved space. John Nash proved in [31] that every Riemannian manifold can be isometrically embedded into some Euclidean space. So one might get tempted to think that if we are able to reconstruct curves in $\mathbb{R}^n$ we must also be able to reconstruct curves in Riemannian manifolds. But it is difficult to construct such an isometric embedding. This inadequacy of knowledge of the isometric embedding has prompted researchers to work in Riemannian manifolds intrinsically. And for that we refer to the intrinsic geometrical ideas in differential geometry [22]. That brings us to the junction of the computational geometry and differential geometry. We use the well developed theory of differential geometry and extend the results of curve reconstruction in $\mathbb{R}^n$ to Riemannian manifolds. The motivation is the growing applications

of manifold methods in robotics, graphics and computer vision.

Since our work focuses on curves in Riemannian manifolds we begin by defining a distance metric on manifolds useful in applications. We use variational as well as geodesic curvature based approaches for computing geodesics. Both the formulations lead to the same system of non-linear ordinary differential equations as shown in [22]. The geodesics are computed numerically in practice.

A Riemannian manifold $\mathcal{M}$ is defined as a differentiable manifold with the Riemannian metric defined at every point of the manifold in [17]. This Riemannian metric defines an inner product in the tangent space at every point on the manifold. The inner product in turn equips the connected Riemannian manifold $\mathcal{M}$ with a distance metric. The distance between two points on $\mathcal{M}$ is defined as the distance of the shortest geodesic path connecting them. As an example, consider the distance between two points in $\mathbb{R}^n$, with the standard inner product defined on $\mathbb{R}^n$. It is computed as the length of the straight line segment connecting them. Geodesics on a manifold are similar to straight line segments in euclidean space. In this way, we can construct the distance metric for every connected Riemannian manifold.

We compute geodesics on the sphere and a few surfaces. Since surfaces are isometrically embedded in the $\mathbb{R}^3$, it is relatively straight forward to work with surfaces. The standard inner product on $\mathbb{R}^3$ can be used to find lengths of the curve on surfaces. But for many useful manifolds such isometric embeddings are not known, for example $SE(3)$, the special euclidean group acting on objects in $\mathbb{R}^3$. Along with being a smooth manifold, $SE(3)$ is also a group. Such groups are called Lie groups. In general, the group of rigid body motions in $\mathbb{R}^n$ is the semi-direct product of the special orthogonal group $SO(n)$ and $\mathbb{R}^n$. There does not exist any bi-invariant Riemannian metric on $SE(3)$. In [33], a physically meaningful left-invariant Riemannian metric is defined on $SE(3)$. The physical implication of the left invariance is the freedom of choice of the inertial frame. Moreover, with a particular choice of Riemannian metric on $SE(3)$, closed form expressions for $\exp$ and $\log$ maps are derived in [52]. The formulation can be easily generalized to any $n$. We compute

geodesic path between two configurations of $SE(3)$ and compute the distance between them using the $\exp$ map, a map which maps a Lie algebra diffeomorphically to its Lie group, and the $\log$ map.

With the distance metric defined, $\mathcal{M}$ becomes a metric space. Since $\mathcal{C}$ is a compact submanifold of $\mathcal{M}$, there exists a finite subcover of $\mathcal{C}$ for every open cover, [17]. This indicates a possibility of sampling the curve at finite locations. The concept of $\varepsilon$ net, defined in [50], captures the idea of such a sampling very well.

The medial axis $M$ of a curve $\mathcal{C} \subset \mathcal{M}$, is the closure of the set of points in $\mathcal{M}$ that have at least two closest points in $\mathcal{C}$. We present a few observations related to the medial axis for a curve on a surface embedded in $\mathbb{R}^3$. The curve in space and the curve in surface are two different entities. For some cases, it is possible to define surfaces so that the curve when lying on the surface requires coarser sampling than the same curve lying in $\mathbb{R}^3$. But this demands knowledge of the underlying surface.

With the help of an example of a curve on a surface we show that medial axis based sampling becomes meaningless on arbitrary manifolds. And we point out that the reason for the breakdown is the gaussian curvature of the surface at the points in the region enclosed by the closed curve. The injectivity radius of the underlying manifold is key in understanding this difficulty in sampling a curve. Our sampling criterion is based on the tubular neighborhood of the curve which is well within the injectivity radius of the manifold. It can be shown that if $q \in \mathcal{M} - C_m(p)$ then there exists a unique minimizing geodesic joining $p$ and $q$, where $C_m(p)$ is the cut locus of the point $p$ in $\mathcal{M}$. In [17], $i(\mathcal{M}) = \inf_{p \in \mathcal{M}} d(p, C_m(p))$ is defined as the injectivity radius of $\mathcal{M}$. In [42] the tubular neighborhood for a curve is constructed by taking the union of all the normal geodesics to the curve, assuring the injectivity of the $\exp$ map along these normal directions. Instead, as shown in [40], we propose to work inside the injectivity radius to deal with the problem in sampling.

We give an alternate proof for curve reconstruction by EMST in $\mathbb{R}^2$. We present a result giving relationship between the sampling density and the curvature of the curve. The claim about the flatness of the sample inside a tubular neighborhood was proved in [13]. The argument rests on what

happens outside the tubular disc. In our argument we do not use the curvature center explicitly. And with the help of the orthogonality of the boundary of the geodesic ball centered at a point and the geodesics passing through this point, we extend this proof to arbitrary Riemannian manifolds. The crucial argument in the proof is Gauss's lemma [17]. It defines the local geodesic polar coordinates at a point on the Riemannian manifold. Once the flatness of a sample is assured, the proof for re-ordering by EMST is essentially the same as in [13].

Once we have introduced an order on the sample we propose to use the de Castelaju algorithm prescribed in [1], for interpolating the ordered points in $\mathcal{M}$. For illustrating the algorithm, we interpolate ordered points in $\mathbb{R}^n$, on a sphere, and surfaces. We interpolate between two configurations in $SE(3)$ and compare the results with different initial conditions. We also introduce a partial geodesic interpolation scheme for interpolation in $SE(3)$, where geodesic interpolation is used to interpolate between rotations and spline segments are used to interpolate between positions for smoothness.

For experimentation we have taken up examples of curves on a sphere and a few other surfaces. We compute the distances between sample points of a curve on these surfaces numerically and reconstruct the curve with MST. We show a potential application of curve reconstruction in $SE(2)$ for ordering the video frames. Here we take the clue from an object in a video which is undergoing a rigid motion, and re-order the frames by re-ordering the sample points in $SE(2)$. Next we experiment with curves in $SE(3)$ and show successfully reconstructed curves with applications to graphics and robot path planning. We consider a manifold which has elements of similar kind to $SE(2)$. The difference is that it also includes scaling with respect to the center of mass of the object. We present an example of a successfully reconstructed curve in this manifold. This manifold is useful for applications which involve object tracking, for example the study of cell growth.

In conclusion, this work shows that the MST gives the correct geodesic polygonal approximation to smooth, closed and simple curves in Riemannian manifolds, assuming the sample is dense enough and we work inside the injectivity radius. We have worked out a conservative bound for

uniform sampling of a curve in a Riemannian manifold. The effect of the local topological behavior of the underlying manifold is clearly identified and resolved by working inside the injectivity radius. In general the scheme works for smooth arcs with endpoints also. If we work inside the injectivity radius of the underlying manifold we have taken care of the topological changes but to take care of geometric changes we need to work inside the convexity radius as well, as discussed in [27]. We believe that, with careful modifications, results of non-uniform sampling for curves in $\mathbb{R}^n$ are transferable to curves in a Riemannian manifold. As an extension to this work, we would like to work out the necessary proofs and carry out simulations in this direction to support our claim.

# List of Symbols

| | |
|---|---|
| $\mathbb{R}$ | Set of real numbers |
| $\mathbb{R}^+$ | Set of positive real numbers including zero |
| $\mathbb{R}^n$ | $n$-dimensional real vector space |
| $I$ | Closed unit interval $[0, 1] \subset \mathbb{R}$ |
| $d(,)$ | Distance metric |
| $B_\varepsilon(s)$ | Open ball of radius $\varepsilon > 0$ centered at point $s$ |
| $S_\varepsilon(s)$ | Close ball of radius $\varepsilon > 0$ centered at point $s$ |
| $S^2$ | Unit 2-Sphere of in $\mathbb{R}^3$ |
| $\gamma, \mathcal{C}$ | Smooth curves |
| $\mathcal{S} \subset \mathcal{C}$ | A finite sample of curve $\mathcal{C}$ |
| $M$ | Medial Axis |
| $f(p)$ | Feature size at point $p$ on the curve |
| $LFS$ | Least feature size |
| $\ell_a^b$ | Length of the curve segment with $a$ and $b$ as end points |
| $\mathcal{M}, \mathcal{N}$ | Riemannian manifolds |
| $T_p\mathcal{M}$ | Tangent space at point $p \in \mathcal{M}$ |
| $<,>_p$ | Riemannian inner product defined at point $p \in \mathcal{M}$ |

| | |
|---|---|
| $X, Y$ | Vector fields on $\mathcal{M}$ |
| $T\mathcal{M}$ | Tangent bundle of $\mathcal{M}$ |
| $C^\infty(\mathcal{M})$ | Ring of smooth real valued functions on $\mathcal{M}$ |
| $\nabla$ | Levi-Civita connection on Riemannian manifold |
| $\frac{D}{dt}$ | Covariant derivative |
| $\Gamma_{ij}^k$ | Christoffel symbols |
| $SO(2),\ SO(3)$ | Special orthgonal groups of rotations in dimensions 2 and 3 respectively |
| $so(2),\ so(3)$ | Tangent spaces at identities of $SO(2)$ and $SO(3)$ |
| $SE(3)$ | Special euclidean group acting on $\mathbb{R}^3$ |
| $se(3)$ | Tangent space at identity of $SE(3)$ |
| $\exp$ | Exponential map from tangent space to the manifold |

# List of Figures

# Chapter 1

# Introduction

## 1.1 Introduction

With the advent of digital scanning technologies and digital processing media, people are trying to come up with sampling strategies that will preserve the information content of signals even after sampling. Take for example a document scanner. Let's say a lot of handwritten documents are required to be preserved by converting them into digital form. Since documents have different features in terms of hand writing, font sizes, languages in which the documents are written etc., the decision regarding the minimum resolution of the scanner becomes important. This in some sense is similar to Nyquist's sampling criterion for band limited signals in signal processing.

To motivate the problem of *curve reconstruction* from sample points, let us consider the game of connecting the dots. Connect the dots is a classic puzzle, see Figure 1.1(a), wherein for a given set of dots we are supposed to connect the dots based on the proximity criterion to form a closed figure as shown in Figure 1.1(b).

The curve reconstruction problem can be thought of as one of connecting the dots. The idea is quite similar to reconstruction theorem for band limited signals in signal processing. The difference is in terms of ordering of the sample points. When we talk about signals being sampled we have

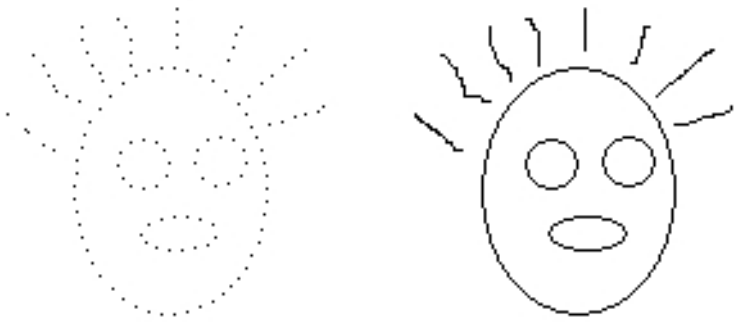

(a) Given dots (b) After connecting the dots

Figure 1.1: Connect the dots

a predefined ordering available on the sample. And by reconstruction we mean an interpolation scheme that approximates the original digitized signal. On the other hand in case of reconstruction of curves, the samples are required to be ordered based on the proximity criterion, and then a suitable interpolation scheme is used to approximate the original curve.

Thus the problem of curve reconstruction can be divided into three parts:

1. Establish a proper sampling criterion for the curve.

2. Suggest a provable ordering algorithm based on the sampling criterion.

3. Interpolate the ordered sample and approximate the original curve.

Curve reconstruction falls in the class of geometrical modeling problems. It is an instance of the more general manifold learning problem, where the objects to be reconstructed are not only curves but surfaces, volumes, and higher dimensional geometrical entities. The problem of reconstruction starts with a point cloud (sample) of an object and the expectation is to come up with a parametric model for the object. This model is then used for computational purposes.

A curve $\mathcal{C}$ is a function $\mathcal{C} : [0, 1] \to \mathcal{M}$, where $[0, 1] \subset \mathbb{R}$ and $\mathcal{M}$ is a differentiable manifold. To start with, let us assume that the curve is lying in an $n$- dimensional Euclidean space so that $\mathcal{M}$ is $\mathbb{R}^n$ for some $n > 0$. In general, reconstructing the curve from given sample points is a non-trivial

problem, since there may be a variety of ways to connect the points. In practice the curves we examine are mostly differentiable. The class of curves that are smooth (infinitely differentiable), closed ($\mathcal{C}(0) = \mathcal{C}(1)$) and simple (no self intersections) is of vital importance in pattern recognition, graphics, image processing and computer vision*. For example the objects in images are identified by closed contours representing their shapes.

To begin with, it is essential to see whether it is in fact possible at all to sample the curve at finite locations without losing the details of the curve. In this context we may recall that for a compact set, every open cover has a finite sub-cover. To appreciate the possibility that a compact set provides us with, let us look at a definition of an $\varepsilon$-net. If $\varepsilon > 0$ is given, a subset $\mathcal{S}$ of $\mathcal{C}$ is called an $\varepsilon$-net if $\mathcal{S}$ is finite and $\mathcal{C} \subset \cup_{s \in \mathcal{S}} B_\varepsilon(s)$, where $B_\varepsilon(s)$ is an open ball in $\mathcal{M}$ with radius $\varepsilon$. In other words, if $\mathcal{S}$ is finite and its points are scattered through $\mathcal{C}$ in such a way that the distance of each point of $\mathcal{C}$ is less than $\varepsilon$ from at least one point of $\mathcal{S}$. This shows a possibility of a finite representative sample set of $\mathcal{C}$. The concept of $\varepsilon$-net captures the idea of sampling very well. We see in the literature that the bounds on $\varepsilon$ for uniform sampling and the ways in which non-uniform sampling criteria are suggested try to essentially capture the very notion of $\varepsilon$-net.

The definition of a curve in a differentiable manifold is suggestive of the fact that the curves we are interested in are lying in more general spaces than Euclidean. We do have an isometric embedding theorem by Nash which says that every compact Riemannian manifold can be embedded into a Euclidean space $\mathbb{R}^n$ for sufficiently large $n$. However, it is difficult to construct such an isometric embedding. So we work in the domain of curved spaces and develop results about reconstructing curves on Riemannian manifolds. This work is at the junction of two disciplines of mathematics namely, differential geometry and computational geometry. During the course of this work, we have created a wide range of examples and simulations. These will help us understand concepts from both the domains.

*Each of the terms smooth, closed, simple will be discussed in detail in Chapter 3.

## 1.2 Problem Statement

We pose the problem of curve reconstruction in Riemannian manifolds as follows.

> Let $\mathcal{C}$ be a smooth, simple, and closed curve in a Riemannian manifold $\mathcal{M}$ . Given a *finite sample*, $\mathcal{S} \subset \mathcal{C}$, reconstruct $\mathcal{C}$.

The first step towards a solution of the problem of curve reconstruction requires us to define a criterion for obtaining an appropriate sample $\mathcal{S}$. Next, it requires us to suggest a provable algorithm to introduce an order on the sample. The final step involves suggesting a suitable interpolation scheme for the ordered sample set.

For example take an object in space undergoing a rigid body motion. Suppose we have captured some frames of this motion, but these frames are jumbled up (the ordering is lost). We want to reconstruct the original motion from this sample set (a set of motion frames). If this motion is represented by a curve in the special euclidean group then the problem is of reconstructing the curve in a Riemannian manifold.

Think of a graphic game designer designing a game. To design a path of an object and the way the object moves along that path he must first create a sequence of orientations and displacements in the space. A typical approach to animation is to begin with the first frame and end with the last frame. The graphic designer will create in between frames iteratively For the movement along the path, he may create intermediate frames in an order which best suits his imagination. Now he provides these frames to an interpolator. At this stage he is also required to provide an ordering of the frames to the interpolator.

Results presented in this work provide a way to automate the process of ordering the frames created by a graphic designer. In this work we present a sampling criterion, an ordering algorithm and an interpolation scheme that reconstructs an approximation to the original motion. We have made an attempt to extend the computational geometric curve reconstruction approach to curved spaces (Riemannian Manifolds). Instances of applications of curve reconstruction in curved spaces

are sparsely present in literature, see for example, edge grouping in [9], and DT-MRI tractography in [8]. In [9], voronoi diagram construction is used for perceptual grouping of points on a curved surface.

To the best of our knowledge, no results have so far been reported in this direction, where the curve to be reconstructed is embedded in a curved space. John Nash proved in [31] that every Riemannian manifold can be isometrically embedded into some Euclidean space. So one might get tempted to think that if we are able to reconstruct curves in $\mathbb{R}^n$ we must also be able to reconstruct curves in Riemannian manifolds. But it is difficult to construct such an isometric embedding. This inadequacy of knowledge of the isometric embedding has prompted researchers to work in Riemannian manifolds intrinsically. For that we refer to the intrinsic geometrical ideas in differential geometry [22]. That brings us to the junction of computational geometry and differential geometry. We use the well-developed theory of differential geometry and extend the results on curve reconstruction in $\mathbb{R}^n$ to Riemannian manifolds. The motivation is the growing application of manifold methods in robotics, graphics and computer vision.

The Riemannian manifold we are interested in, i.e. the euclidean motions $SE(3), SE(2)$, are endowed with an additional structure of a group and thereby give us Lie groups to work on. $SE(3)$ is well-studied in physics and mathematics. $SE(2)$ is used to model the set of configurations of an object under euclidean motion and is explored in the domain of image processing for segmentation as well as in object tracking where one is interested in the constrained evolution of a curve under the action of $SE(2)$, [29]. $SE(3)$ is used extensively in robotics for path planning and motion planning of robots. It is also useful in computer vision and graphics. No bi-invariant metric exists on $SE(3)$. With the Riemannian metric defined on it, the *exponential map* and further a left invariant distance metric on $SE(3)$ is expressed in a closed form. We give examples of successfully reconstructed curves in $SE(2)$ and $SE(3)$. We show an application of curve reconstruction in $SE(2)$ for ordering video frames. We show that for densely sampled curves, the *minimal spanning tree* (MST) gives a correct polygonal reconstruction of curves in Riemannian manifolds. It can be

shown that the problem of curve reconstruction is equivalent to that of traveling salesman problem. In [2], the authors show that in the context of curve reconstruction, the traveling salesman tour can be constructed in polynomial time. After ordering, we interpolate the ordered point set by a partial geodesic interpolation scheme. To ensure smoothness at the sample points, we also propose to interpolate samples using de Casteljau algorithm assuming that the boundary conditions are known. It is possible to tackle a noisy sample both in combinatorial and variational curve reconstruction approaches, see for example [13] and [49]. However, in this work, we do not discuss issues related to noisy samples.

## 1.3 Literature Survey

There exist a variety of approaches for reconstructing a curve embedded in $\mathbb{R}^n$ from its sample points. In a broad sense, we can be divide them into two categories: algebraic and combinatorial. In an algebraic approach the set of sample points is used for arriving at an estimate of the curve in terms of a parametric or an implicit form. This leads to a variational formulation as prescribed in [49]. The well developed theory of deformable models, presented in [48], is the driving force behind this development.

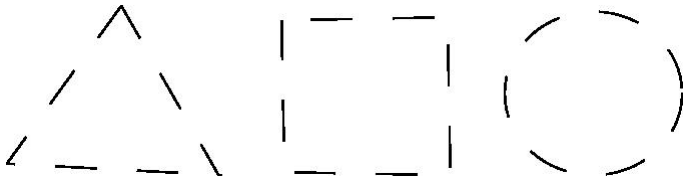

(a) Discontinuity in the curves

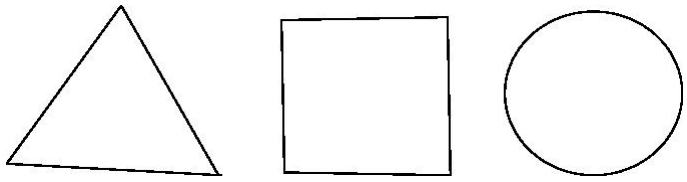

(b) Contours latched on to the discontinuous curves

Figure 1.2: An application of deformable models (active contours) to detect a connected boundary of an object from given disconnected edges

In Figure 1.2, active contours are used to provide connected boundaries for the disconnected edges of various shapes. To latch on to the disconnected object boundaries we have used gradient vector flow based active contours. More on gradient vector flow force field can be found in [51]. This example is taken from the work carried out by Pratik Shah and Asim Banerjee in [39].

The intersection of two surface patches is, usually a non-planar curve. This observation is explored in [45] to implicitly describe a curve which best fits the given sample points. This approach tries to minimize the approximate mean square distances between the curve and the sample points. To illustrate this approach we provide here a simple example of a circle. Let us consider that a sample of points of this circle is given. In Figure 1.3, we show an estimate of the curve as an

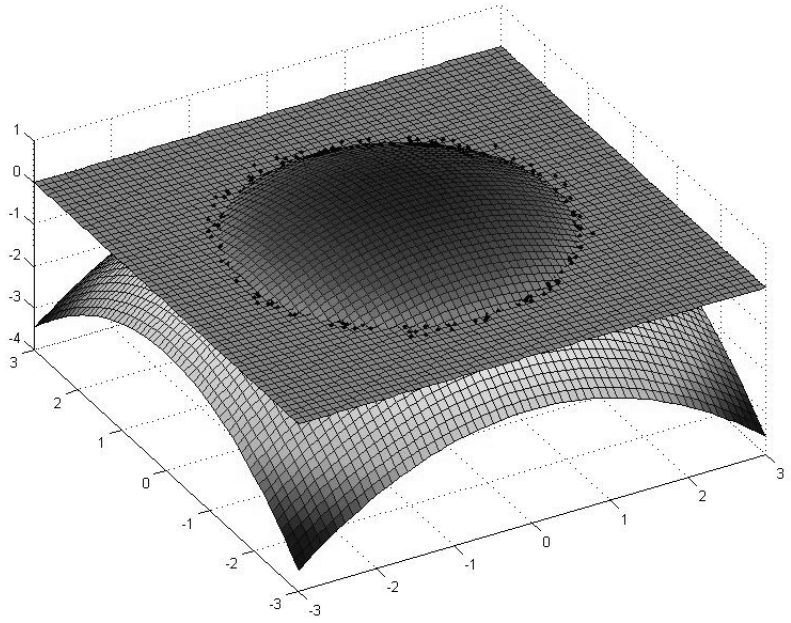


Figure 1.3: Intersection of two surfaces as a least square fit to noisy sample points of a circle

intersection of two surfaces, a plane and a parabolic surface. The work carried out in the field of algebraic curve and surface fitting can be followed in [46], [47]. In [7] the authors present least squares fitting for surface data.

The other approach, which is based on voronoi diagrams and computational morphology based sampling conditions is, known in the literature as combinatorial curve reconstruction. The literature in this field has grown rapidly. Since we will be following this approach, we prefer to discuss it in detailed fashion. We begin with a quick review of curve reconstruction in the plane, keeping the notations and definitions as general as possible. A curve, for our purpose, is a function $\mathcal{C} : [0, 1] \rightarrow \mathcal{M}$. More specifically looking at the application at hand, we restrict $\mathcal{M}$ to be a differentiable manifold. We will use the symbol $\mathcal{C}$ interchangeably for this function and its image. A subclass of curves, that are smooth and simple is of vital importance in pattern recognition, graphics, image processing and computer vision. Since it is an image of a compact interval, $\mathcal{C}$ is a one dimensional compact manifold.

If $\mathcal{M}$ is $\mathbb{R}^2$ then the problem is of reconstructing curves in a plane and $\mathcal{C}$ is planar. $\mathbb{R}^2$ along with the standard Euclidean distance metric becomes a metric space. Naturally the question arises that, *is it always possible to have a finite sample set $\mathcal{S} \subset \mathcal{C}$ which captures everything about $\mathcal{C}$?* As discussed earlier the concept of an $\varepsilon$-net captures the idea of sampling criterion very well. Since the domain of $\mathcal{C}$ is compact every cover of it will have a finite subcover, this shows a possibility of a finite representative sample set of $\mathcal{C}$. In other words if $\mathcal{S}$ is finite and its points are scattered through $\mathcal{C}$ in such a way that each point of $\mathcal{C}$ is distant by less than $\varepsilon$ from at least one point of $\mathcal{S}$.

In [13], based on a uniform sampling criterion, an Euclidean MST is suggested for the reconstruction. In the initial phase of the development, use of a uniform sampling criterion was the bottleneck. The first breakthrough came with the non-uniform sampling criterion suggested based on local feature size by [4]. Unlike uniform sampling, it samples the curve more where the details are more. Non-uniform sampling is based on the medial axis of the curve. The *medial axis* of a curve $\mathcal{C}$ is closure of the set of points in $\mathcal{M}$ which have two or more closest points in $\mathcal{C}$. A simple closed curve in a plane divides the plane into two disjoint regions. Medial axis can be thought of as the union of disjoint skeletons of the regions formed by the curve. The *local feature size*, $f(p)$, of a point $p \in \mathcal{C}$ is defined as the Euclidean distance from $p$ to the closest point $m$ on the medial axis.

$\mathcal{C}$ is $\varepsilon$-*sampled* by a set of sample points $\mathcal{S}$ if every $p \in \mathcal{C}$ is within distance $\varepsilon \cdot f(p)$ of a sample point $s \in \mathcal{S}$. The algorithm suggested in [4] is based on voronoi and its dual delaunay triangulation. All delaunay based approaches can be put under a single formalism, the restricted delaunay complex, as shown in [18]. Every approach is similar in construction and differs only in how it restricts the delaunay complex. The crust [4], and further the NN-CRUST, an improvement suggested in [14], can handle smooth curves. In some cases, it is possible to tackle curves with boundaries and also curves in $\mathbb{R}^d$, [14]. euclidean space. The CRUST and NN-CRUST assume that the sample $\mathcal{S}$ is derived from a smooth curve $\mathcal{C}$. The question of reconstructing non-smooth cuves has also been studied. Extensive experimentation with various curve reconstruction algorithms is carried out in [3]. In [15] an extension of NN-CRUST to $\mathbb{R}^d$ is presented, which opens up possibilities of extending the existing delaunay based reconstruction algorithms to higher dimensional euclidean spaces. We show an example of a curve in $SE(2)$ reconstructed by NN-CRUST.

Looking at the importance of the results and the amount of work carried out in this field, in the next chapter we give a systematic development of results in the domain of combinatorial curve reconstruction. This will help us to understand the current status of the problem. It will also provide us with the machinery required to understand the curve reconstruction problem in more detailed fashion.

## 1.4 Contributions

To the best of our knowledge no efforts are reported in the domain of curve reconstruction for reconstructing curves in a curved space. We pose the problem of curve reconstruction for curves embedded in Riemannian manifolds for the first time. Take for example a curve in $SE(3)$ with its sample points as shown in Figure 1.4. This work utilizes the concepts from the intrinsic geometrical approach taken by differential geometry to handle curved space. In this thesis, we extend the computational geometry based approach for curve reconstruction to higher dimensional curved

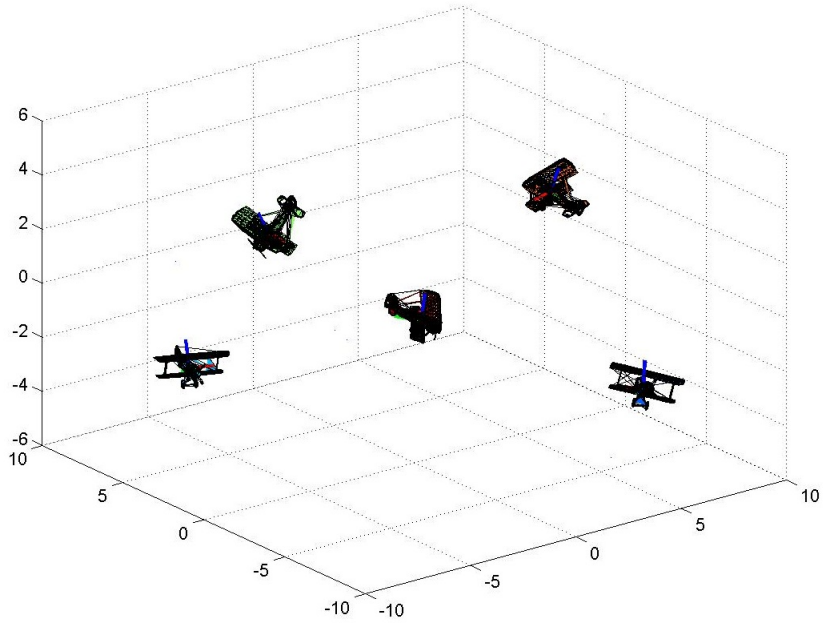


Figure 1.4: A sample $\mathcal{S}$ of a curve $\mathcal{C} \subset SE(3)$

spaces. First we present a few observations and a counter-example for the sampling criterion based on medial axis. We show that the necessary condition on $\varepsilon$, to form a tubular neighborhood of a simple closed curve, is explicitly given by;

$$\varepsilon < \frac{1}{k} \tag{1.1}$$

where $k = \max_{p \in \mathcal{C}} k(p)$, refer to Proposition. 5.4. Further we give a revised sampling criterion for curves in the Riemannian manifold as

$$\varepsilon < \min \{\inf_{p \in \mathcal{C}} f(p), i(\mathcal{M})\} \tag{1.2}$$

where, $i(\mathcal{M})$ is the injectivity radius of the manifold $\mathcal{M}$, refer to Proposition 5.8 . In this work we provide an alternate proof of the flatness of a curve inside a tubular neighborhood for curves in the plane. Next the proof of flatness of curve segment inside a tubular neighborhood is extended

to the general Riemannian manifold. We show that it is possible to re-order the samples by Minimal Spanning Tree (MST). For the ordered sample points in Riemannian manifold, we present an interpolation scheme based on the de Casteljau algorithm, refer to Chapter 6. Finally to validate our proposed scheme we provide a few examples of curve reconstruction for curves on Riemannian manifolds. We have selected underlying Riemannian manifolds that are widely used in engineering applications (sphere, surfaces, $SE(3)$ and $SE(2)$ with scaling). See for example, a point sample and the reconstructed curve in $SE(3)$ in Figure 1.5.

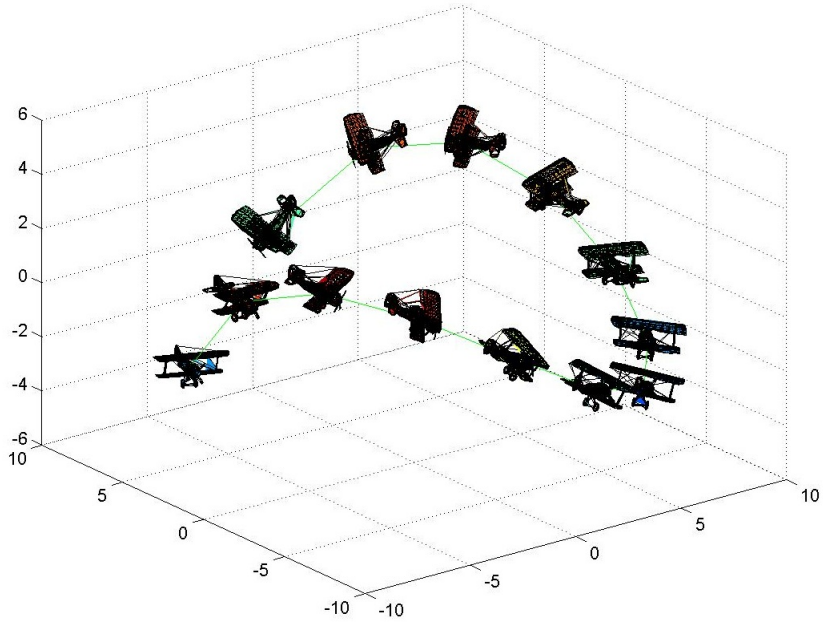


Figure 1.5: Reconstructed curve in $SE(3)$

## 1.5 Thesis Organization

This section briefly describes the organization of the thesis.

The thesis is divided into eight chapters. The first chapter provides an introduction to the problem and motivation for the study. It also provides a basic literature survey which is then extended with the help of suitable examples in Chapter 2. Chapter 2 is an extended literature survey,

where we discuss and present the important results on curve reconstruction in $\mathbb{R}^n$ from the literature on combinatorial curve reconstruction. We also show a few instances of curves reconstructed in $\mathbb{R}^n$ using results in the literature available. We have implemented these algorithms and have created a set of examples of curve reconstruction which are presented in Chapter 2. To show that the NN-CRUST takes care of disjoint components of a curve, we have experimented with curves in $\mathbb{R}^3$ and we exhibit an example at the end of Chapter 2.

In this thesis, as clearly stated in the introduction, we pose the problem of curve reconstruction in higher dimensional curved spaces. To deal with samples on curved spaces, we first examine the notion of distance on surfaces and then we move on to define distances on more general manifolds. In Chapter 3 we give a short review of the definitions and concepts required to work on Riemannian manifolds.

The Riemannian manifolds we are interested in and which will be used in simulations are explicitly presented in Chapter 4. In this chapter we show that how a particular metric is actually defined on the Riemannian manifolds from the Riemannian metric (inner product). This chapter contains examples of Riemannian manifolds starting from $\mathbb{R}^n$ to the curved spaces like surfaces and the Euclidean motion group $SE(3)$. We also take up an example of an implicitly defined Riemannian manifold and describe a way to compute geodesics on it. Geodesics on each of the Riemannian manifolds discussed in this chapter are computed using MATLAB.

Once we have a distance metric defined on Riemannian manifolds, in Chapter 5 we define the tubular neighborhood of a given smooth curve in a Riemannian manifold. We propose a bound on $\varepsilon$ for construction of a tubular neighborhood of a curve based on the radius of curvature at each point of the curve in plane. With the help of two example curves on surfaces, we present observations to show how the underlying manifold affects the sampling density. We give a counter example to the local feature size based sampling process and also show that the cause of the failure - the gaussian curvature of the underlying manifold which is associated with the cut-locus. In this chapter, we give a proof of flatness of the curve segment connecting two consecutive sample points

of the dense sample of the curve.

In Chapter 6, we prove that the Minimum Spanning Tree (MST) correctly re-orders the dense sample. Here we will model the point sample on the curve as vertices of a graph and form a complete graph with edge weights equal to the distances between two points on the underlying Riemannian manifold. In this chapter we also propose a Bezier interpolation scheme for interpolating the sample to approximate the original curve.

The simulations and examples of the reconstructed curves are presented in Chapter 7 of the thesis. Here we consider curves on a sphere ($S^2$), and on special Euclidean groups ($SE(2)$, $SE(3)$) and on $SE(2)$ with scaling. We present successfully reconstructed curves in all the above mentioned Riemannian manifolds. We also show an application of curve reconstruction for ordering motion frames.

Finally we conclude in Chapter 8 with comments on noise in the sampling process. We also discuss possible future direction for work on the curve reconstruction problem.

# Chapter 2

# Curve Reconstruction in $\mathbb{R}^n$

The curve reconstruction problem has its roots in edge-detection in images and in applications such as shape analysis in pattern recognition and classification. The idea behind curve reconstruction is to build a parametric model of a point cloud (sample) which is representative of the original object from which the point cloud was derived. In 1980s, a few graph based algorithms were suggested to tackle this problem in $\mathbb{R}^2$. Examples of these graph theory based approaches are the $\beta$-skeleton of Kirkpatrick and Radke [26]; the $\alpha$ shapes of Edelsbrunner, Kirkpatrick and Seidel [19] and the influence graph of Toussaint [6]. With the advent of scanning technologies, one started looking at efficient sampling mechanisms for objects with various shapes and sizes. This was the motivation for most of the work done on shape modeling with the help of finite sample points. This includes algorithms that guarantee reconstruction of the shape from these finite sample points, up to some topological correctness. Usually, we would like to have a homeomorphism between the shape and the approximation reconstructed from the finite sample of that shape. The shape of an object in plane is represented by the boundary curve of that object. In this chapter, we will discuss the methods for reconstructing curves in the plane and $\mathbb{R}^n$. In other words we assume that the curve is in $\mathbb{R}^n$.

We present here a systematic development of the concepts and algorithms in the field of combi-

natorial curve reconstruction. We have implemented and experimented with various algorithms for curve reconstruction that are available in literature. All the example curves and figures presented in this chapter are results of simulations that we have carried out in MATLAB.

## 2.1 A Curve in the Plane

Given an arbitrary set of sample points of a curve, it is not possible to reconstruct the curve based on the proximity criterion, since, there are varieties of ways in which we can connect the sample points. Let us first look at the difficulty involved in the reconstruction process based on the proximity criterion. To illustrate the point let $\mathcal{S} \subset \mathcal{C}$ be a finite sample of the curve $\mathcal{C} \in \mathbb{R}^2$ with points

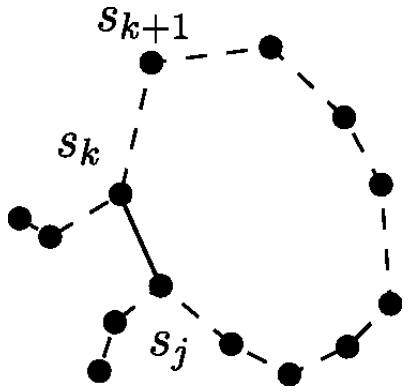


Figure 2.1: Confusion due to lack of samples at the corners or the high curvature region of the curve

$\{s_1, s_2, \ldots, s_k, s_{k+1}, \ldots, s_j, \ldots, s_{N-1}\}$. As shown in Figure 2.1, if we try to connect the sample points based on the nearest neighbor criterion or if we try to re-order the sample via Minimal Spanning Tree as suggested in [13], the confusion at $s_k$ is clearly visible. The reason is proximity based decision : $d(s_k, s_{k+1}) > d(s_k, s_j)$, where $d(\ )$ is the standard Euclidean distance metric defined on $\mathbb{R}^2$. Similar examples can be found in [4]. In a word, it is not possible to re-order an arbitrary sample of the curve. The above argument indicates that we must take care and avoid the possibility of confusion in the high curvature region of the curve by taking a sufficiently large sample. The problem is not resolved fully, since there might be a situation where even though the

curvature of the curve is not high, the re-ordering is still difficult. This is shown in Figure 2.2 below. In this example, sample points on opposite sides $s_k$ and $s_m$ are taken as neighbors.

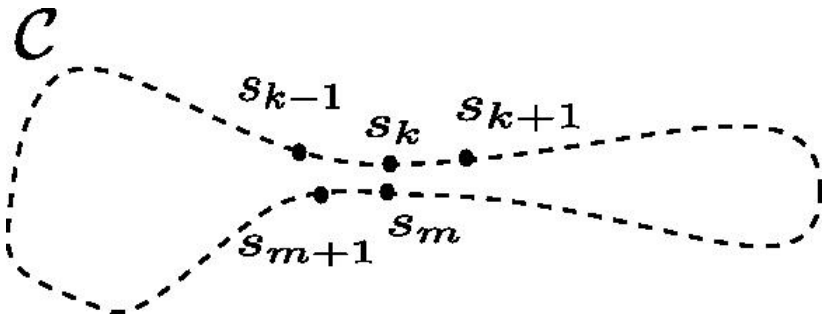


Figure 2.2: Confusion at a region of low curvature

In conclusion, these issues motivated a sampling criterion based on the medial axis. The medial axis $M$ of a curve $\mathcal{C}$ is defined as the closure of the set of points in the plane which have two or more closest points in $\mathcal{C}$. The voronoi diagram of the finite sample $\mathcal{S}$ of $\mathcal{C}$ tries to approximate the medial axis of $\mathcal{C}$. In fact, in practice the medial axis (skeleton) of any shape is approximated by the voronoi vertices of the voronoi diagram, see for example [16]. The concept of least feature size has emerged in the search for a uniform sampling criterion for a given curve, based on its medial axis. In Figure 2.3, the feature size function is evaluated at point $s_{k+1} \in \mathcal{C}$ denoted by $f(s_{k+1})$, which is

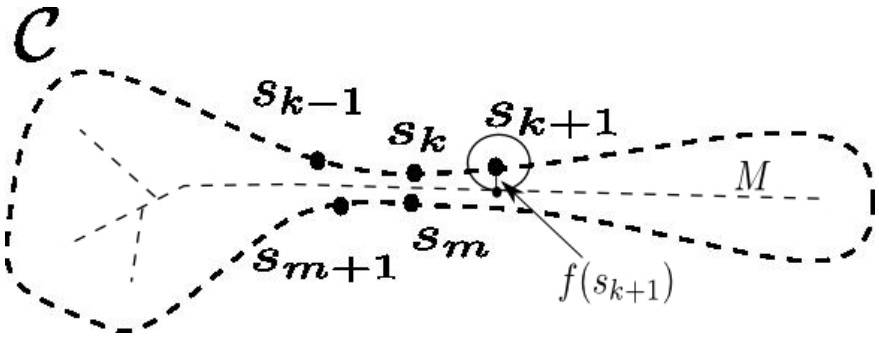


Figure 2.3: Medial axis and the feature size function

the distance of point $s_{k+1}$ to the medial axis $M$ of $\mathcal{C}$. Least feature size ($LFS(\mathcal{C})$) is defined as the least distance from $\mathcal{C}$ to the medial axis $M$.

To begin with, a tubular neighborhood based criterion for curve reconstruction was suggested in [13]. The authors suggested to sample the curve with the least feature size (LFS) $\varepsilon$. A tubular neighborhood for a curve $\mathcal{C}$ is defined as a set $T$ containing $\mathcal{C}$ such that every point of $T$ belongs to exactly one line segment totally contained in $T$ and normal to $\mathcal{C}$. They define a dense sample as a sample $\mathcal{S} \subset \mathcal{C}$, such that for some $\varepsilon > 0$, no two consecutive sample points are more than $\varepsilon$ apart, and the closed disks of radius $\varepsilon$ centered at the sample points, form a tubular neighborhood of $\mathcal{C}$. Such an $\varepsilon > 0$ always exists for smooth simple curves and smooth non-intersecting arcs, see [42]. It is proved in [13] that given a dense sample of a curve $\mathcal{C}$, it is possible to reorder the sample and reconstruct the curve with a polygonal approximation. It is not difficult to show that, for $\varepsilon$ less than the least feature size the generated sample will always be dense. In fact, we will prove this in Proposition in Chapter . Furthermore, de Figueiredo and de Miranda Gomes in [13] also provide a simple heuristic and suggest a graph theoretical approach to deal with noisy samples of a curve. Moreover, they also show that EMST can reconstruct curves with boundaries from a sufficiently dense uniform sample.

But, this requires a high uniform sampling of the curve. A sample $\mathcal{S}$ of a curve $\mathcal{C}$ is called $\delta$-uniform if each point $x \in \mathcal{C}$ has a sample point withing a fixed distance $\delta$. In [4], the authors show a way to reduce the sampling density. This was the first breakthrough in reconstructing curves from a given non-uniform sample. The CRUST and $\beta$-skeleton proposed by Amenta, Bern and Eppstein in [4] provided a way to relax the sampling density criterion from uniform to non-uniform samples. The required sampling density varies with the local feature size on the curve. The suggested thumb rule is, sample the curve more frequently where the details are more, similarly the regions of less details are sampled less densely. By details we mean curvature at points on that curve. The motivation for the CRUST, defined in [4], is based on the voronoi construction. It essentially considers the fact that voronoi vertices in the voronoi diagram of a finite point set $\mathcal{S}$, approximate the medial axis of $\mathcal{S}$. If $\mathcal{S}$ is a finite set of points in the plane, and $V$ is the set of vertices of the Voronoi diagram of $\mathcal{S}$, then an edge between $s_1,\ s_2 \in \mathcal{S}$ belongs to the CRUST of

$\mathcal{S}$ if there is a disk, empty of points in $\mathcal{S} \cup V$, touching $s_1$ and $s_2$. For an alternate characterization of CRUST refer to [4].

The condition for sampling a smooth curve in [4] is based on a local feature size function, which reveals the local level details of the curve at a given point. The local feature size, $f(p),\ p \in \mathcal{C}$ is defined as the Euclidean distance from $p$ to the closest point $m$ on the medial axis. It can be seen that it is an extension to the global feature of the curve defined by least feature size. In fact, it is easy to see that the least feature size $LFS(\mathcal{C}) = \min\{f(p),\ p \in \mathcal{C}\}$. A curve $\mathcal{C}$ is said to be $r$-sampled by a set of sample points $\mathcal{S}$ if every $p \in \mathcal{C}$ is within $r.LFS(p)$ distance of a sample point $s \in \mathcal{S}$.

With the help of empty circle property of voronoi diagram and profound geometrical arguments, the authors in [4] prove a theorem which states that the CRUST of an $r$-sampled smooth curve does not contain any edge between nonadjacent vertices, for $r < 0.252$. This result is considered to be the first breakthrough in reconstructing curves from nonuniform samples. In Figure 2.4, using the CRUST algorithm, a curve is reconstructed from a finite sample.

The essence of the CRUST algorithm is captured in the above example of a reconstructed curve, Figure 2.4. To begin with we assume that we have $\mathcal{S} \subset \mathcal{C}$, an $r$-sample of a smooth curve $\mathcal{C} \subset \mathbb{R}^2$. Using voronoi construction find out $V$, the set of voronoi vertices. Now perform delaunay triangulation on the set $G := \mathcal{S} \cup V$. The final stage of the algorithm involves removal of edges that do not have end points in $\mathcal{S}$. Another example of a reconstructed curve is shown in Figure 2.5. For the detailed analysis of the CRUST algorithm refer to [4].

Some of the effective approaches namely $r$-regular shapes, $\mathcal{A}$-shapes, $\alpha$-shapes are recorded in [5], [30], [19] respectively. A delaunay based method is also suggested in [10]. The use of voronoi vertices as the approximate medial axis (skeleton) of a shape is the essence for defining the sampling criteria. More discussions on voronoi diagrams and the continuous skeleton (medial axis) can be found in [25] and [10].

In [18], a comprehensive survey of these methods is presented. Although there are various

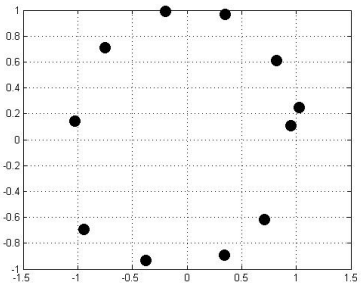

(a) Sample points $\mathcal{S}$

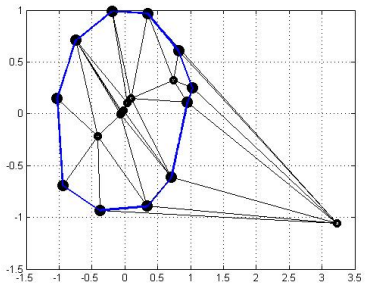

(b) Delaunay triangulation of $G = \{\mathcal{S}, V\}$

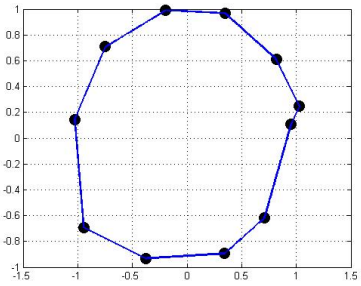

(c) After removing unwanted edges

Figure 2.4: A curve reconstructed by CRUST

instances of curve reconstruction algorithms present in the literature, we will see that Edelsbrunner identifies the common thread and gives a unified view of algorithmic solutions proposed in the computer science literature based on the delaunay approach.

## 2.2 A Curve in the Space

On the basis of the work carried out by Amenta, Bern and Eppstein, in [4], a provable reconstruction algorithm, nearest neighbor CRUST (NN-CRUST), is suggested by T Dey and P Kumar in [15]. Their proposed algorithm is easily adaptable to higher dimensional curve reconstruction problems. It also improves the sampling density from $r < 0.252$, as obtained in [4], to $r < 1/3$. The definition of medial axis is still meaningful in case of higher dimensional euclidean spaces $\mathbb{R}^n$. The medial axis $M$ of a smooth curve $\mathcal{C} \subset \mathbb{R}^n$ is defined as the closure of all points that have two or more

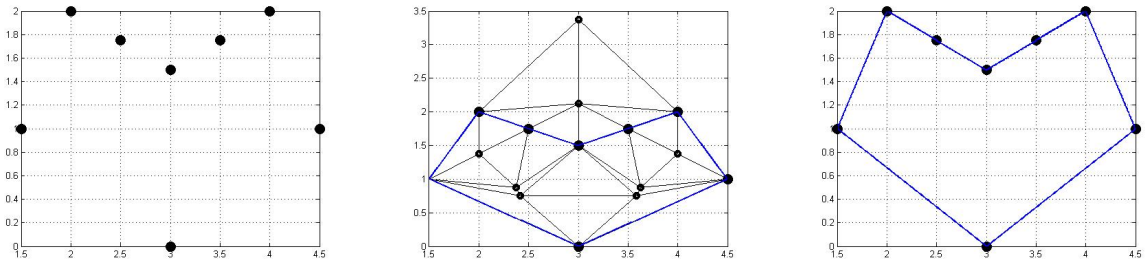

(a) (b) (c)

Figure 2.5: As long as the curve is simple and closed, CRUST gives a correct polygonal reconstruction to the original curve

closest points in $\mathcal{C}$. The local feature size $f(p)$ at a point $p \in \mathcal{C}$ is the least euclidean distance of $p$ from $M$. Other definitions related to sampling also apply.

The algorithm begins with an $r$-sample, $\mathcal{S} \subset \mathcal{C}$, of a smooth curve $\mathcal{S} \subset \mathbb{R}^n$. It is known from [4] that the desired polygonal reconstruction is contained in the delaunay triangulation $T$ of $\mathcal{S}$. What is left is to develop a the polygonal reconstruction. The authors, in [15], provide simple restrictions on $T$ in terms of the nearest neighbor and an angle criterion for curve reconstruction. The first step in the algorithm connects nearest neighbors in $\mathcal{S}$ via edges. Next, points that are incident with only one edge are identified. Suppose $s_k$ is such a point with a single edge $e$. The second step computes the shortest edge incident with $s_k$ amongst all the edges that make an angle more than $\frac{\pi}{2}$ with $e$. The third step includes all such shortest edges in the nearest neighbor edge set. For the proof of correctness of this algorithm refer to [15].

An example of a sample $\mathcal{S} \subset \mathcal{C}$ and the reconstructed polygonal approximation to the helical curve in $\mathbb{R}^3$ is shown in the Figure 2.6. This reconstruction is done using NN-CRUST algorithm. In the first step, the nearest neighbor is searched for each sample point in the delaunay triangulation of the sample. Next a half neighbor, as proposed in [14], is identified for points with single neighbor. These two steps include all the edges required in a polygonal approximation of the original curve $\mathcal{C}$ from which the sample $\mathcal{S}$ is derived.

It is not difficult to see that NN-CRUST also works for smooth curves with more than one

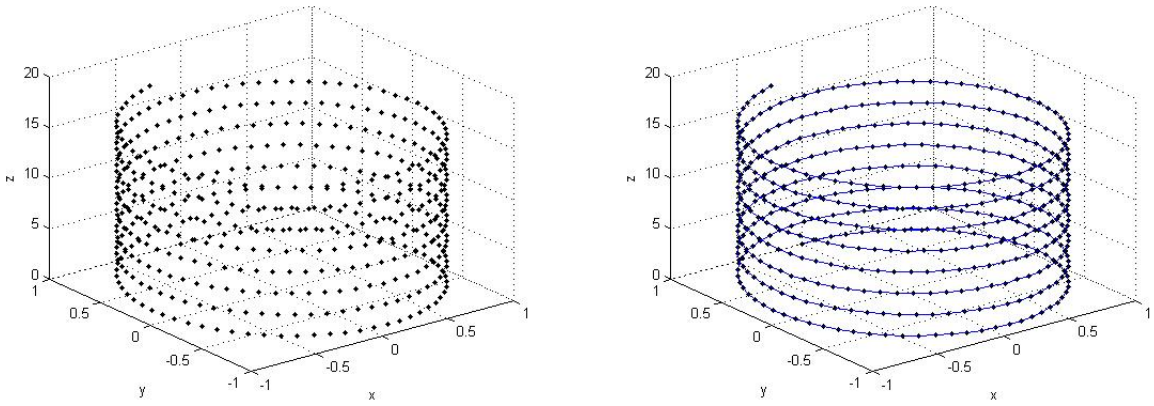


(a) Sample of helical curve in $\mathbb{R}^3$ (b) Reconstructed curve

Figure 2.6: A helical curve reconstructed using NNCRUST

component, since the algorithm prescribed above implicitly allows for only two neighbors for any sample point. To show the behavior of the algorithm on multiple component curves we present an example in Figure 2.7.

Both the examples presented above are of curves in $\mathbb{R}^3$. In general the NN-CRUST can be used to reconstruct smooth curves in $\mathbb{R}^n$. For the development of ideas and extensive proofs of the claims made in [15], one may refer to the book by Tamal K Dey [14]. It presents a comprehensive study in the domain of shape reconstruction. It includes curve as well as surface reconstruction strategies.

Before we begin to explore Riemannian manifolds, consider the situation presented below. Suppose we are given a set of video frames. Assume that the ordering of this video sequence is lost, in other words the frames are jumbled up. We need to re-order the video frames. Suppose we also know that in this video there is an object undergoing rigid motion. Let us try to exploit this information and see if we can re-order the video frames. A set of video frames with the segmented object under motion is shown in Figure 7.2.

We compute the translation $T_{ij}$, and rotation $\theta_{ij}$ between object locations and orientations for frames $i$ and $j$. The Euclidean motions in $\mathbb{R}^2$ form a group $SE(2)$. A typical element of $SE(2)$

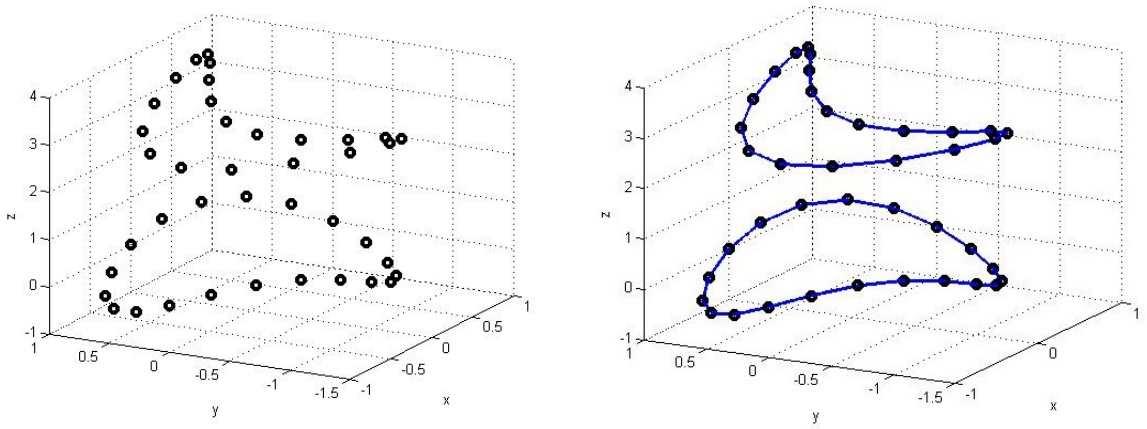

(a) $\mathcal{S} \subset \mathcal{C}$ (b) Reconstructed curve

Figure 2.7: Two connected components reconstructed correctly

is represented using $(Tij, \theta_{ij})$. We will discuss $SE(2)$ in more detail in Chapter 4. So the problem of ordering video frames is translated into the problem of reconstructing a curve in $SE(2)$ (a Riemannian manifold). Considering the distance metric on $SE(2)$ as given in (4.5), if we scale the three axis properly, the problem of curve reconstruction in $SE(2)$ reduces to the problem of curve reconstruction in $\mathbb{R}^3$ and we may use voronoi diagram based reconstruction algorithms assuming dense sampling condition. In other words, in this case it is possible to embed each video frame into $\mathbb{R}^3$ with the help of rotations and translations. To illustrate the point, we use the NN-CRUST algorithm to reconstruct the curve above in the motion sequence and we get the correct ordering as expected. Figure 7.4 shows the correct ordering of the euclidean motions and hence the video frames. In general it may not be possible to identify an embedding from given curved spaces to $\mathbb{R}^n$. Although this example looks like a fabricated one, it suffices to provide a useful insight for further developments.

In next chapter, we present basic definitions and concepts from differential geometry. The objective of the next two chapters is to equip the given Riemannian manifold with a distance metric. A list of useful examples is presented throughout these chapters.

# Chapter 3

# Riemannian Manifolds - I

The subject of this thesis is to extend the combinatorial curve reconstruction approach to curves embedded in Riemannian manifolds. A Riemannian manifold is an abstraction of a curved space in which it is possible to measure geometric quantities such as length of a curve segment, the area of an enclosed region, angle between two curves at a point, etc. Our interest is to equip the manifold with the metric structure, which involves the idea of geodesics and the shortest distance between two point on the given manifold. Riemannian manifolds arise in variety of engineering applications. For example, meteorological studies involve the surface of earth which is a surface like a sphere, it is indeed a Riemannian manifold. The euclidean motion group used in graphics applications is also an example of a Riemannian manifold. In this chapter, we will define a few basic terms and state some of the results from Riemannian geometry which will serve as the building blocks for the development of the ideas ahead. At the end we will present examples of Riemannian manifolds relevant to the problem we will deal with. The focus will be on the sphere - $S^2$ and surface patches, euclidean motion group - $SE(3)$, and $SE(2)$ with scaling.

## 3.1 Differentiable Manifolds

A manifold $\mathcal{M}$ can be considered as a topological space which locally resembles a Euclidean space. A differentiable manifold allows partial differentiation and consequently all the features of differential calculus on $\mathcal{M}$. We will briefly present the essentials of manifold theory to the extent that is required for our work. The vector space $\mathbb{R}^n$ is a topological space, and the vector operations are continuous with respect to the topology. In addition we have the notion of differentiability for real valued functions on $\mathbb{R}^n$, i.e. $f : \mathbb{R}^n \to \mathbb{R}$ is differentiable if the partial derivatives

$$\frac{\partial^{i_1+\ldots+i_r} f}{\partial u_1^{i_1} \ldots \partial u_r^{i_r}}$$

of all order exist and are continuous. Such functions are called $C^\infty$ functions.

The *natural coordinate functions* of $\mathbb{R}^n$ are mappings $u_i : \mathbb{R}^n \to \mathbb{R}$ defined by

$$u_i(x_1, \ldots, x_n) = x_i$$

for $i = 1, 2, \ldots, n$. A function $\phi : \mathbb{R}^m \to \mathbb{R}^n$ is differentiable, continuous or linear if and only if each $u_i \cdot \phi$ is differentiable, continuous or linear, respectively.

**Definition 3.1.** A patch (or chart) on a topological apace $\mathcal{M}$ is a pair $(\mathrm{x}, \mathcal{U})$, where $\mathcal{U}$ is an open subset of $\mathbb{R}^n$ and

$$\mathrm{x} : \mathcal{U} \to \mathrm{x}(\mathcal{U}) \subset \mathcal{M}$$

is a homeomorphism of $\mathcal{U}$ onto an open set $\mathrm{x}(\mathcal{U})$ of $\mathcal{M}$. Let

$$x_i = u_i \circ \mathrm{x}^{-1} : \mathrm{x}(\mathcal{U}) \to \mathbb{R}$$

for $i = 1, \ldots, n$. Then $(x_1, \ldots, x_n)$ is called a system of local coordinates for $\mathcal{M}$.

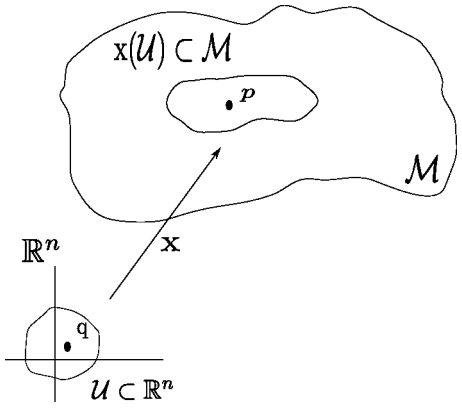


Figure 3.1: A coordinate patch $\mathrm{x} : \mathbb{R}^n \to \mathcal{M}$, with $\mathrm{x}(q) = p$.

**Definition 3.2.** An atlas $\mathcal{A}$ on a topological space $\mathcal{M}$ is a collection of patches $(\mathrm{x}_\alpha, \mathcal{U}_\alpha)$ such that $\mathrm{x}_\alpha : \mathcal{U}_\alpha \subset \mathbb{R}^n \to \mathcal{M}$ and $\cup_\alpha \mathrm{x}_\alpha(\mathcal{U}_\alpha) = \mathcal{M}$. A topological space $\mathcal{M}$ equipped with an atlas is called a topological manifold.

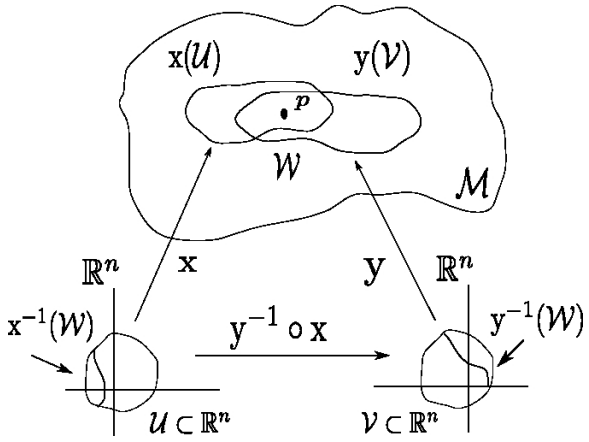


Figure 3.2: Change of coordinates $\mathrm{y}^{-1} \circ \mathrm{x}$. If it is differentiable for every pair of intersecting patches on $\mathcal{M}$ then the manifold $\mathcal{M}$ is called a differentiable manifold.

Let $\mathcal{A}$ be an atlas on a topological space $\mathcal{M}$. If $(\mathrm{x}, \mathcal{U})$ and $(\mathrm{y}, \mathcal{V})$ are any two patches in $\mathcal{A}$ such that $\mathrm{x}(\mathcal{U}) \cap \mathrm{y}(\mathcal{V}) = \mathcal{W}$ is a nonempty subset of $\mathcal{M}$, then the map

$$\mathrm{y}^{-1} \circ \mathrm{x} : \mathrm{x}^{-1}(\mathcal{W}) \to \mathrm{y}^{-1}(\mathcal{W}) \tag{3.1}$$

is a homeomorphism between open subsets of $\mathbb{R}^n$. We call $\mathrm{y}^{-1} \circ \mathrm{x}$ a change of coordinates.

**Definition 3.3.** A differentiable manifold is a topological space $\mathcal{M}$ equipped with an atlas $\mathcal{A}$ such that the change of coordinates (3.1) is differentiable (that is, of class $C^\infty$) in the ordinary Euclidean sense*. The dimension of the manifold $\mathcal{M}$ (denoted by $dim\ \mathcal{M}$) is $n$.

**Example 3.1.** *The Euclidean space $\mathbb{R}^n$ is a differentiable manifold. The identity map $\mathbf{1} : \mathbb{R}^n \to \mathbb{R}^n$*

$$(u_1, \ldots, u_n) : \mathbb{R}^n \to \mathbb{R}^n$$

*constitutes an atlas $\mathcal{A} := \{(\mathbf{1}, \mathbb{R}^n)\}$ for $\mathbb{R}^n$ by itself.*

**Example 3.2.** *A regular surface $\mathcal{M}$ in $\mathbb{R}^n$ is a differentiable manifold.*

1. *A Monge patch is a patch $\mathrm{x} : \mathcal{U} \to \mathbb{R}^3$ of the form*

$$\mathrm{x}(u, v) = (u, v, h(u, v)),$$

   *where $\mathcal{U}$ is an open set in $\mathbb{R}^2$ and $h$ is a differentiable function. Paraboloid defined as $\mathrm{h}(u, v) := (u, v, au^2 + bv^2)$, where $a, b \neq 0$, and monkey saddle defined as $\mathrm{h}(u, v) := (u, v, u^3 - 3uv^2)$ are examples of regular surfaces each parametrized by a single patch.*

2. *A sphere is an example of a regular surface which needs an atlas with at least two patches to cover it. Refer to section 4.3 for more details.*

## 3.2 Tangent Vectors and Tangent Space

The tangent space to a differentiable manifold $\mathcal{M}$ at a point $p \in \mathcal{M}$ can be thought of as the best linear approximation to $\mathcal{M}$ at $p$. For surfaces in $\mathbb{R}^3$, a tangent vector at a point $p$ of the surface is

*In order to ensure uniqueness of convergence and avoid pathological situations, we will always take $\mathcal{M}$ to be a connected, Hausdroff topological space.

defined as the velocity in $\mathbb{R}^3$ of a curve in the surface passing through $p$. But one of the main aims of modern differential geometry is to present ideas in a way that is intrinsic to the manifold itself, in particular, is not dependent on an embedding in some higher dimensional vector space. For example, the definition of a differentiable manifold itself made no reference to such an embedding, and neither should the definition of a tangent space. In the following, we define the tangent vector as an equivalence class of curves on the manifold.

**Definition 3.4.** Let $\mathcal{M}$ be a differentiable manifold. A differentiable function $\alpha : (-\varepsilon, \varepsilon) \to \mathcal{M}$ is called a differentiable curve in $\mathcal{M}$. Suppose that $\alpha(0) = p \in \mathcal{M}$, and let $\mathcal{D}$ be the set of functions on $\mathcal{M}$ that are differentiable at $p$. The tangent vector to the curve $\alpha$ at $t = 0$ is a function $\alpha'(0) : \mathcal{D} \to \mathbb{R}$ given by

$$\alpha'(0)f = \left.\frac{d(f \circ \alpha)}{dt}\right|_{t=0}, \ f \in \mathcal{D}.$$

A tangent vector at $p$ is the tangent vector at $t = 0$ of some curve $\alpha$ with $\alpha(0) = p$. The set of all tangent vectors to $\mathcal{M}$ at $p$ will be indicated by $T_p\mathcal{M}$.

If we choose a parametrization $\mathrm{x} : \mathcal{U} \to \mathcal{M}$ at $p = \mathrm{x}(0)$, we can express the function $f$ and the curve $\alpha$ in this parametrization by

$$f \circ \mathrm{x}(q) = f(x_1, \ldots, x_n), \ q = (x_1, \ldots, x_n) \in \mathcal{U}$$

and

$$\mathrm{x}^{-1} \circ \alpha(t) = (x_1(t), \ldots, x_n(t)),$$

respectively. Therefore, restricting $f$ to $\alpha$, we obtain

$$\alpha'(0)f = \left.\frac{d}{dt}(f \circ \alpha)\right|_{t=0} = \left.\frac{d}{dt} f(x_1(t), \ldots, x_n(t))\right|_{t=0} = \sum_{i=1}^{n} x_i'(0) \left(\frac{\partial f}{\partial x_i}\right) = \left(\sum_{i=1}^{n} x_i'(0) \left(\frac{\partial}{\partial x_i}\right)_0\right) f.$$

So the vector $\alpha'(0)$ can be expressed in the parametrization x by

$$\alpha'(0) = \sum_i x_i'(0) \left(\frac{\partial}{\partial x_i}\right)_0. \tag{3.2}$$

where $\left(\frac{\partial}{\partial x_i}\right)_0$ is the tangent vector at $p$ of the coordinate curve $x_i \to \mathrm{x}(0, \ldots, 0, x_i, 0, \ldots, 0)$.

The expression 3.2 shows that the tangent vector to the curve $\alpha$ at $p$ depends only on the derivative of $\alpha$ in a coordinate system. It follows from 3.2 that the set $T_p\mathcal{M}$, with the usual operations of functions, forms a vector space of dimension $n$, and that the choice of parametrization $\mathrm{x} : \mathcal{U} \to \mathcal{M}$ determines an associated basis $\left\{\left(\frac{\partial}{\partial x_1}\right)_0, \ldots, \left(\frac{\partial}{\partial x_n}\right)_0\right\}$ in $T_p\mathcal{M}$. The linear structure in $T_p\mathcal{M}$ defined above does not depend on the parametrization. The vector space $T_p\mathcal{M}$ is called the tangent space of $\mathcal{M}$ at $p$.

**Example 3.3.** *Tangent space at a point on a 2-sphere is the tangent plane at a point. Depending upon the parametrization of a 2-sphere we can find orthogonal vectors spanning the tangent space at a given point. See section 4.3 for a particular parametrization of 2-sphere and the corresponding tangent space at a point on a 2-sphere.*

We state the definition of differential of a differentiable mapping without proof. It will be used when we will discuss issues related to isometric embedding.

**Definition 3.5.** Let $\mathcal{M}$ and $\mathcal{N}$ be differentiable manifolds and let $\phi : \mathcal{M} \to \mathcal{N}$ be a differentiable mapping. For every $p \in \mathcal{M}$ and for each $v \in T_p\mathcal{M}$, choose a differentiable curve $\alpha : (-\varepsilon, \varepsilon) \to \mathcal{M}$ with $\alpha(0) = p$, $\alpha'(0) = v$. Take $\beta = \phi \circ \alpha$. The mapping $d\phi_p : T_p\mathcal{M} \to T_{\phi(p)}\mathcal{N}$ given by $d\phi_p(v) = \beta'(0)$ is a linear mapping that does not depend on the choice of $\alpha$. The linear mapping $d\phi_p$ is called the differential of $\phi$ at $p$. Some times $\phi_{*p}$ is also used iin place of $d\phi_p$ to denote the differential.

In addition it can be shown that if $m$ and $n$ are the dimensions of $\mathcal{M}$ and $\mathcal{N}$ respectively,

$$\beta'(0) = d\phi_p(v) \;=\; \left(\frac{\partial y_i}{\partial x_j}\right)(x_j'(0)),$$

where $i = 1, \ldots, m$ and $j = 1, \ldots, n$ and $\left(\frac{\partial y_i}{\partial x_j}\right)$ denotes an $m \times n$ matrix and $x_j'(0)$ denotes a column matrix with $n$ elements obtained from the parametrizations x and y.

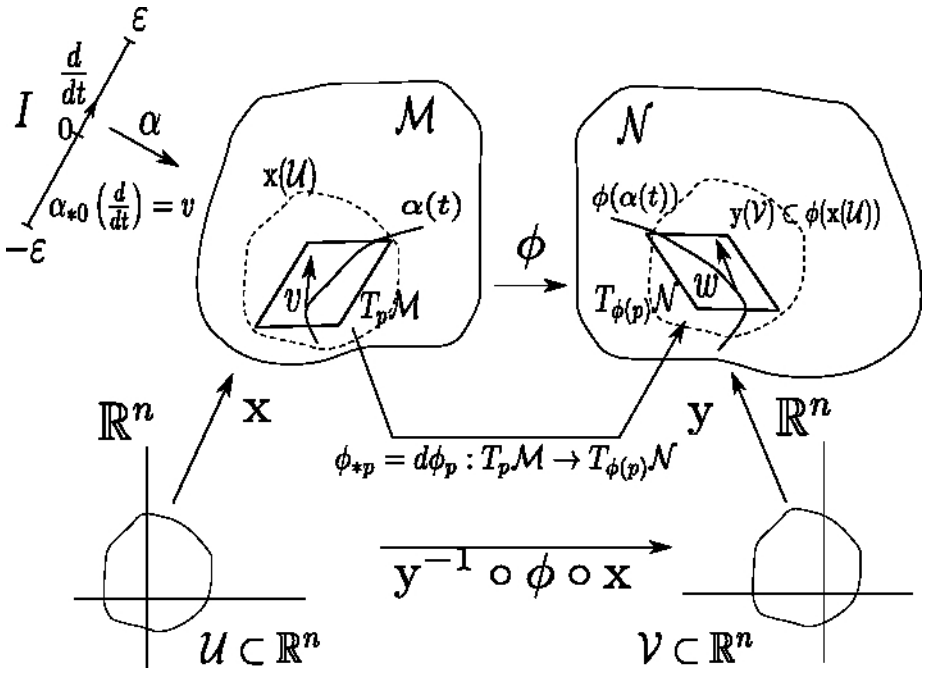


Figure 3.3: Differential of map $\phi : \mathcal{M} \to \mathcal{N}$ and representation of $\phi$ in local coordinates.

**Definition 3.6.** Let $\mathcal{M}$ and $\mathcal{N}$ be differentiable manifolds. A mapping $\phi : \mathcal{M} \to \mathcal{N}$ is called a diffeomorphism if it is differentiable, bijective and its inverse is also differentiable. The concept of a diffeomorphism is the natural idea of equivalence between differentiable manifolds.

**Definition 3.7.** Let $\mathcal{M}$ be an $n$ dimensional differentiable manifold and let $T\mathcal{M} = \{(p, v);\ p \in \mathcal{M},\ v \in T_p\mathcal{M}\}$. $T\mathcal{M}$ is called the tangent bundle of $\mathcal{M}$.

**Definition 3.8.** A vector field $X$ on a differentiable manifold $\mathcal{M}$ is a correspondence that associates to each point $p \in \mathcal{M}$ a vector $X(p) \in T_p\mathcal{M}$. In terms of mappings, $X$ is a mapping of $\mathcal{M}$ into the tangent bundle $T\mathcal{M}$. The field is differentiable if the mapping $X : \mathcal{M} \to T\mathcal{M}$ is differentiable.

Considering a parametrization $\mathrm{x} : \mathcal{U} \subset \mathbb{R}^n \to \mathcal{M}$ we can write

$$X(p) = \sum_{i=1}^{n} a_i(p) \frac{\partial}{\partial x_i}, \tag{3.3}$$

where each $a_i : \mathcal{U} \to \mathbb{R}$ is a function on $\mathcal{U}$ and $\left\{ \frac{\partial}{\partial x_i} \right\}_{i=1,\ldots,n}$ is the basis associated to $\mathrm{x}$. It is clear that $\mathrm{x}$ is differentiable if and only if the functions $a_i$ are differentiable for some parametrization.

A vector field can also be thought of as a mapping $X : \mathcal{D}(\mathcal{M}) \to \mathcal{D}(\mathcal{M})$. $\mathcal{D}(\mathcal{M}) := C^\infty(\mathcal{M})$ denotes the ring of smooth functions on $\mathcal{M}$.

## 3.3 Riemannian Manifolds

**Definition 3.9.** A Riemannian metric (or Riemannian structure) on a differentiable manifold $\mathcal{M}$ is a correspondence which associates to each point $p \in \mathcal{M}$ an inner product $\langle , \rangle_p$, a symmetric, bilinear, positive-definite form on the tangent space $T_p\mathcal{M}$, which varies differentiably in the sense that if $\mathrm{x} : \mathcal{U} \subset \mathbb{R}^n \to \mathcal{M}$ is a system of coordinates around $p$, with $\mathrm{x}(x_1, \ldots, x_n) = q \in \mathrm{x}(\mathcal{U})$ and $\frac{\partial}{\partial x_i}(q) = d\mathrm{x}_q(0, \ldots, 1, \ldots, 0)$, then $\langle \frac{\partial}{\partial x_i}(q), \frac{\partial}{\partial x_j}(q) \rangle_q = g_{ij}(x_1, \ldots, x_n)$ is a differentiable function on $\mathcal{U}$.

Whenever there is no possibility of confusion the index $p$ in the function $\langle , \rangle_p$ is discarded. The function $g_{ij} = g_{ji}$ is called the local representation of the Riemannian metric in the coordinate system $\mathrm{x} : \mathcal{U} \subset \mathbb{R}^n \to \mathcal{M}$. A differentiable manifold with a given Riemannian metric will be called a Riemannian manifold.

Let $\mathcal{M}$ and $\mathcal{N}$ be Riemannian manifolds. A diffeomorphism $f : \mathcal{M} \to \mathcal{N}$ is called an isometry if:

$$\langle u, v \rangle_p = \langle df_p(u), df_p(v) \rangle_{f(p)}, \tag{3.4}$$

for all $p \in \mathcal{M}$ and $u, v \in T_p\mathcal{M}$.

**Example 3.4.** $\mathbb{R}^2$ *with the usual inner product defined as the vector dot product is a Riemannian*

*manifold. Suppose* $\mathbb{R}^2$ *is equipped with a different inner product, say* $g_{ij} = \begin{pmatrix} 2 & 1 \\ 1 & 1 \end{pmatrix}$. *It is certainly a valid Riemannian metric since it is symmetric and positive definite.*

*Now since* $g_{ij}$ *is constant at all points on* $\mathbb{R}^2$, *we can find a linear isometry* $f : (\mathbb{R}^2, \langle , \rangle_{g_{ij}}) \to (\mathbb{R}^2, \langle , \rangle)$, *given by,* $f(x, y) = (x, x + y)$.

*The differential, i.e. the Jacobian of* $f$, *of the isometry is* $f_* = df = \begin{pmatrix} 1 & 0 \\ 1 & 1 \end{pmatrix}$.

Moreover it can be shown that every differentiable manifold $\mathcal{M}$ (Hausdorff with countable basis) has a Riemannian metric. Now by using the Riemannian inner product we will proceed to calculate the lengths of curves in Riemannian manifolds.

**Definition 3.10.** A differentiable mapping $c : I \to \mathcal{M}$ of $I := [0, 1] \subset \mathbb{R}$ into a differentiable manifold $\mathcal{M}$ is called a curve.

A parametrized curve can admit self-intersection as well as corners. To avoid difficulties at singularities we assume that the curve under study is always a smooth (infinitely differentiable) curve.

**Definition 3.11.** A vector field $V$ along a curve $c : I \to \mathcal{M}$ is a differentiable mapping that associates to every $t \in I$ a tangent vector $V(t) \in T_{c(t)}\mathcal{M}$. To say that $V$ is differentiable means that for any differentiable function $f$ on $\mathcal{M}$, the function $t \to V(t)f$ is a differentiable function on $I$.

The vector field $dc(\frac{d}{dt})$, denoted by $\frac{dc}{dt}$, is called the velocity field of $c$. The restriction of a curve $c$ to a closed interval $[a, b] \subset I$ is called a segment. If $\mathcal{M}$ is a Riemannian manifold, we define the length of the segment by

$$\ell_a^b(c) = \int_a^b \left\langle \frac{dc}{dt}, \frac{dc}{dt} \right\rangle^{1/2} dt. \tag{3.5}$$

## 3.4 Covariant Derivative, Parallel Transport and Geodesics

Let $S \subset \mathbb{R}^3$ be a surface and let $c : I \to S$ be a curve in $S$, with $X : I \to \mathbb{R}^3$ a vector field along $c$ tangent to $S$. The vector $\frac{dX}{dt}(t),\ t \in I$ does not in general belong to $T_{c(t)}S$. To make sure that the differentiation is an intrinsic geometric notion on $S$, instead of usual derivative $\frac{dX}{dt}(t)$, the orthogonal projection of $\frac{dX}{dt}(t)$ on $T_{c(t)}S$ is considered. This is called the covariant derivative and is denoted by $\frac{DX}{dt}(t)$. Still it is interesting to note that this process of taking the derivative is valid only by making use of the ambient space in which the manifold is embedded. To overcome the orthogonal projection, we need to define a so called Levi-Civita connection, denoted as $\nabla$, on a Riemannian manifold. In fact it can be shown that $\nabla$ is uniquely determined from a given metric $\langle , \rangle$.

It is occasionally helpful to visualize covariant derivative as the intrinsic directional derivative, where we take the definition of directional derivative and replace the vector difference by vector difference of parallel translated vector. For more on the above notions, the reader may refer to [17].

**Definition 3.12.** On a differential manifold $\mathcal{M}$, an affine connection $\nabla$ is defined as a mapping

$$\nabla : \mathcal{V}(\mathcal{M}) \times \mathcal{V}(\mathcal{M}) \to \mathcal{V}(\mathcal{M}) \tag{3.6}$$

where $\mathcal{V}(\mathcal{M})$ is the set of all vector fields of class $C^\infty$ on $\mathcal{M}$. It is denoted by $(X, Y) \to \nabla_X Y$ and satisfies the following properties:

1. $\nabla_{fX+gY} Z = f\nabla_X Z + g\nabla_Y Z$.
2. $\nabla_X (Y + Z) = \nabla_X Y + \nabla_X Z$.
3. $\nabla_X (fY) = f\nabla_X Y + X(f)Y$,

where $X, Y, Z \in \mathcal{V}(\mathcal{M})$ and $f, g \in \mathcal{D}(\mathcal{M})$.

Let $\mathcal{M}$ be a differentiable manifold with an affine connection $\nabla$. There exists a unique correspondence which associates to a vector field $X$ along the differentiable curve $c : I \to \mathcal{M}$ an another vector field $\frac{DX}{dt}$ along $c$, called the covariant derivative of $X$ along $c$, such that

1. $\frac{D}{dt}(X+Y) = \frac{DX}{dt} + \frac{DY}{dt}$.
2. $\frac{D}{dt}(fX) = \frac{df}{dt}X + f\frac{DX}{dt}$, where $Y$ is a vector field along $c$ and $f \in \mathcal{D}(\mathcal{M})$.
3. If $X$ is induced by a vector field $V \in \mathfrak{X}(\mathcal{M})$, i.e., $X(t) = V(c(t))$, then $\frac{DX}{dt} = \nabla_{dc/dt}V$.

Let $\mathrm{x} : \mathcal{U} \subset \mathbb{R}^n \to \mathcal{M}$ be a system of coordinates with $c(I) \cap \mathrm{x}(\mathcal{U}) \neq \emptyset$ and let $(x_1(t), \ldots, x_n(t))$ be the local expression of $c(t),\ t \in I$. Let $X_i = \frac{\partial}{\partial x_i}$. then we can express the field $X$ locally as $X = \sum_j x^j X_j,\ j = 1, \ldots, n$, where $x^j = x^j(t)$ and $X_j = X_j(c(t))$.

$$\frac{DX}{dt} = \sum_j \frac{dx^j}{dt} X_j + \sum_{i,j} \frac{dx_i}{dt} x^j \nabla_{X_i} X_j. \tag{3.7}$$

The correspondence expressed in (3.7) satisfies the above three conditions. The above expression is the expression of covariant derivative in terms of a connection.

**Definition 3.13.** Let $\mathcal{M}$ be a differentiable manifold with an affine connection $\nabla$. A vector field $X$ along curve $c : I \to \mathcal{M}$ is called parallel if $\frac{DX}{dt} = 0$.

Suppose there exists such a parallel field $X$ in $\mathrm{x}(\mathcal{U})$ along $c$ with $X(t_0) = X_0$. Then $X = \sum_j x^j X_j$ satisfies

$$0 = \frac{DX}{dt} = \sum_j \frac{dx^j}{dt} X_j + \sum_{i,j} \frac{dx_i}{dt} x^j \nabla_{X_i} X_j.$$

Putting $\nabla_{X_i} X_j = \sum_k \Gamma_{ij}^k$, called the Christoffel symbols, and replacing $j$ wit $k$ in the first sum, we obtain

$$\frac{DX}{dt} = \sum_k \left\{ \frac{dx^k}{dt} + \sum_{i,j} x^j \frac{dx_i}{dt} \Gamma_{ij}^k \right\} X_k = 0.$$

The system of $n$ differential equations in $x^k(t)$,

$$\frac{dx^k}{dt} + \sum_{i,j} x^j \frac{dx_i}{dt} \Gamma^k_{ij} = 0,\ k = 1, \ldots, n, \tag{3.8}$$

posses a unique solution satisfying the initial condition. Moreover, since the system is linear, any solution is defined for all $t \in I$. As an example, we present parallel transport of a vector on a sphere in Appendix C.

**Theorem 3.14.** *(Levi-Civita). Given a Riemannian manifold $\mathcal{M}$, there exists a unique affine connection $\nabla$ on $\mathcal{M}$ satisfying the conditions;*

1. *$\nabla$ is symmetric, i.e. $\nabla_X Y - \nabla_Y X = [X, Y]$ for all $X, Y \in \mathfrak{X}((M))$. $[X, Y] = XY - YX$ is called the bracket.*

2. *$\nabla$ is compatible with the Riemannian metric.*

We will encourage reader to follow the definition of compatibility from [17]. A connection is defined in terms of the Christoffel symbols. Observe that for Euclidean space $\mathbb{R}^n$ the $\Gamma^k_{ij} = 0$. Observer also that the covariant derivative (3.7) differs from the usual derivative in $\mathbb{R}^n$ by terms which involve the Christoffel symbols.

**Definition 3.15.** A parametrized curve $\gamma : I \to \mathcal{M}$ is a geodesic at $t_o \in I$ if $\frac{D}{dt}\left(\frac{d\gamma}{dt}\right) = 0$ at the point $t_0$; if $\gamma$ is geodesic $\forall t \in I$, we say $\gamma$ is a geodesic.

This definition describes the geodesic as a curve with zero acceleration. In other words the magnitude of the velocity vector is constant. We will see that a geodesic minimizes the arc length for points which are close enough. Geodesics are local length minimizers.

## 3.5 Riemannian Manifold as a Metric Space

Suppose in a system of coordinates $(\mathrm{x}, \mathcal{U})$ about $\gamma(t_0)$, $\gamma$ is a geodesic. From the definition above the curve $\gamma(t) = (x_1(t), \ldots, x_n(t))$ is a geodesic iff,

$$\frac{D}{dt}\left(\frac{d\gamma}{dt}\right) = \sum_k \left(\frac{d^2x^k}{dt^2} + \sum_{i,j} \frac{dx_i}{dt}\frac{dx_j}{dt}\Gamma_{ij}^k\right)\frac{\partial}{\partial x^k} = 0.$$

So we get a second order system of nonlinear ordinary differential equations,

$$\frac{d^2x^k}{dt^2} + \sum_{i,j} \frac{dx_i}{dt}\frac{dx_j}{dt}\Gamma_{ij}^k = 0,\ k = 1, \ldots, n. \tag{3.9}$$

Existence of solution for a given initial value problem is guaranteed locally. One may refer to the results on existence in [17]. Geodesic starting from a point $q$ in the direction $v \in T_q\mathcal{M}$ within small interval $(-\delta, \delta)$ will be denoted by $\gamma(t, q, v)$. In regard to this the exponential map is defined next.

Let $p \in \mathcal{M}$ and let $U \subset T\mathcal{M}$ be a suitable open set. Then the map $\exp : U \to \mathcal{M}$ given by

$$\exp(q, v) = \gamma(1, q, v),\ (q, v) \in U$$

is called the exponential map on $U$. It is a differentiable map. If we restrict it to tangent space $T_q\mathcal{M}$, we get

$$\exp_q : B_\varepsilon(0) \subset T_q\mathcal{M} \to \mathcal{M}$$

denoted by $\exp_q(v) = \exp(q, v)$, where $B_\varepsilon(0)$ is an open ball with center at the origin $0$ of $T_q\mathcal{M}$.

On manifold $\mathcal{M}$, $\exp_q(v)$ is a point obtained by traveling the length equal to $|v|$, starting from $q$, along a geodesic which passes through $q$ with velocity $\frac{v}{|v|}$. We state the following result which will play a crucial role in development of tubular neighborhood for a curve on manifold without proof.

**Proposition 3.16.** *Given $p \in \mathcal{M}$, there exists an $\varepsilon > 0$ such that $\exp_p : B_\varepsilon \subset T_p\mathcal{M} \to \mathcal{M}$ is a*

*diffeomorphism of $B_\varepsilon(0)$ onto an open subset of $\mathcal{M}$.*

For Lie groups the exponential map plays an important role. The elements of lie algebra (tangent space at the group identity) are mapped to group elements via $\exp$.

**Definition 3.17.** A Riemannian manifold $\mathcal{M}$ is geodesically complete if for all $p \in \mathcal{M}$, the $\exp_p$ is defined for all $v \in T_p\mathcal{M}$, i.e. geodesic $\gamma(t)$ starting from $p$ is defined for all values of $t \in \mathbb{R}$.

Now we define distance function on a Riemannian manifold $\mathcal{M}$. Given two points $p, q \in \mathcal{M}$, consider all the piecewise differentiable curves joining $p$ and $q$. Such curves exist since $\mathcal{M}$ is connected.

**Definition 3.18.** The distace $d(p, q)$ is defined by $d(p, q) =$ infimum of the lengths of all curves $c_{p,q}$, where $c_{p,q}$ is a piecewise differentiable curve joining $p$ and $q$. With the distance $d$, $\mathcal{M}$ is a metric space, i.e.,

1. $d(p, r) \leq d(p, q) + d(q, r)$,
2. $d(p, q) = d(q, p)$,
3. $d(p, q) \geq 0$, and $d(p, q) = 0$ iff $p = q$.

If there exists a minimizing geodesic $\gamma$ joining $p$ to $q$ then $d(p, q) =$ length of $\gamma$. To be in a position to work with manifolds as metric spaces we need the Hopf-Rinow-de Rham Theorem which is stated here without proof:

**Theorem 3.19.** *Let $\mathcal{M}$ be a Riemannian manifold and let $p \in \mathcal{M}$. The following are equivalent:*

1. *$\exp_p$ is defined on all of $T_p\mathcal{M}$.*
2. *$\mathcal{M}$ is complete as a metric space.*
3. *$\mathcal{M}$ is geodesically complete.*

4. *For any $q \in \mathcal{M}$ there exists a geodesic $\gamma$ joining $p$ to $q$ with $\ell(\gamma) = d(p, q)$.*

The Riemannian manifolds we are concerned with, which arise in engineering applications, are complete in the above sense. Having equipped Riemannian manifolds with a metric structure, we will turn our attention to suitable examples in the next chapter.

# Chapter 4

# Riemannian Manifolds - II : Examples

## 4.1 $\mathbb{R}^n$

The Euclidean space, $\mathbb{R}^n$ can be thought of as a Riemannian manifold with the usual *vector inner product* as the Riemannian metric. The tangent space at a point of $\mathbb{R}^n$ is also an $n$-dimensional vector space. With the help of the vector inner product the length of the curve $x : [0,1] \to \mathbb{R}^n$ is defined as: $L(x) = \int_0^1 \sqrt{\langle x'(t), x'(t)\rangle} dt$. It turns out that the minimum length curve between two points in the Euclidean space is a straight line segment connecting them. So the distance between two points in $\mathbb{R}^n$ is given by $d(x,y) = \sqrt{\sum_{i=1}^n (x_i - y_i)^2}$. With this as a metric $(\mathbb{R}^n, d)$ is a metric space.

**Example 4.1** (Curvature Flow)**.** *For example consider $\mathbb{R}^2$. Let a curve in $\mathbb{R}^2$ connect two points $P(0,0)$ and $Q(1,1)$. Now if it is not a straight line it will have non zero curvature function. Suppose we evolve this curve such that at each point on the curve under evolution the curvature reduces. There will be a moment when the curve will have zero curvature everywhere, see Figure 4.1.*

*Curvature flow of a parametric curve $C(t=0,s)$, where $C : [0,a) \times [0,1] \to \mathbb{R}^2$ with $C(t,0) = P$ and $C(t,1) = Q$ is given by*

$$\frac{\partial C(t,s)}{\partial t} = \kappa \hat{N}. \tag{4.1}$$

*$\kappa$ is the curvature of the curve and $\hat{N}$ is the unit normal to the curve. As discussed earlier the curvature measures the amount by which a curve curves away from the straight line segment. As evolution progresses the $C(t,p)$ converges to a straight line segment in $\mathbb{R}^2$. Now the distance between points, $d(P,Q)$, is computed as the length of this straight line segment which matches with the definition of metric on $\mathbb{R}^2$.*

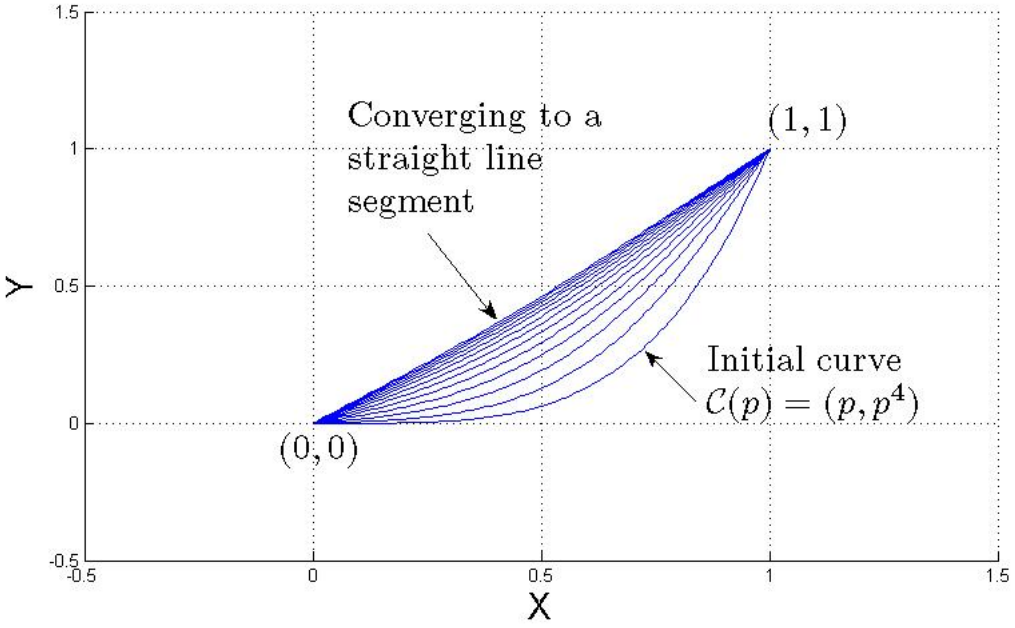


Figure 4.1: Curvature flow : $\frac{\partial}{\partial t}\mathcal{C}(t,p) = \kappa\hat{N}$

## 4.2 Monge Patch

Now let us look at a two dimensional surface $\mathcal{S}$ embedded in $\mathbb{R}^3$. *Two dimensions* here indicate that each point $p \in \mathcal{S}$ has a neighborhood diffeomrophic to a subset of $\mathbb{R}^2$. In other words, if we associate with each point $p \in \mathcal{S}$ a tangent space $T_p\mathcal{S}$ then the dimension of $T_p\mathcal{S}$ is two , i.e. two linearly independent vectors are required to span $T_p\mathcal{S}$. It is now this tangent space and the basis

vectors of this space which decide the Riemannian metric for a given surface. Let us consider a surface patch $\mathrm{x}(u,v) \subset \mathbb{R}^3$ parametrized by $(u,v) \in \mathcal{U} \subset \mathbb{R}^2$. In this case $\mathrm{x}(u,v)$ is our Riemannian manifold $\mathcal{S}$. Riemannian metric is defined as:

$$g_{ij} = \begin{bmatrix} E = \langle \mathrm{x}_u, \mathrm{x}_u \rangle & F = \langle \mathrm{x}_u, \mathrm{x}_v \rangle \\ F = \langle \mathrm{x}_v, \mathrm{x}_u \rangle & G = \langle \mathrm{x}_v, \mathrm{x}_v \rangle \end{bmatrix} \tag{4.2}$$

where $\mathrm{x}_u$ and $\mathrm{x}_v$ are partial derivatives of $\mathrm{x}(u,v)$ w.r.t. $u$ and $v$ respectively. Any vector in $T_p\mathcal{S}$ can be expressed in terms of these basis vectors $\mathrm{x}_u$ and $\mathrm{x}_v$. The inner product for vectors $v_1, v_2 \in T_p\mathcal{S}$ is given by $\langle v_1, v_2 \rangle_g = v_1^T g_{ij} v_2$, where $v_1$ and $v_2$ are column vectors. Given a curve $\gamma(t) \in \mathcal{S}$, the length of the curve segment, for $t \in [a,b]$, is defined as :

$$\ell_a^b(\gamma) = \int_a^b \sqrt{\langle \gamma'(t), \gamma'(t) \rangle_g} dt \tag{4.3}$$

Given $p, q \in \mathcal{S}$, let $\gamma$ be a curve lying in $\mathcal{S}$ with $p = \gamma(a), q = \gamma(b)$ as end points. Then

$$d(p,q) = \inf \ell_a^b(\gamma) \tag{4.4}$$

is a valid metric on $\mathcal{S}$. A $\gamma^*$ for which the distance between two points is minimized is called a *geodesic* curve on the surface $\mathcal{S}$. As we will see in the following example, even for a simple looking parametrized surface finding a closed form expression for the geodesic curve is difficult. In practice, $\gamma^*$ is obtained by numerical approximations.

**Example 4.2.** *Let* $\mathrm{x}(u,v) = (u, v, u \cdot v)$ *which leads to* $\mathrm{x}_u = (1, 0, v)$, $\mathrm{x}_v = (0, 1, u)$ *and* $E = 1 + v^2$, $F = u \cdot v$ *and* $G = 1 + u^2$. *A curve in* $\mathrm{x}(u,v)$ *is,* $\gamma(t) = \mathrm{x}(u(t), v(t)) = (u(t), v(t), u(t) \cdot v(t))$.

*In this example, the system of differential equations corresponding to (3.9) is:*

$$\frac{d^2u}{dt^2} + 2\frac{v}{1+u^2+v^2}\frac{du}{dt}\frac{dv}{dt} = 0 \tag{4.5}$$

$$\frac{d^2v}{dt^2} + 2\frac{u}{1+u^2+v^2}\frac{du}{dt}\frac{dv}{dt} = 0 \tag{4.6}$$

*When we try to minimize the length functional by Euler-Lagrange minimization (Appendix. B), we get for each of the co-ordinates the same system of second order ordinary non-linear differential equations.*

*The length of the curve* $\gamma(t)$, $t \in [t_0, t_1]$ *is* $\int_{t_0}^{t_1} \sqrt{Eu'^2 + 2 \cdot F \cdot u' \cdot v' + Gv'^2}dt$, *where* $u'$ *and* $v'$ *are* $du/dt$ *and* $dv/dt$ *respectively.*

*Let the boundary points, i.e. the points between which we are trying to find the geodesic distance, be* $(1,1,1)$ *and* $(-1,-1,1)$. *We solve the BVP for the above system of equations with MATLAB boundary value solver. The resultant geodesic and the initial guess are shown in the Figure.4.2(a).*

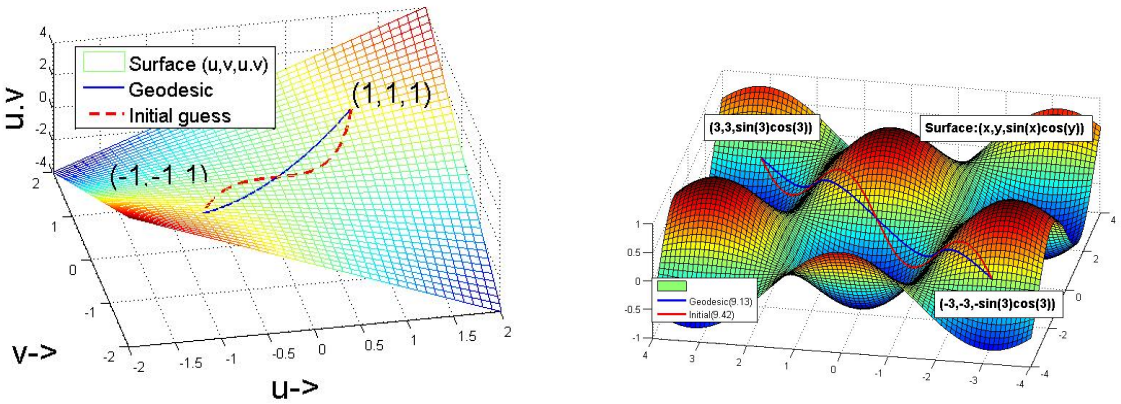


(a) (b)

Figure 4.2: Monge patches and geodesic connecting two points on them.

**Example 4.3.** *Let* $\mathrm{x}(x,y) = (x, y, \sin(x) \cdot \cos(y))$ *be a surface patch. The Figure.4.2(b) shows an initial guess and the stabilized geodesic on the surface. The solution is found with MATLAB*

*boundary value solver with boundary points* $(x_1, y_1) = (-3, -3)$ *and* $(x_2, y_2) = (3, 3)$.

### 4.2.1 Level Set Front Propagation

In the literature, alternate formulations are available for finding the shortest paths on meshed surfaces. We give here an example based on level set front propagation approach suggested in [24]. We take a surface patch as shown in Figure 4.3. In the next Figure 4.4, we show intermediate iterations of the front propagation, front starting from a point $P_1$. Finally in Figure 4.5(a) two shortest paths connecting points $P_1$ and $P_2$ are computed from the distance maps as suggested in [24].

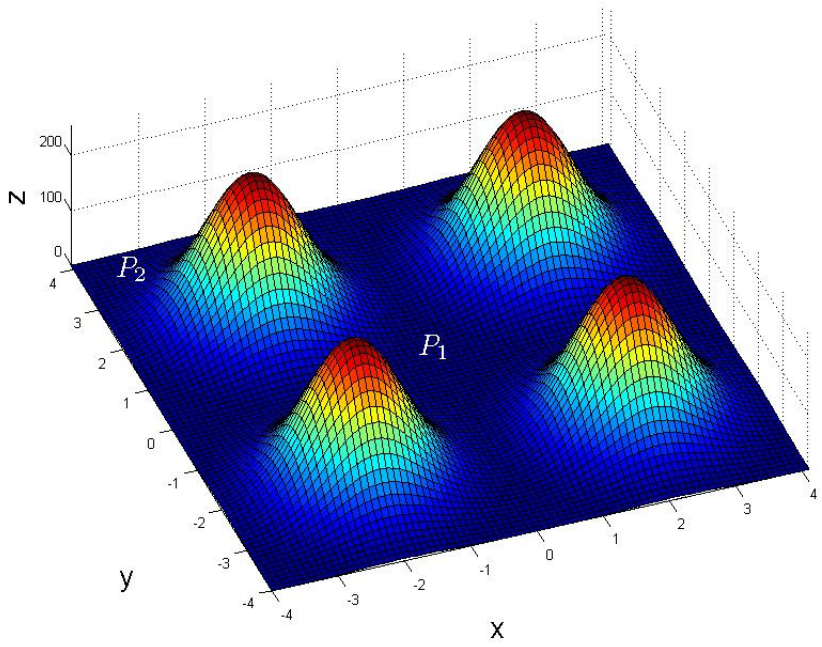


Figure 4.3: Points $P_1$ and $P_2$ on the surface.

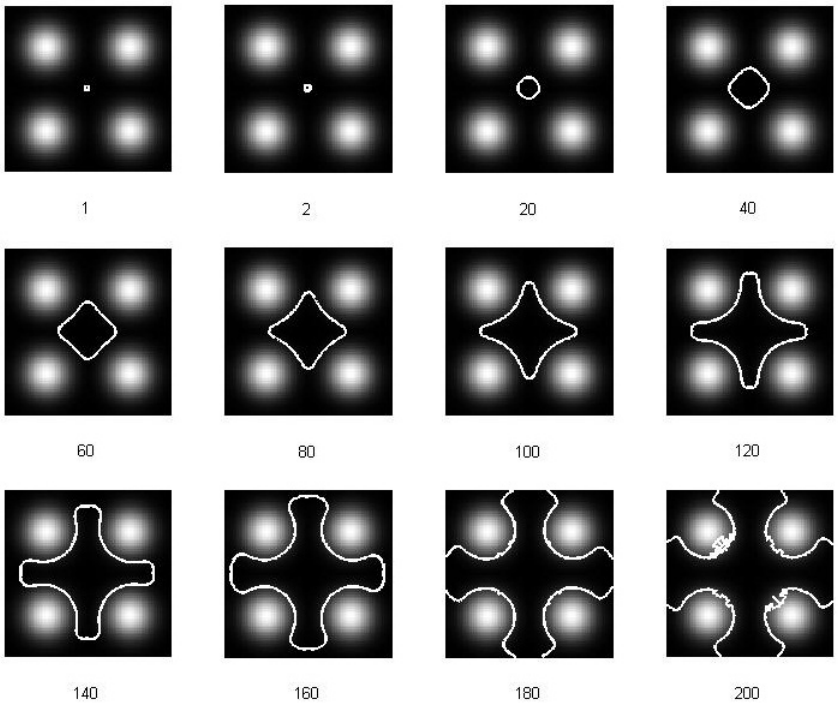


Figure 4.4: Intermediate iterations of front propagation $\frac{\partial}{\partial t}\mathcal{C}(t,p) = \hat{N}$

## 4.3 The Unit Sphere $S^2 \subset \mathbb{R}^3$

A unit sphere embedded in $\mathbb{R}^3$ is an example of a closed surface which can not be patched up with a single patch. It needs at least two patches to be covered up. One such parametrization is the stereographic projection from the poles to the plane cutting the equator, if we consider the sphere to be an approximation to the earth's surface.

For this example, it will be sufficient to work with a single patch given by the parametrization $\mathrm{x} : \mathcal{U} \subset \mathbb{R}^2 \to \mathbb{R}^3$, as

$$\mathrm{x}(u,v) = (\sin u \cos v, \sin u \sin v, \cos u),\ u \in (0,\pi),\ v \in (0,2\pi). \tag{4.7}$$

The Figure 4.6 shows the sphere with parameters $u$ and $v$; $u$ equal to constant are arcs of great circles, the longitudes and $v$ equal to constant are latitudes.

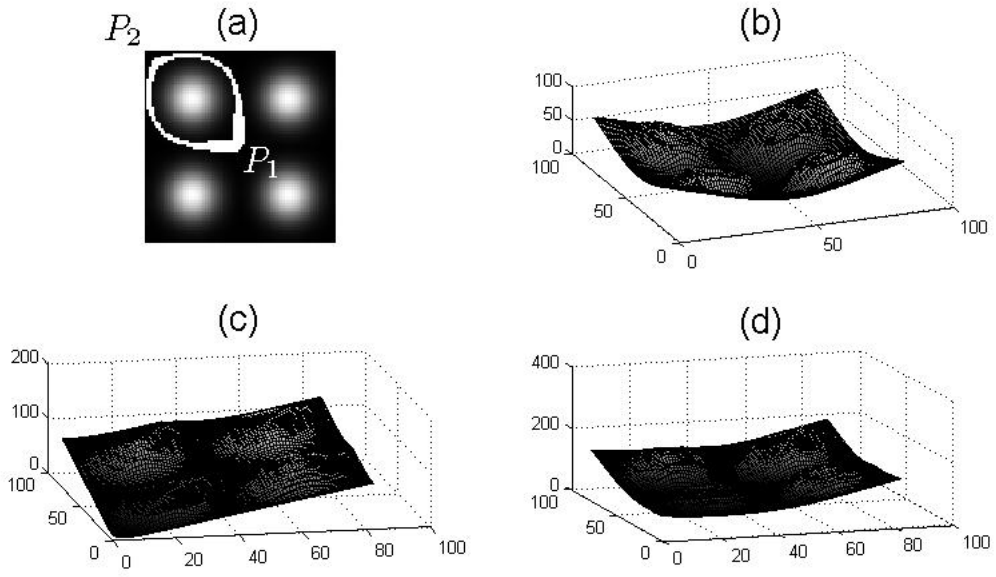


Figure 4.5: Calculated distance maps on surfaces using level set front propagation $\frac{\partial}{\partial t}\mathcal{C}(t,p) = \hat{N}$

Let us express the Riemannian metric in terms of this system of local coordinates. A point on the sphere is expressed in terms of two coordinates $u, v$ by (4.7), see Figure 4.6. The coordinate curves are given by

$$c_1(t) = \mathrm{x}(t,v) \; and \; c_2(t) = \mathrm{x}(u,t).$$

The basis of the tangent space at point $p$ is expressed by using the velocity vectors of theses curves:

$$\frac{d}{dt}c_1(t)_{t=u} = \frac{\partial}{\partial t}\mathrm{x}(t,v)_{t=u} = \mathrm{x}_u(u,v) = (\cos u \cos v, \cos u \sin v, -\sin v),$$

$$\frac{d}{dt}c_2(t)_{t=v} = \frac{\partial}{\partial t}\mathrm{x}(u,t)_{t=v} = \mathrm{x}_v(u,v) = (-\sin u \sin v, \sin u \cos v, 0).$$

The Riemannian metric in terms of these local coordinates, since the sphere is embedded in $\mathbb{R}^3$, is computed $g_{11}(u,v) = \langle \mathrm{x}_u, \mathrm{x}_u \rangle = 1$, $g_{12}(u,v) = g_{21}(u,v) = \langle \mathrm{x}_u, \mathrm{x}_v \rangle = 0$ and $g_{22}(u,v) =$

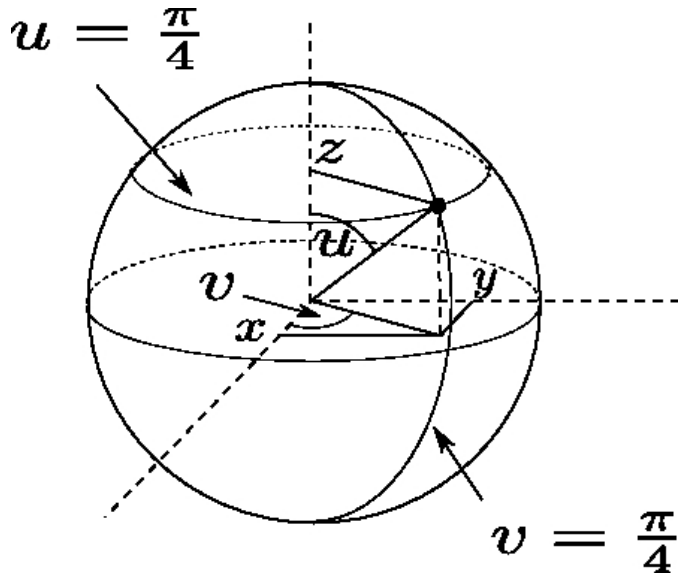


Figure 4.6: A parametric unit sphere with longitude and latitudes.

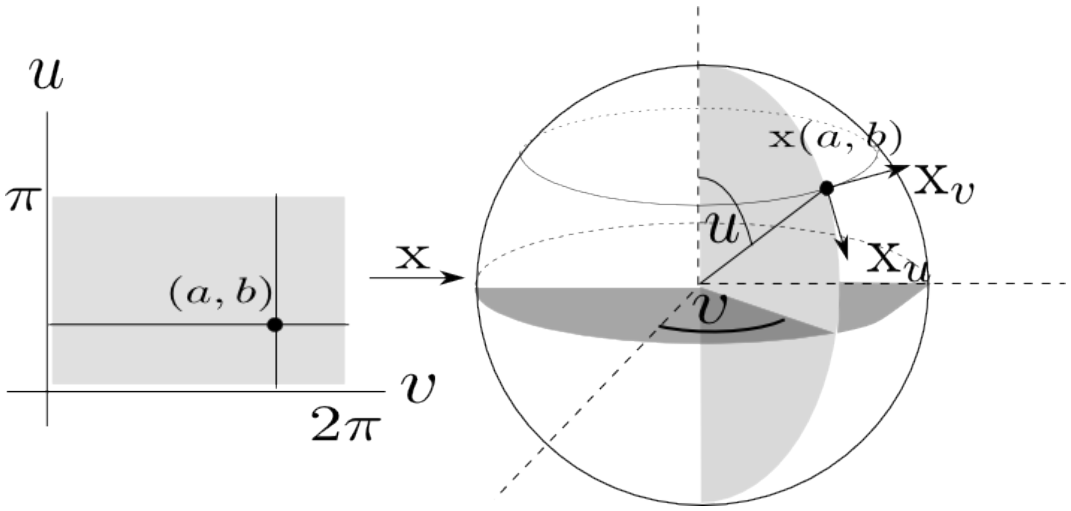


Figure 4.7: Local coordinates and the tangent vectors to coordinate curve on the unit sphere.

$\langle \mathrm{x}_v, \mathrm{x}_v \rangle = \sin^2 u$. Thus the matrix of the Riemannian metric is:

$$g_{ij} = \begin{pmatrix} 1 & 0 \\ 0 & \sin^2 u \end{pmatrix} \tag{4.8}$$

Let us now compute the length of the latitude curve $c(t) = \mathrm{x}(u(t), v(t))$, $u(t) = \frac{\pi}{4},\ v(t) = 2\pi t, t \in [0, 1]$. Since it is evident that everywhere on the curve $c(t)$ the tangent vector $c'(t)$ is expressed as $c'(t) = 0 \cdot \mathrm{x}_u + 2\pi \cdot \mathrm{x}_v$.

Length of this curve is calculated from (3.5) as:

$$\ell_0^1(c(t)) = \int_0^1 2\pi \sin \pi/4 \, dt \ = \ 2\pi \sin \pi/4$$

since, $\langle c'(t), c'(t) \rangle_{g_{ij}} = \begin{pmatrix} 0 & 2\pi \end{pmatrix} \begin{pmatrix} 1 & 0 \\ 0 & \sin^2 u(t) \end{pmatrix} \begin{pmatrix} 0 \\ 2\pi \end{pmatrix} = (2\pi \sin \pi/4)^2$. It is easy to derive that the geodesics on a sphere are the arcs of the great circles. So in case given two points on a sphere the distance between them is calculated as the length of the shortest arc of the great circle passing through these two points. Great circle is found by intersection of a plane passing through given two points and the center of the sphere with the sphere. The image of the $\exp_p$ map as described in section 3.5 is computed for a given point $p \in S^2$ as a unit distance point $q \in S^2$ from $p$ traveled on the great circle in the direction suggested by the tangent vector at $p$.

With the help of Riemannian metric defined it is possible to compute the area of a region enclosed by a curve on the sphere. The closely connected idea of curvature of the surface and parallel transport along with area is presented in Appendix C. It is supported by a simulated example. It is seen to be an instance of the Gauss-Bonnet theorem.

## 4.4 Implicitly Defined Manifold

**Example 4.4.** *Consider the function* $F : \mathbb{R}^4 \to \mathbb{R}$ *defined by,*

$$F(x_1, x_2, y_1, y_2) = (x_1 - y_1)^2 + (x_2 - y_2)^2 - 1.$$

*The level set* $\mathcal{M} := F^{-1}(0)$ *is a manifold. It is the set of end points of all unit line segments in a plane.*

For this manifold the normal space basis vector at a given point can be identified with the maximum change direction, i.e. the gradient vector,

$$\nabla F = [2(x_1 - y_1)\ 2(x_2 - y_2)\ -2(x_1 - y_1)\ -2(x_2 - y_2)]^T.$$

The tangent space vector can be identified with the vectors which are orthogonal to the gradient at a given point. For example at the point $P := (0, 0, 1/\sqrt{2}, 1/\sqrt{2})$ the gradient is $\nabla F = [-\sqrt{2}\ -\sqrt{2}\ \sqrt{2}\ \sqrt{2}]^T$ and the basis for tangent space vectors are given by

$$\nabla F^{\perp} = \left\{ \begin{bmatrix} 1 \\ 0 \\ 1 \\ 0 \end{bmatrix}, \begin{bmatrix} 0 \\ 1 \\ 0 \\ 1 \end{bmatrix}, \begin{bmatrix} 1 \\ -1 \\ -1 \\ 1 \end{bmatrix} \right\}. \tag{4.9}$$

The first two vectors in the tangent space corresponds to the geodesic translation and the third vector corresponds to the rotation of the line segment in the plane. So between two points on $\mathcal{M}$ the distance metric is computed based on the geodesic curve segment connecting these two points. It turns out that in this case the geodesic curves are just made up of translations and rotations. We can in fact show an isomorphism between the basis of $se(2)$ denoted by $\{T_x, T_y, R\}$ and $\nabla F^{\perp}$, where $T_x, T_y$ represents operators corresponding to the translation in $\mathbb{R}^2$ and $R$ is the rotation matrix

operating on the objects of $\mathbb{R}^2$.

Here we have followed the formulation given in [44] for computing the $\exp_p$ map. It is formed in terms of an Initial Value Problem. The Figures 4.8,4.9 and 4.10 show the geodesics emanating from different tangent vectors.

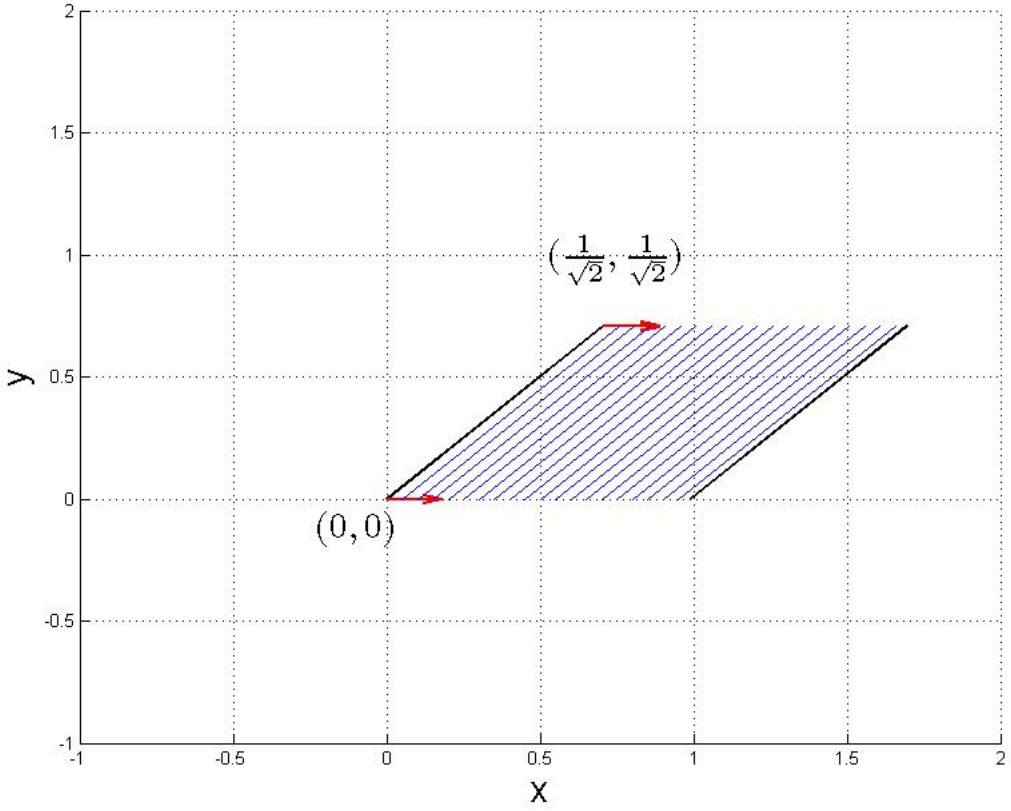


Figure 4.8: $\exp_p$ map in the direction of $[1\ 0\ 1\ 0]^T$

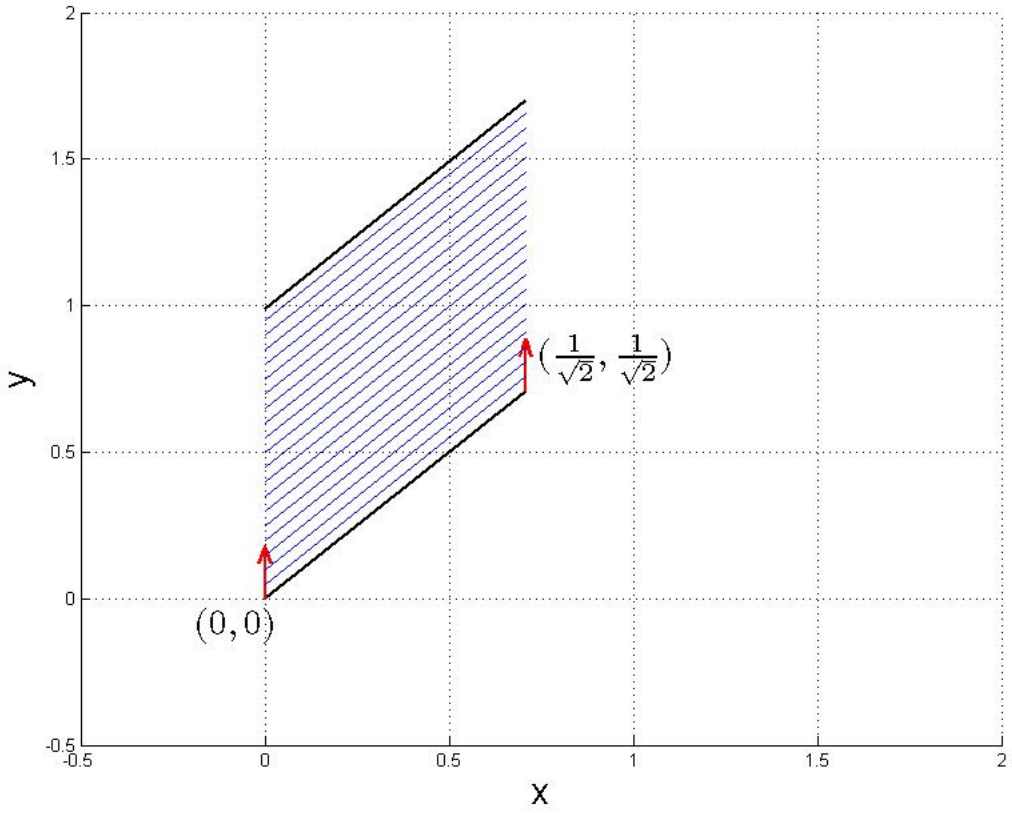


Figure 4.9: $\exp_p$ map in the direction of $[0\ 1\ 0\ 1]^T$

## 4.5 Euclidean Motion Groups

Consider an object in plane undergoing a rigid body euclidean motion. This motion can be decomposed into a rotation with respect to the center of mass of the object and a translation of the center of mass of the object. All possible configurations of an object in plane can be represented by $(\theta, u, v)$ (i.e. orientation of the principle axis and the co-ordinates of the center of mass of the object), where $0 \leq \theta \leq 2\pi$ and $(u, v) \in \mathbb{R}^2$. Let all such configurations form a set $\mathbb{S}$. It is rather intuitive to define a metric on $\mathbb{S}$ so as to compare two configurations of an object. If $A_1 = (\theta_1, u_1, v_1)$ and $A_2 = (\theta_2, u_2, v_2)$ be two configurations in $\mathbb{S}$ then it is easy to verify that

$$d(A_1, A_2) := \sqrt{a(\theta_1 - \theta_2)^2 + b(u_1 - u_2)^2 + b(v_1 - v_2)^2} \tag{4.10}$$

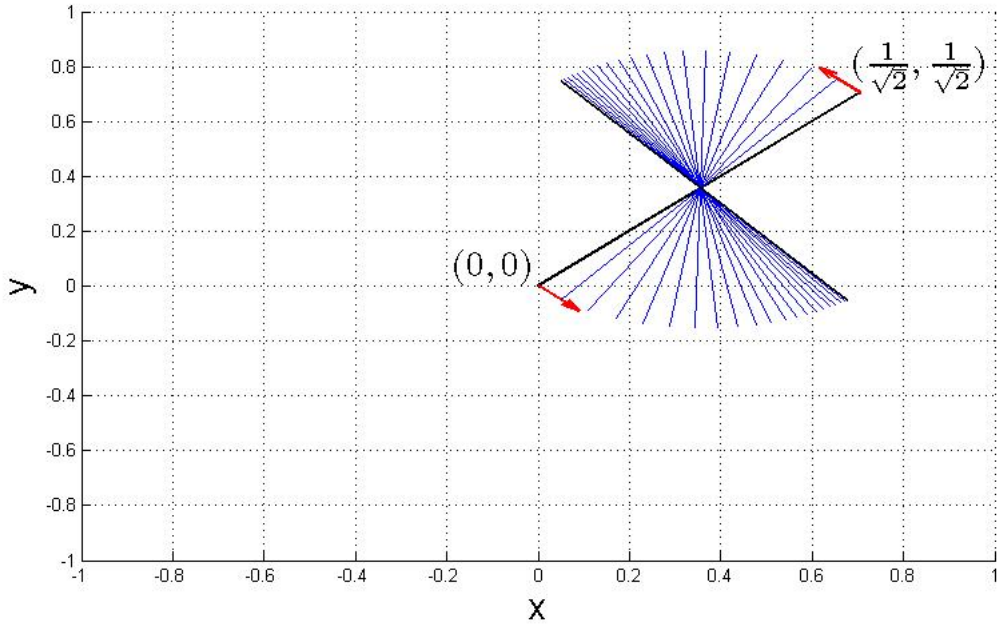


Figure 4.10: $\exp_p$ map in the direction of $[1\ -1\ -1\ 1]^T$

is a valid metric on $\mathbb{S}$ corresponding to the Riemannian inner product $\langle A_1, A_2 \rangle_R = A_1^T R A_2$, and $R = \begin{bmatrix} a & 0 \\ 0 & bI_2 \end{bmatrix}$ a positive definite matrix. Moreover for given $A_1, A_2$, left composition with $A \in \mathbb{S}$, i.e $A(A_1) = (\theta + \theta_1, u + u_1, v + v_1)$, the above defined metric leads to $d(A_1, A_2) = d(A(A_1), A(A_2))$. Hence we have a left invariant metric defined on $\mathbb{S}$. Physical interpretation of the left invariance is the freedom in choice of the inertial reference frame. The matrix representation of $\mathbb{S}$, the euclidean motion group, is denoted by $SE(2)$. A typical element of $SE(2)$ is made up of a rotation matrix and a translational vector. Correspondence between $\mathbb{S}$ and $SE(2)$ is given by

$$(\theta, u, v) \Leftrightarrow \begin{bmatrix} \cos\theta & \sin\theta & u \\ -\sin\theta & \cos\theta & v \\ 0 & 0 & 1 \end{bmatrix}$$

A typical curve between two configurations in $SE(2)$ and the geodesic segment from $A_1$ to $A_2$ are show in Fig.4.11.

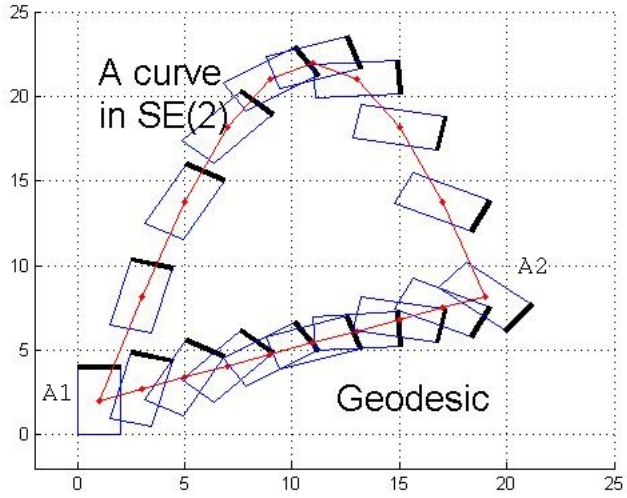


Figure 4.11: Comparison of a curve and a geodesic in $SE(2)$ between two configurations $A_1$ and $A_2$.

$SE(2)$ is exploited in the domain of image processing for segmentation in object tracking where one is interested in constrained evolution of the curve under the action of $SE(2)$, a Lie group. In general the group of rigid body motions in $\mathbb{R}^n$ is the semi-direct product [38] of the special orthogonal group with $\mathbb{R}^n$ itself.

$$SE(n) = SO(n) \ltimes \mathbb{R}^n$$

Unlike $\mathbb{R}^2$, rotations in $\mathbb{R}^3$ are not commutative, and that reflects in the group composition of $SO(3)$, $R_1R_2 \neq R_2R_1$, $R_1, R_2 \in SO(3)$. The product of two rigid body motions $(R_1, d_1), (R_2, d_2) \in SE(3)$ is given by $(R_2, d_2)(R_1, d_1) = (R_2R_1, R_2d_1 + d_2)$. Elements of $SE(3)$ are represented in matrix form as:

$$SE(3) = \{A|A = \begin{bmatrix} R & d \\ 0 & 1 \end{bmatrix}, R \in SO(3), d \in \mathbb{R}^3\} \tag{4.11}$$

The tangent space at the group identity in $SO(3)$ and $SE(3)$ are the Lie algebras $so(3)$ and

$se(3)$ respectively.

$$so(3) = \{[\omega] | [\omega] \in \mathbb{R}^{3\times 3}, [\omega]^T = -[\omega]\}, \tag{4.12}$$

$$se(3) = \{S = \begin{bmatrix} [\omega] & v \\ 0 & 0 \end{bmatrix}, [\omega] \in so(3), v \in \mathbb{R}^3\} \tag{4.13}$$

In the above $[\omega]$ is a skew symmetric matrix [22] corresponding to the vector $\omega = [\omega_x, \omega_y, \omega_z] \in \mathbb{R}^3$. The $||\omega||_2$ gives the amount of rotation with respect to the unit vector along $\omega$. The exponential map is a diffeomorphism [52] connecting the lie algebra to the lie group. The $\exp : se(3) \to SE(3)$ is given by the usual matrix exponential as $\exp(S) = \sum_{n=0}^{\infty} \frac{S^n}{n!}$.

Consider a rigid body moving in free space. We fix any inertial reference frame $\{B\}$ at $o$ and a frame $\{E\}$ to the body at some point $o'$ of the body as shown in Fig.4.12. At each instance the configuration of the rigid body is described via a transformation matrix, $A \in SE(3)$, corresponding to the displacement from frame $\{B\}$ to frame $\{E\}$.

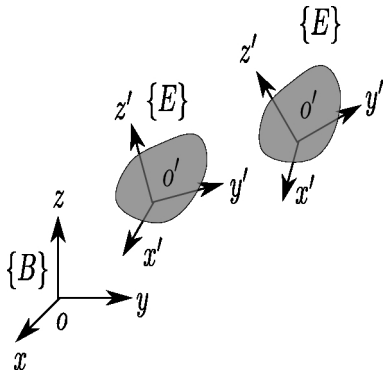


Figure 4.12: Inertial frame $\{B\}$ and body fixed frames $\{E\}$

So a rigid body motion becomes a curve in $SE(3)$, let $A(t)$ be such a curve given by $A(t) : [-c, c] \to SE(3), A(t) = \begin{bmatrix} R(t) & d(t) \\ 0 & 1 \end{bmatrix}$. The Lie algebra element $S(t) \in se(3)$ can be identified

with the tangent vector $A'(t)$ at an arbitrary t by:

$$S(t) = A^{-1}(t)A'(t) = \begin{bmatrix} [\omega](t) & v(t) \\ 0 & 0 \end{bmatrix} \tag{4.14}$$

The $\omega$ physically corresponds to the angular velocity of the body, while $v$ is the linear velocity of the origin $O'$. Let us assign a Riemannian metric $g = \begin{bmatrix} \alpha I_3 & 0 \\ 0 & \beta I_3 \end{bmatrix}$ over $SE(3)$ as prescribed in [33]. And so for $V = (\omega, v) \in se(3)$, $\langle V, V \rangle_g = \alpha\omega^T\omega + \beta v^T V$. It was proved in [52] that the analytic expression for the geodesic between two configurations $A_1$ and $A_2$ in $SE(3)$, with $g$ as Riemannian metric, is given by;

$$R(t) = R_1 \exp([\omega_0]t) \tag{4.15}$$

$$d(t) = (d_2 - d_1)t + d_1 \tag{4.16}$$

where $[\omega_0] = log(R_1^T R_2)$ and $t \in [0, 1]$. The path is unique for $Trace(R_1^T R_2) \neq -1$. The distance between two configuration in $SE(3)$ is given by

$$d(A_1, A_2) = \sqrt{\alpha \| \log(R_1^{-1} R_2) \|^2 + \beta \| d_2 - d_1 \|^2}. \tag{4.17}$$

All the formulas required for computing $\exp$ and $\log$ maps are given in the Appendix C for completeness.

**Example 4.5.** *Consider two configurations $A_1$ and $A_2$, as shown in Fig.4.13, given by vectors $(\omega_1, v_1)$ and $(\omega_2, v_2)$ respectively, where $\omega_1 = \frac{\pi}{4}\begin{bmatrix} 1 & 0 & 0 \end{bmatrix}$, $v_1 = \begin{bmatrix} -6 & 0 & 0 \end{bmatrix}$, $\omega_2 = \frac{\pi}{2}\begin{bmatrix} 1 & 1 & 0 \end{bmatrix}$ and $v_2 = \begin{bmatrix} 0 & 6 & 2 \end{bmatrix}$.*

$SE(3)$ is used extensively in robotics for path planning and motion planning of robots. It is also useful in computer vision and graphics.

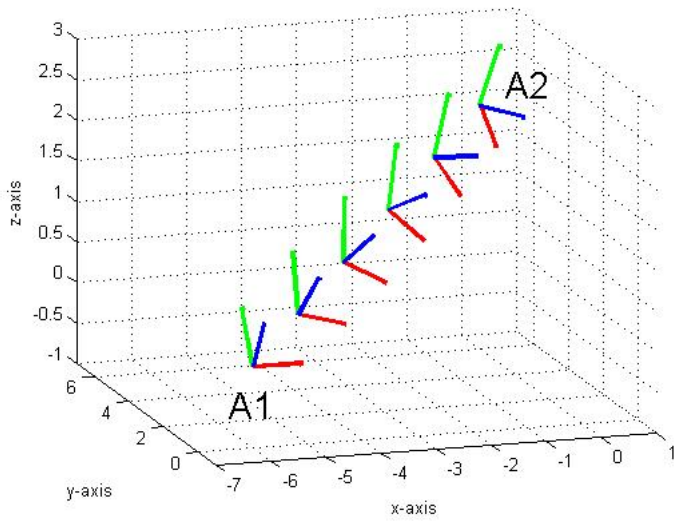


Figure 4.13: A geodesic between $A_1, A_2 \in SE(3)$.

## 4.6 $SE(2)$ with Scaling

Suppose for a planar object in motion, we include scaling with respect to the center of mass along with rotation and translation. The resultant element will be of the following form

$$A = \begin{bmatrix} e^{\lambda}R & d \\ 0 & 1 \end{bmatrix}. \tag{4.18}$$

This element operates individually on each point of the object in plane. It scales (by the factor $e^{\lambda}$) and rotates ($R \in SO(3)$) the object with respect to its center of mass and then translates (by vector $d \in \mathbb{R}^3$) the center of mass. With each such element we can associate a vector $[\lambda, \theta, d_x, d_y]$. The elements of the form given by (4.18) with standard matrix multiplication form a Lie group. We can extend the notions of tangent space and exponential map to this Lie group. This group is a semi-direct product of elements of scaled rotations and translations. The tangent space elements at

identity, Lie algebra elements, for scaled rotations are given by

$$[a] = \lambda \begin{bmatrix} 1 & 0 \\ 0 & 1 \end{bmatrix} + \theta \begin{bmatrix} 0 & -1 \\ 1 & 0 \end{bmatrix} \tag{4.19}$$

The usual matrix exponentiation gives

$$\exp[a] = e^{\lambda} \begin{bmatrix} \cos\theta & -\sin\theta \\ \sin\theta & \cos\theta \end{bmatrix}. \tag{4.20}$$

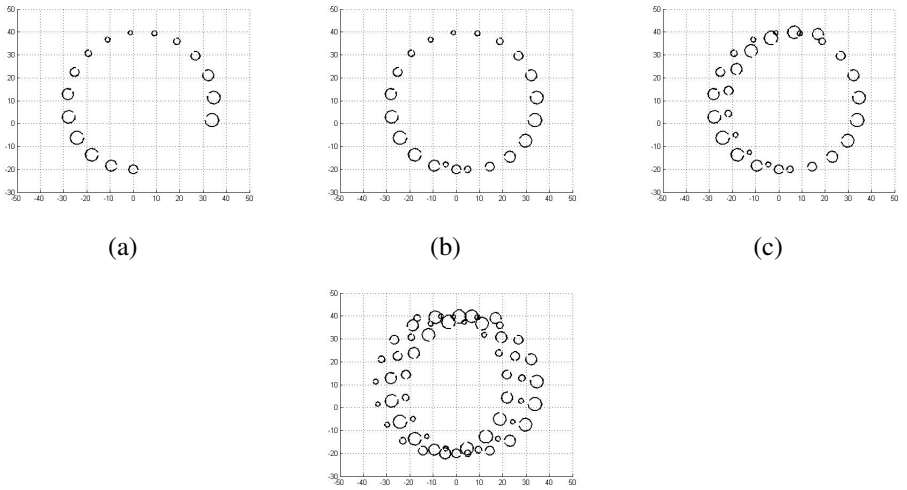

(a) (b) (c)

(d)

Figure 4.14: Various instances of a curve in $SE(2)$ with scaling.

We can construct a left-invariant Riemannian metric on this group. It can be shown that for two elements $A_1, A_2$ in this group

$$d(A_1, A_2) = \sqrt{\alpha((\lambda_1 - \lambda_2)^2 + (\theta_1 - \theta_2)^2) + \beta \parallel d_1 - d_2 \parallel} \tag{4.21}$$

is a valid distance metric. In Figure 4.14, a circular object under the action of this group is shown for various time steps.

Once the Riemannian metric is identified we can construct a distance metric on the manifold. With the distance metric $d(\cdot, \cdot)$ (corresponding to the geodesic path) defined on the Riemannian manifold we are now ready to talk about the medial axis and the sampling criterion for a curve on the manifold.

# Chapter 5

# Medial Axis, Dense Sample and Flatness

## 5.1 Medial Axis Based Sampling

We commence by revisiting the definition of the medial axis stated previously. Let $\mathcal{M}$ be a Riemannian manifold and $d(\cdot,\cdot) : \mathcal{M} \times \mathcal{M} \to \mathbb{R}$ be the corresponding distance metric.

**Definition 5.1.** The medial axis $M$ of a curve $\mathcal{C} \subset \mathcal{M}$, is the closure of the set of points in $\mathcal{M}$ that have at least two closest points in $\mathcal{C}$.

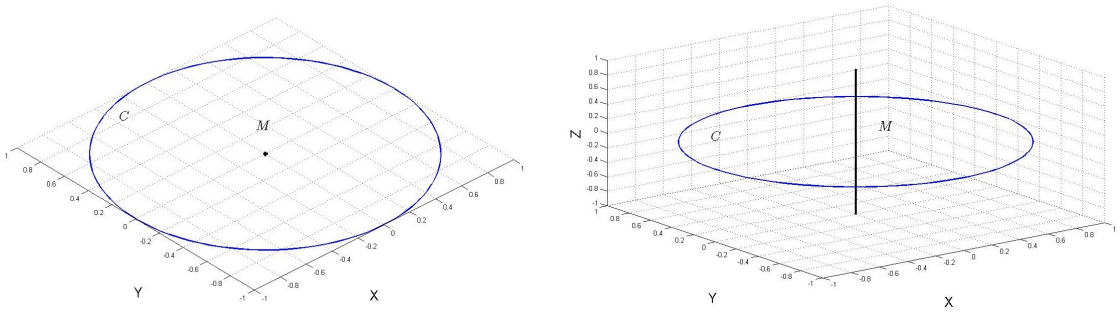


(a) (b)

Figure 5.1: Medial axis of a circle in plane and in $\mathbb{R}^3$

In Figure 5.1, medial axis ($M$) of a circle ($\mathcal{C}$) is presented here as an example. In general the medial axis depends upon the curve as well as the space in which the curve is embedded. Further

in Figure 5.2 we show examples of medial axis of closed curves on a half cylinder and in a plane.

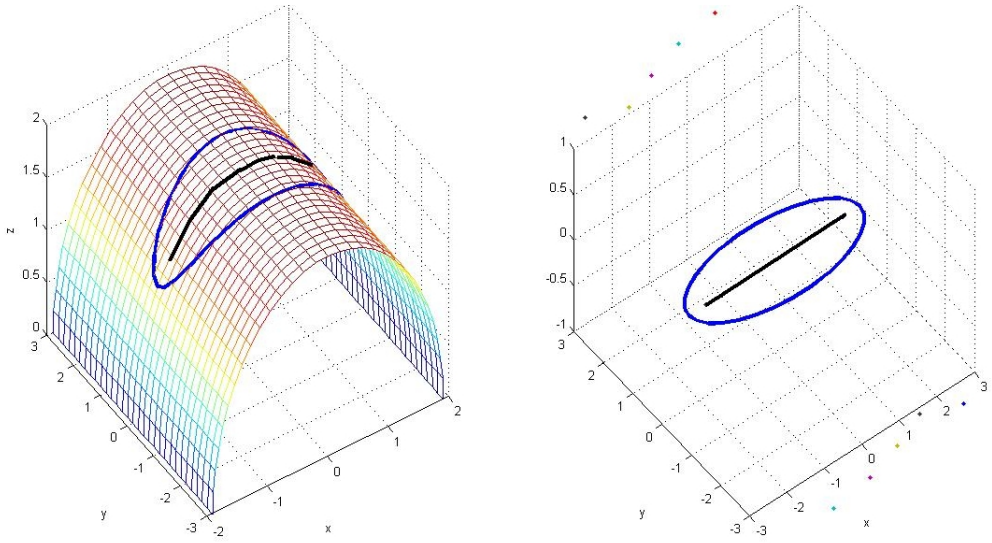


Figure 5.2: Medial axis of a curve on a surface and a curve in a plane

It should be noted that the medial axis, as defined above, is a subset of the underlying manifold in which the curve lies. Note that a curve embedded in a Riemannian manifold in $\mathbb{R}^3$ will have a different medial axis from its medial axis in $\mathbb{R}^3$. The open disc (ball) of radius $\varepsilon > 0$ in $\mathcal{M}$ with $s \in \mathcal{M}$ as a center is defined as $S_\varepsilon(s) = \{x \in \mathcal{M} | d(s,x) < \varepsilon\}$. In the same manner $B_\varepsilon(s) = \{x \in \mathcal{M} | d(s,x) \leq \varepsilon\}$ is a closed disc (ball) in $\mathcal{M}$ with radius $\varepsilon$ and the center $s$. The set $\partial B_\varepsilon(s) = \{x \in \mathcal{M} | d(x,s) = \varepsilon\}$ is the boundary of $B_\varepsilon(s)$.

**Definition 5.2.** At a point $p$ on the curve $\mathcal{C}$ the local feature size $f(p) = d(p, M)$, where $d(p, M) = \inf\{d(p,m), \forall m \in M\}$.

The local feature size at a point on the curve captures the behavior of the curve in the neighborhood of that point. In practice it is difficult to identify the medial axis for arbitrary curves. Looking at the construction of the *voronoi* diagram [32] for a given sample of points on a curve, the voronoi vertices do capture the behavior of the medial axis of the sampled curve. So for a densely sampled curve the voronoi vertices of such a sample are taken to be an approximation for the medial axis of

the given curve. It is computationally challenging to construct voronoi diagrams on curved spaces [27].

## 5.2 Tubular Neighbourhood

A tubular neighborhood of a curve in a plane is defined as a subset of the plane such that every point of the subset belongs to exactly one line segment totally contained in the subset and normal to the curve. A disk centered on the curve contained in a tubular neighborhood of the curve is called a tubular disk. Let us generalize this definition to curves in manifolds. We will also define the notion of a dense sample of a curve in a manifold using the concept of tubular neighborhood.

**Definition 5.3.** Let $\mathcal{C} \subset \mathcal{M}$ be a smooth curve. Consider segments of geodesics that are normal to $\mathcal{C}$ and start from points on $\mathcal{C}$. If $\mathcal{C}$ is compact, then there exists an $\varepsilon > 0$ such that no two segments of length $\varepsilon$ and starting at different points of $\mathcal{C}$ intersect [42]. The union of all such segments of length $\varepsilon$ is an open neighborhood $T$ of $\mathcal{C}$, and is called a tubular neighborhood of $\mathcal{C}$.

We denote the open segment with center $p \in \mathcal{C}$ and radius $\varepsilon$ in the normal geodesic segment of $\mathcal{C}$ at $p$ by $N_\varepsilon(p)$. Revisiting the definition of the tubular neighbourhood: the union $N_\varepsilon(\mathcal{C}) = \cup_{p\in\mathcal{C}} N_\varepsilon(p)$ is called a tubular neighbourhood of radius $\varepsilon$ if it is open as a subset of $\mathcal{M}$ and the map $F : \mathcal{C} \times (-\varepsilon, \varepsilon) \to N_\varepsilon(\mathcal{C})$ is a diffeomorphism. Let $\mathcal{C} \subset \mathbb{R}^2$, be a simple closed smooth curve. Existence of the tubular neighbourhood is evident from the compactness of the curve in $\mathbb{R}^2$. We show something more about the value of $\varepsilon$ in next proposition.

**Proposition 5.4.** *If $N_\varepsilon(\mathcal{C})$ is a tubular neighbourhood of $\mathcal{C}$, then $\varepsilon < \frac{1}{k}$, where $k = \max\{k(p), p \in \mathcal{C}\}$ and $k(p)$ is the curvature of the curve at point $p$.*

*Proof.* Let us define a curve $\alpha(s)$ in $\mathbb{R}^2$ by

$$\alpha(s) = F(\mathcal{C}(s), t) = \mathcal{C}(s) + tN(\mathcal{C}(s)),$$

for a fixed $t \in (-\varepsilon, \varepsilon)$ such that $\alpha(0) = p$. $N(p)$ is the unit normal to the curve $\mathcal{C}$ at $p$. This new curve belongs to the open set $N_\varepsilon(\mathcal{C})$ and

$$\alpha(0) = p + tN(p) \tag{5.1}$$

$$\alpha'(0) = \mathcal{C}'(0) + tN'(0) \tag{5.2}$$

$$\alpha'(0) = (1 - tk(p))\mathcal{C}'(0) \ = \ (dF)_{(p,t)}(\mathcal{C}'(0)) \tag{5.3}$$

Since $F : \mathcal{C} \times (-\varepsilon, \varepsilon) \to \mathbb{R}^2$ is a diffeomorphism when restricted to $\mathcal{C} \times (-\varepsilon, \varepsilon)$, we have that $(dF)_{(p,t)}(\mathcal{C}'(0))$ is a non-null vector, i.e. $1-tk(p) \neq 0$. Since $(-\varepsilon, \varepsilon)$ is connected and $1-tk(p) > 0$ for $t = 0$, so $1 - tk(p) > 0$ on $\mathcal{C} \times (-\varepsilon, \varepsilon)$. Now if $k = \max k(p), p \in \mathcal{C}$ then $1 - tk > 0$. And we have $\varepsilon = t < \frac{1}{k}$. □

**Definition 5.5.** A finite sample set $\mathcal{S} \subset \mathcal{C}$ is called a *uniform $\varepsilon-$sample* if for a given $\varepsilon > 0$ any two consecutive sample points $r, s \in \mathcal{S}$, $r \in B_\varepsilon(s)$.

**Definition 5.6.** A uniform $\varepsilon$-sample $\mathcal{S}$ of a curve $\mathcal{C} \subset \mathcal{M}$ is dense if there is a real number $\varepsilon > 0$ such that $\cup_{s\in\mathcal{S}} B_\varepsilon(s)$,i.e. the union of the open disks of radius $\varepsilon$ centered at the sample points $s \in \mathcal{S}$, forms a tubular neighborhood of $C$.

**Proposition 5.7.** *For plane curves if $\varepsilon < \min_{p\in\mathcal{C}} f(p)$ then a uniform $\varepsilon$-sample $\mathcal{S}$ of curve $\mathcal{C}$ is a dense sample.*

*Proof.* By the definition of $f(p),\ p \in \mathcal{C}$, for a smooth curve $\mathcal{C}$, $f(.)$ attains maximum value at the points where the curvature of $\mathcal{C}$ is maximum. For $\varepsilon < \min_{p\in\mathcal{C}} f(p)$, let the uniform $\varepsilon$- sample be $\mathcal{S} \subset \mathcal{C}$. From proposition 5.4, we see that $\cup_{s\in\mathcal{S}} B_\varepsilon(s)$ covers the curve $\mathcal{C}$ and is a tubular neighborhood of $\mathcal{C}$. So, $\mathcal{S}$ is dense. □

Before we proceed to the main theorem, we will make a few observations in the next section. We show by an example how the medial axis based sampling fails due to the curvature of the

underlying Riemannian manifold. We also show how to work within the injectivity radius of the manifold to avoid such a problem.

## 5.3 Observations and a Counter Example

The first two observations presented in this section are encouraging. With a counter example to the Least Feature Size based sampling we prescribe in this section a conservative sampling condition. We know that to form a dense sample of a curve in $\mathbb{R}^n$ it is required to sample with an $\varepsilon_1 < \min_{p \in \mathcal{C}} f(p)$. The curve and corresponding $\varepsilon_1$ are shown in Figure 5.3(a). However, if the same

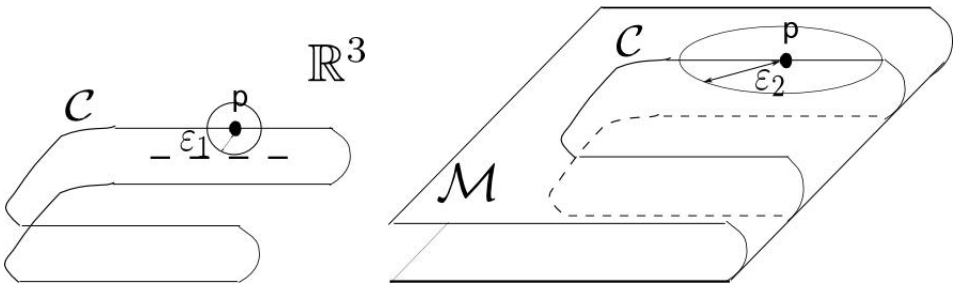


(a) (b)

Figure 5.3: (a) A curve $\mathcal{C} \in \mathbb{R}^3$ and the part of medial axis near $p \in \mathcal{C}$. $\varepsilon_1$ is the distance of the point $p \in \mathcal{C}$ from the medial axis of the curve in space. (b) The same curve $\mathcal{C}$ on a surface $\mathcal{M}$ and the medial axis distance $\varepsilon_2$ from the point $p \in \mathcal{C}$ to the medial axis of the curve on the surface.

curve is embedded in a surface, as shown in Figure 5.3(b), the required $\varepsilon_2$ needs to be evaluated on the surface. In this case it turns out that $\varepsilon_2 < \varepsilon_1$. Let us look at another example. A circle in the $xy$-plane in $\mathbb{R}^3$ can be thought of as some latitude on a sphere of radius $r \geq \frac{L}{2\pi}$, where $L$ is the length of the circle. For these two cases, i.e. the circle on a plane and the circle on a sphere, the sampling required for correct reconstruction is different. On the sphere we need a less dense sample set as compared to on the plane. In fact, as we increase the radius $r$ we need denser and denser sample set for correct reconstruction and the limiting case, $r \to \infty$, is the plane. In $\mathbb{R}^3$, the usual euclidean metric is carried over to the points of the circle. In the case of the sphere, the shortest path between two points is always along the great circle passing through these two points and the

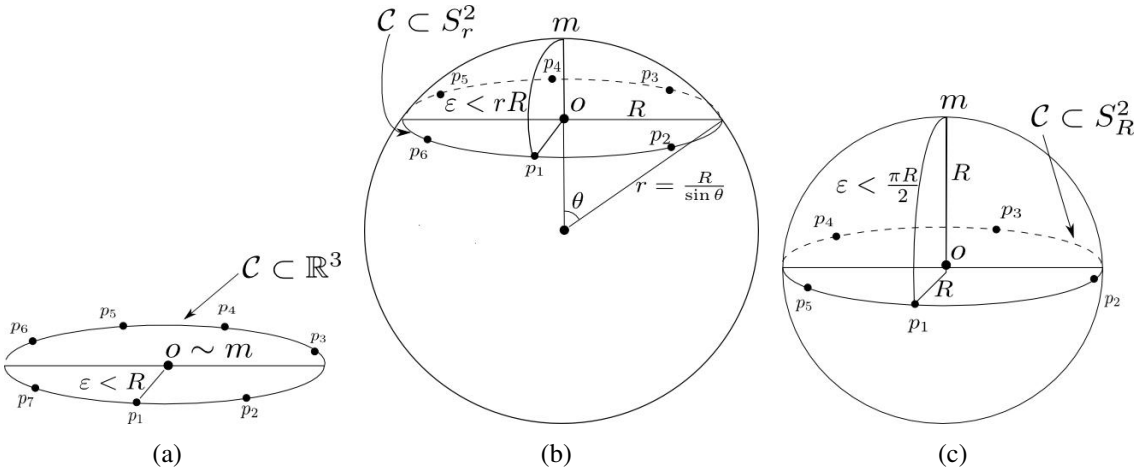


Figure 5.4: (a) Circle with radius R is lying in space (b) Circle resting on a sphere of radius $r = \frac{R}{\sin\theta}$ (c) Circle is the great circle the sphere of radius $R$

length of the shorter of the two segment which is the distance between two points on the sphere. With this distance metric defined, the sphere becomes a metric space, distance between any two points of the circle on the sphere are obtained via this metric. The points of this circle on a sphere are more structured then the points of the same circle in space. The additional knowledge of the underlying surface strengthens the ordering relation between points of the circle. Since we know the surface we know the tangent space and that reduces the efforts required to order the sample points. Interestingly, when generalized to curves on manifolds, the sampling criterion based only on the medial axis becomes meaningless. As an example let us look at a unit circle on the surface shown in Figure 5.5. The medial axis of the circle on the given surface is the point $M = (0, 0, 0)$. For any point on the circle, the distance from the medial axis turns out to be larger than the length of the circle itself. In the limiting case of this surface, i.e. a cylinder, the medial axis is empty.

The above phenomenon can be understood more clearly if we look at the cut locus of the point $p \in \mathcal{M}$. The following can be considered as the defining property of the cut locus of a point on the manifold. If $\gamma(t_0)$ is the cut point of $p = \gamma(0)$ along the geodesic arc $\gamma$ then either $\gamma(t_0)$ is the first conjugate point of $\gamma(0)$ or there exists a geodesic $\sigma = \gamma$ from $p$ to $\gamma(t_0)$ such that $l(\sigma) = l(\gamma)$(lengths of $\sigma$ and $\gamma$ are equal).

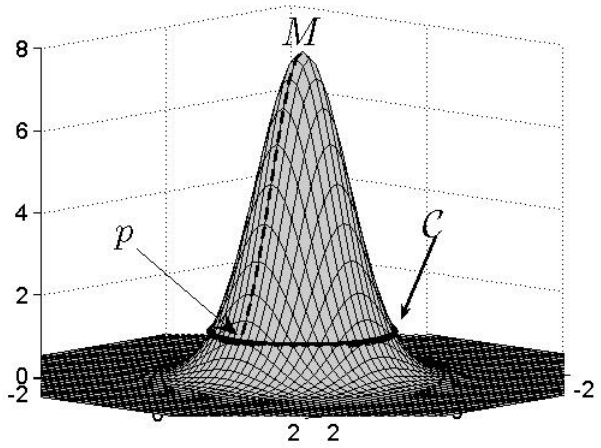


Figure 5.5: A circle $\mathcal{C}$ and the normal geodesic from a point $(1, 0, 1.0629)$ to $M$

For example, if $\mathcal{M}$ is a sphere $S^2$ and $p \in S^2$ then the cut locus of $p$ is its antipodal point. If we consider the sphere of radius $R$ the distance of point $p$ from its cut locus is $\pi R$, whereas the distance of the point $p$ on the circle in Figure 5.4(c) to the medial axis $M$ is $\frac{\pi R}{2}$. Now coming back to the counter example Figure 5.5, we observe that the distance from $p$ to its cut locus, $d(p, C_m(p))$, is less then the distance to the medial axis $M$ of the circle, where $C_m(p)$ is the cut locus of $p \in \mathcal{M}$.

It can be shown that if $q \in \mathcal{M} - C_m(p)$, there exists a unique minimizing geodesic joining $p$ and $q$. In [17]

$$i(\mathcal{M}) = \inf_{p \in \mathcal{M}} d(p, C_m(p)) \tag{5.4}$$

is called the injectivity radius of $\mathcal{M}$. So if $\varepsilon < i(\mathcal{M})$ then $\exp_p$ is injective on the open ball $S_\varepsilon(p)$.

A tubular neighborhood for a curve is constructed by taking only the normal geodesics to the curve at a point and assuring the injectivity of the $exp_p$ map along these normal directions. We now propose to work inside the injectivity radius to straighten out the problem with sampling.

**Proposition 5.8.** *Let $\mathcal{C} \in \mathcal{M}$ be a smooth, simple and closed curve. If $\mathcal{S}$ is a uniform $\varepsilon$- sample of $\mathcal{C}$, then $\mathcal{S}$ is dense for $\varepsilon < \min\{\inf_{p \in \mathcal{C}} f(p), i(\mathcal{M})\}$.*

*Proof.* Let $\mathcal{S}$ be a uniform $\varepsilon$- sample of $\mathcal{C}$ with $\varepsilon < \min\{\inf_{p \in \mathcal{C}} f(p), i(\mathcal{M})\}$. From the definitions

of the injectivity radius and the feature size we know that for the above mentioned $\varepsilon$, $\exp_p$ is injective on $S_\varepsilon(p)$. So, $\cup_{s\in\mathcal{S}} B_\varepsilon(s)$ forms a tubular neighborhood of $\mathcal{C}$, and hence $\mathcal{S}$ is dense. □

## 5.4 Uniform Sampling

### 5.4.1 Flatness of a Curve Segment Inside a Tubular Neighbourhood

If the underlying manifold is a plane and a curve is sampled densely then based on the tubular neighborhood, it is proven, in [13], that the Euclidean minimal spanning tree reconstructs the sampled arc. The crucial ingredient in the proof is the denseness of the sample. It comes from the observation that an arc does not wander too much inside a tubular disk, thus avoiding the possibility of connecting non-consecutive sample points in $\mathcal{S}$ (such connections are called short chords).

We now give an alternate proof of flatness* of the curve segment inside a tubular neighborhood in plane. And after that we extend the proof to curves in the Riemannian manifold.

**Theorem 5.9.** *Let $p$ and $q$ be two points on an arc $\mathcal{C} \subset \mathbb{R}^2$ such that $q$ is inside the tubular disk $B_\varepsilon(p)$ centered at $p$. Then the sub arc $pq$ of $\mathcal{C}$ is completely inside $B_{pq/2}(c)$, where $c$ is the mid-point of diameter $pq$.*

*Proof.* Since $q \in B_\varepsilon(p)$, $pq = d(p,q) \leq \varepsilon$. Now pq being a segment of an arc $\mathcal{C}$ there are three possible ways, as shown in Figure 5.6, in which it intersects with $B_{pq/2}(c)$.

For the possibility shown in Figure 5.6(a), it is evident that center $c$ lies on two normals passing through $p$ and $q$, i.e. $c \in \overline{pq}$, since $B_{pq/2}(c)$ and $\mathcal{C}$ share common tangents at $p$ and $q$. This can not happen since $B_{pq/2}(c) \subset B_\varepsilon(p)$, a subset of a tubular neighborhood.

Let us consider the case in Figure 5.6(b), arc $\mathcal{C}$ touches $B_{pq/2}(c)$ at $p$ and intersects the boundary of $B_{pq/2}(c)$ at $q$ and $q'$. We can find out a point $q''$ on the segment $qq'$ which is nearest to $c$. At $q''$

*The word flatness here indicates that the geodesic curvature at points of the curve segment inside a tubular neighborhood is bounded above and is certainly very small.

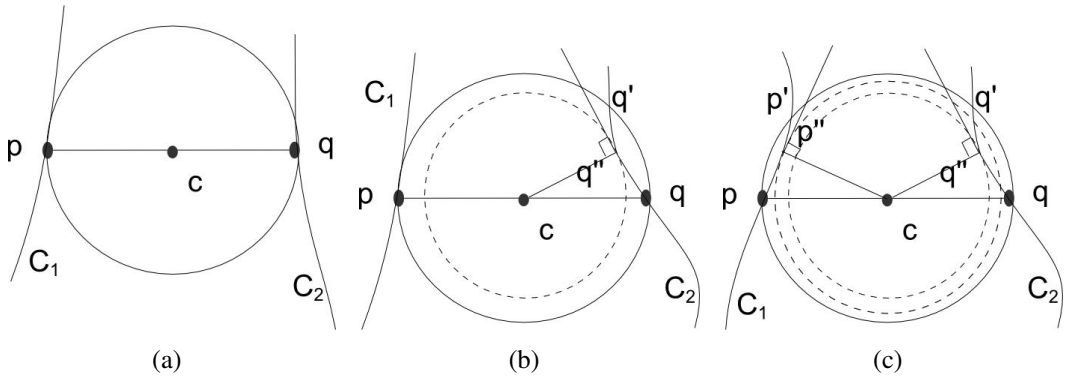


Figure 5.6: (a) The arc touches $B_{pq/2}(c)$ (b) The arc touches $B_{pq/2}(c)$ at $p$ and intersects its boundary at $q'$ while passing through $q$ (c) The arc intersects boundary of $B_{pq/2}(c)$ at $p'$ and $q'$ while passing through $p$ and $q$ respectively

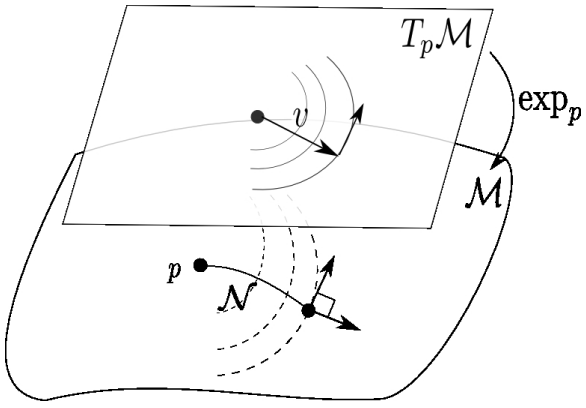


Figure 5.7: Tangent space of a point $p \in \mathcal{M}$ where $||v|| < \varepsilon$ and the corresponding geodesic $\mathcal{N}$.

the circle with center $c$ and radius $d(c, q'')$ shares a common tangent with $\mathcal{C}$. Hence $c$ lies on the two normals $\overline{pc}$ and $\overline{q''c}$. This can not happen inside a tubular neighborhood.

Finally we consider the Figure 5.6(c). On segments $pp'$ and $qq'$ we find $p''$ and $q''$ nearest to $c$. In this case $c$ lies on $\overline{p''c}$ and $\overline{q''c}$. Since $c$ is inside tubular neighborhood this can not happen.

So the only possibility we are left with is that the segment $pq$ of curve $\mathcal{C}$ lies entirely inside $B_{pq/2}(c)$. □

**Theorem 5.10.** *Let $p$ and $q$ be two points on an arc $\mathcal{C} \subset \mathcal{M}$, where $\mathcal{M}$ is any Riemannian manifold, such that $q$ is inside the tubular disk $B_\varepsilon(p)$ centered at $p$. Then the sub arc $pq$ of $\mathcal{C}$ is completely*

*inside $B_{pq/2}(c)$, where $c$ is the mid-point of diameter $pq$.*

*Proof.* For $\mathcal{M} := \mathbb{R}^n$ we know that $\overline{cp}$, $p \in S^{n-1}$, is orthogonal to $T_pS^{n-1}$.

Since we are working inside a tubular neighborhood of the curve $\mathcal{C}$, with $\varepsilon$ as prescribed in Proposition 5.8, $\exp : T_p\mathcal{M} \to \mathcal{M}$ is a diffeomorphism.

Gauss's lemma, in [17], asserts that the image of a sphere of sufficiently small radius($< \varepsilon$) $T_p\mathcal{M}$ under the exponential map is perpendicular to all geodesics originating at $p$ Figure 5.7.

The rest of the proof follows from arguments of the Theorem 5.9. □

# Chapter 6

# Curve Reconstruction in Riemannian Manifolds

## 6.1 MST Reorders the Dense Sample Set

A sample $\mathcal{S}$ of a curve is represented as a set of vertices (vertex set $V$) of a graph and the edges (edge set $E$) indicate an order in which the vertices are to be connected. Since, there are varieties of ways in which vertices can be connected it is appropriate to consider the initial graph as a complete graph. If further we put the distance between two sample points as the edge cost, it becomes a weighted graph. A minimal spanning tree for a weighted graph is a spanning tree for which the sum of edge weights is minimal. To keep the notations consistent, we define the geodesic polygonal path on a Riemannian manifold as the path along which every vertex (sample point) pair is connected by a geodesic segment.

Computing the minimal spanning tree utilizes the following fundamental property: let $X \cup Y$ be a partition of the set of vertices of a connected weighted graph $G$. Then any shortest edge in $G$ connecting a vertex of $X$ and a vertex of $Y$ is an edge of a minimal spanning tree. If we use MST to model an arc, we must ensure that there are no short chords in the MST; this was proved in [13].

As before, we focus on closed, simple, smooth curves. In that case, the MST must have every vertex with degree two. In other words every sample point has exactly two neighbors (sample points) on the curve.

**Theorem 6.1.** *If $\mathcal{S}$ is a dense sample of $\mathcal{C} \subset \mathcal{M}$ then MST gives a correct re-ordering on $\mathcal{S}$ and hence a correct geodesic polygonal reconstruction of $\mathcal{C}$, where $\mathcal{C}$ is a smooth, closed and simple curve.*

*Proof.* We show that the geodesic polygonal path has no short chords. The argument is similar to the proof provided for the planar case in [13]. For the sake of completeness, we restate the argument here. Suppose that MST does not give a correct geodesic polygonal reconstruction of $\mathcal{S}$. It implies that there are two points in MST which are not consecutive. Let these points be $p, q \in \mathcal{S}$. Since $pq$ is a short chord there has to be at least one edge in the sub arc $pq$ which has length greater than that of $pq$. But since the sample $\mathcal{S}$ is dense, the arc $pq$ must be contained in the disc with diameter $pq$, refer to Theorem 5.10. Inside the disc there is no arc with length greater than the length of the diameter. So we have a contradiction. □

In the following section we discuss minimum spanning tree algorithm for its complexity and also look at the nearest-neighbor search.

### 6.1.1 Minimum Spanning Tree

Let $G = (V, E)$ be an undirected graph with edge weights $\omega_e$. A tree $T = (V, E')$, with $E' \subset E$ that minimizes

$$\omega(T) = \sum_{e \in E'} \omega_e \tag{6.1}$$

is called a minimum spanning tree. Minimum spanning tree is a classic example of a greedy algorithm. For basic terminologies and details we refer readers to [12]. The intermediate MST is

grown by adding an edge at a time. This is done keeping in mind the following property. First we need some definitions. A *cut* $(S, V - S)$ of an undirected graph $G$ is a partition of $V$. We say that an edge $e \in E$ crosses the cut if one of its endpoints is in $S$ and the other is in $V - S$. We say that a cut *respects* a set $A$ of edges if no edge in $A$ crosses the cut. An edge is a *light edge* crossing a cut if its weight is the minimum of any edge crossing the cut.

[Cut Property] Let $A$ be a subset of $E$ that is included in some minimum spanning tree for $G$, let $(S, V - S)$ be any cut of $G$ that respects $A$, and let $e$ be a light edge crossing $(S, V - S)$. Then, edge $e \in E$ can be added to $A$ to grow the MST.

Prim's algorithm operates much like Dijkstra's algorithm for finding shortest paths in a graph. Prim's algorithm has the property that the edges in the set $A$ always form a single tree. The tree starts from an arbitrary vertex and grows until the tree spans all the vertices in $V$. At each step, a light edge is added to the tree $A$ that connects $A$ to an isolate vertex of $G_A = (V, A)$. This rule adds edges that are safe for $A$. Considering the cases where curve can have more than one connected components, algorithm must provide a *forest* (a collection of trees). Kruskal's algorithm is a greedy algorithm and gives us (a forest) MST. Both the algorithms have the same computational complexity, i.e $O(|E| \log |V|)$. For details on calculation of complexities and pseudocodes refer to [11].

For arcs (open curve segments), a nearest neighbor search algorithm that is similar to Prim's algorithm is used to find the correct ordering. In this case we provide the starting vertex as one of the end points as input to the Prim's algorithm. We have used this approach to order samples of smooth arcs.

## 6.2 Interpolation in Riemannian Manifolds

Once we have ordered the given set of points of the curve on a curved manifold the next step is to interpolate this point set to the desirable granularity. The easiest way to interpolate the points

is to connect the points via straight line segments, a linear interpolation. In general for a manifold like $SE(3)$, the geodesics are the $\exp$ segments. But this scheme will not produce a differentiable curve which might be necessary for some applications. Based on the need and application one may chose the interpolation scheme. In [41] and [23] a quaternion based approach is suggested, which is very useful in computer graphics and animation. Since we have represented $SE(3)$ using matrices, we prefer a matrix based approach. Motivated by motion planning purposes various interpolation schemes based on variational minimization techniques have been proposed and some of them turn out to be quite easily implementable. For a broad overview, see [34] and [28]. For completing the reconstruction process, we have used the *de Casteljau* construction as prescribed in [1]. It is a generalization of the multi linear interpolation on $SE(3)$, where a piecewise $C^2$ curve is used to connect two frames with given velocities. The advantage is that we have a closed form expression with exponential and log maps.

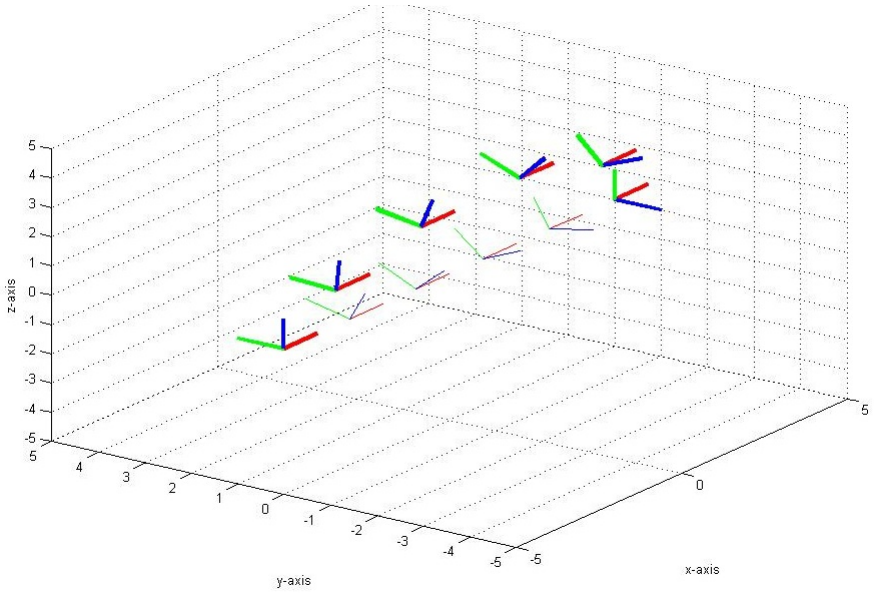


Figure 6.1: Comparison of Exponential map and $C^2$ smooth interpolation in $SE(3)$ between $g_0 = [0,0,0] \ltimes [-5,0,0]$ and $g_1 = [\pi/2,0,0] \ltimes [5,0,0]$, with tangents $v_0^1 = [0,0,0,3,1,1]$ and $v_2^1 = [\pi/2,0,0,-1,-3,-1]$.

Suppose we do not know the velocities at the node points. For such a case we have used a

partial geodesic scheme to interpolate between two elements of $SE(3)$, where the rotational part is interpolated by the $\exp$ map and the translational component is interpolated with spline segments.

In the next section we give the details of the interpolation scheme that we have used.

### 6.2.1 Cubic Spline Interpolation

To begin with, we describe the cubic spline interpolation algorithm used to interpolate between points in $\mathbb{R}^n$. In general, the data or control points determine a parametric curve segment $P(t)$, $t \in [0, 1]$, and curvature, tangent vectors and continuity constraints etc. are used to join the parametric curve segments to generate a complete parametric curve.

In practice, a complete curve is made up of segments. There are two types of curve continuities: geometric and parametric. If two consecutive segments meet at a point, the total curve is said to have $G^0$ geometric continuity. If, in addition, the directions of tangent vectors of the two segments are the same at the point, the curve has $G^1$ geometric continuity at the point. In general, a curve has geometric continuity $G^n$ at a join point if every pair of the first $n$ derivatives of the two segments have the same direction at the point. If the same derivatives also have identical magnitudes at the point, then the curve is said to have $C^n$ parametric continuity at the point.

The cubic spline method constructs a smooth curve passing through $n$ data points. This curve consists of $n-1$ individual Hermite segments that are smoothly connected at the interior data points, i.e. segments meeting at an interior point must have their tangent vectors and second derivatives same.

The parametric form of the Hermite segment is determined from two points $P_1$ and $P_2$ and two tangent vectors $P_1^t$ and $P_2^t$. It is a curve segment that starts at $P_1$, going in direction $P_1^t$ and ends at $P_2$ moving in direction $P_2^t$. Hermite segment is easy to derive. It is a parametric curve, a degree-3 polynomial in $t$, with four coefficients that depend on the two points and two segments.

$$P(t) = at^3 + bt^2 + ct + d = [t^3\ t^2\ t\ 1][a\ b\ c\ d]^T = T(t)A \tag{6.2}$$

This is an algebraic representation of the curve, in which the four coefficients can be expressed in terms of known geometric quantities (points and vectors). Let us find these unknowns from the known. The tangent vector to a curve $P(t)$ is the derivative $dP(t)/dt$, denoted by $P^t(t)$. The tangent vector is therefore

$$P^t(t) = 3at^2 + 2bt + c \tag{6.3}$$

Using the above two expressions and known geometric quantities we can easily derive the following:

$$\begin{aligned} P(t) &= (2t^3 - 3t^2 + 1)P_1 + (-2t^3 + 3t^2)P_2 + (t^3 - 2t^2 + t)P_1^t + (t^3 - t^2)P_2^t \\ &= F_1(t)P_1 + F_2(t)P_2 + F_3(t)P_1^t + F_4(t)P_2^t \\ &= F(t)B \end{aligned} \tag{6.4}$$

where

$$F_1(t) = (2t^3 - 3t^2 + 1), \;\; F_2(t) = (-2t^3 + 3t^2), \;\; F_3(t) = (t^3 - 2t^2 + t), \;\; F_4(t) = (t^3 - t^2), \tag{6.5}$$

$B$ is the column $[P_1 \; P_2 \; P_1^t \; P_2^t]^T$, and $F(t)$ is the row $[F_1(t) \; F_2(t) \; F_3(t) \; F_4(t)]$. Functions $F_i(t)$ are the Hermite blending functions. In matrix notation this becomes

$$F(t) = [t^3 \; t^2 \; t \; 1] \begin{bmatrix} 2 & -2 & 1 & 1 \\ -3 & 3 & -2 & -1 \\ 0 & 0 & 1 & 0 \\ 1 & 0 & 0 & 0 \end{bmatrix} = T(t)H. \tag{6.6}$$

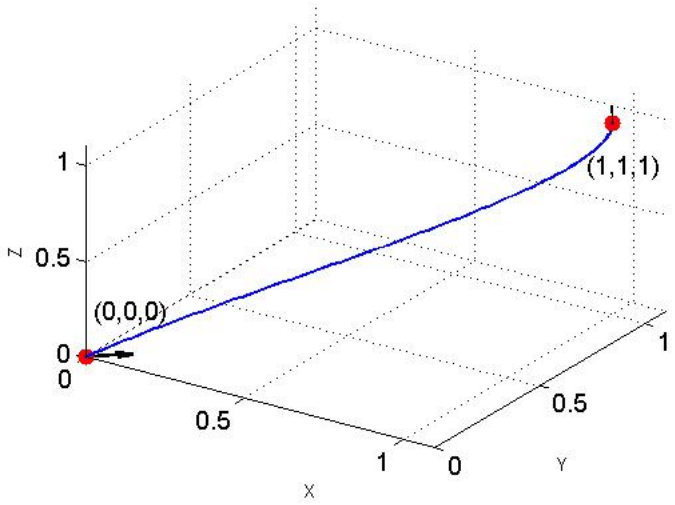


Figure 6.2: A parametric Hermite interpolated curve segment

The curve can now be written as

$$P(t) = T(t)HP = [t^3\ t^2\ t\ 1] \begin{bmatrix} 2 & -2 & 1 & 1 \\ -3 & 3 & -2 & -1 \\ 0 & 0 & 1 & 0 \\ 1 & 0 & 0 & 0 \end{bmatrix} \begin{bmatrix} P_1 \\ P_2 \\ P_1^t \\ P_2^t \end{bmatrix}. \tag{6.7}$$

Matrix $H$ in (6.7) is called the Hermite basis matrix. An example at this stage will help understand the role of tangent vectors at the points.

**Example 6.1.** *Let the two three dimensional points $P_1 = (0, 0, 0)$ and $P_2 = (1, 1, 1)$ and the two tangent vectors $P_1^t = (1, 1, 0)$ and $P_2^t = (0, 0, 1)$ be given. The curve segment turns out to be a cubic polynomial*

$$P(t) = (-t^3 + t^2 + t,\ -t^3 + t^2 + t,\ t). \tag{6.8}$$

*as shown in the Figure 6.2.*

Now, coming back to spline interpolation, let $P_1, P_2, \ldots, P_n$ be given $n$ points. We have $n - 1$

parametric cubics (Hermite segments) $P_1(t), P_2(t), \ldots, P_{n-1}(t)$, where $P_k(t)$ is the polynomial segment from point $P_k$ to $P_{k+1}$. These parametric curves are required to be smoothly connected at the $n-2$ interior points $P_2, P_3, \ldots, P_{n-1}$; this implies that their first derivatives must match at every interior point. Moreover, the definition of a spline requires that their second derivatives match too. So in essence if the user provides the tangent vectors at $P_1$ and $P_n$ we get a system of equations which we can solve and derive the spline interpolation in terms of Hermite segments $P_1(t), P_2(t), \ldots, P_{n-1}(t)$.

The unknown tangent vectors at the interior points are found from the following system of $n-2$ equations:

$$\begin{bmatrix} 1 & 4 & 1 & 0 & \ldots & 0 \\ 0 & 1 & 4 & 1 & \ldots & 0 \\ & & & \ddots & \ddots & \vdots \\ 0 & \ldots & \ldots & 1 & 4 & 1 \end{bmatrix}_{(n-2)\times n} \begin{bmatrix} P_1^t \\ P_2^t \\ \vdots \\ P_n^t \end{bmatrix}_{n\times 1} = \begin{bmatrix} 3(P_3 - P_1) \\ 3(P_4 - P_2) \\ \vdots \\ 3(P_n - P_{n-2}) \end{bmatrix}_{(n-2)\times 1} . \tag{6.9}$$

An advantage is that the user can vary the shape of the curve by entering new values for $P_1^t$ and $P_n^t$ and recalculating. This approach is called the *clamped* end conditions. It is possible to let the user specify any two tangent vectors, not just the two extreme ones. However, it is more natural to edit and reshape the curve by varying the two extreme tangent vectors in practical situations. We refer the reader to [37] for more details and examples on various end point conditions for cubic splines.

### 6.2.2 Closed Cubic Splines

Condition that the tangent vectors ($P_1^t$, $P_n^t$) and the second derivatives (curvatures) at the two end-points are equal, i.e. $P_1^t = P_n^t$ and $P_1^{tt} = P_n^{tt}$, is called a *cyclic* end condition. Cyclic end condition is ideal for a closed cubic spline. A closed cubic spline has an extra curve segment from $P_n$ to $P_1$ that closes the curve. Expression (6.9) with this additional constraint becomes

$$\begin{bmatrix} 1 & 4 & 1 & 0 & \dots & 0 \\ 0 & 1 & 4 & 1 & \dots & 0 \\ & & \ddots & \ddots & \ddots & \vdots \\ 0 & \dots & \dots & 1 & 4 & 1 \\ 1 & \dots & \dots & \dots & 1 & 4 \\ 4 & 1 & 0 & \dots & 0 & 1 \end{bmatrix}_{n\times n} \begin{bmatrix} P_1^t \\ P_2^t \\ \\ \vdots \\ P_{n-1}^t \\ P_n^t \end{bmatrix}_{n\times 1} = \begin{bmatrix} 3(P_3 - P_1) \\ 3(P_4 - P_2) \\ \\ \vdots \\ 3(P_1 - P_{n-1}) \\ 3(P_2 - P_n) \end{bmatrix}_{n\times 1} . \tag{6.10}$$

In Figure 6.3, an example interpolating the points in $\mathbb{R}^2$ lying on a closed curve using the above closed cubic spline formulation is shown. The points in the order of connectivity are

$$P := \begin{bmatrix} x \\ y \end{bmatrix} = \begin{bmatrix} 2 & 3 & 4 & 3 & 2 & 2 & 3 & 4 & 2 & 1 & 1 \\ 0 & 0 & 1 & 2 & 1.5 & 2 & 2.5 & 4 & 4 & 2 & 1 \end{bmatrix} . \tag{6.11}$$

We have used (6.10) for interpolating the translation part in the examples of curves on $SE(3)$, see Figure 7.6 and Figure 7.7. It is interesting to note that there are ways to generalize spline interpolation to curves on surfaces and Riemannian manifolds, see for example [36, 35].

### 6.2.3 de Casteljau Construction

In this section we will extend a multi-linear interpolation scheme developed by de Casteljau for interpolation on Riemannian Manifolds. The essential part of the algorithm is the concept of a geodesic. On Riemannian manifolds this interpolation scheme will begin with geodesics which are similar to straight line segments in $\mathbb{R}^n$. We begin with explaining the algorithm in $\mathbb{R}^n$ and then show its extension to Riemannian manifolds.

In previous sections we saw interpolation schemes where the interpolating curve passes through given points. Let us look at an interpolation scheme where the interpolating curve do not pass through given data points but it considers a few points as control points and controls the tangents

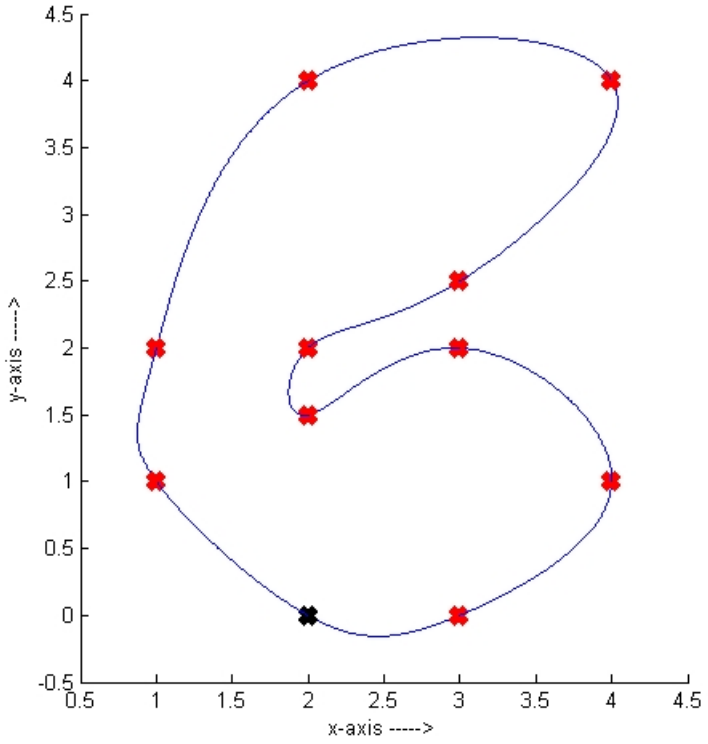


Figure 6.3: Example of a closed cubic spline interpolation

at the intermediate points on the curve.

In Figure 6.4, the interpolating curve $P(t)$ (the envelope) passes through two data points $P_1$ and $P_3$ and the tangents at points $P_1$ and $P_3$ are controlled by the point $P_2$. Curve $P(t)$ is constructed using a multi-linear interpolation scheme. Construction of $P(t)$ involves straight line segments connecting points on the line segments $P_{12}(t)$ and $P_{23}(t)$. Let us look at the construction in detail:

$$
\begin{aligned}
P_{12}(t) &= (1-t)P_1 + tP_2 \\
P_{23}(t) &= (1-t)P_2 + tP_3 \\
P(t) &= (1-t)P_{12}(t) + tP_{23}(t) \\
&= (1-t)^2 P_1 + 2t(1-t)P_2 + t^2 P_3
\end{aligned}
\tag{6.12}
$$

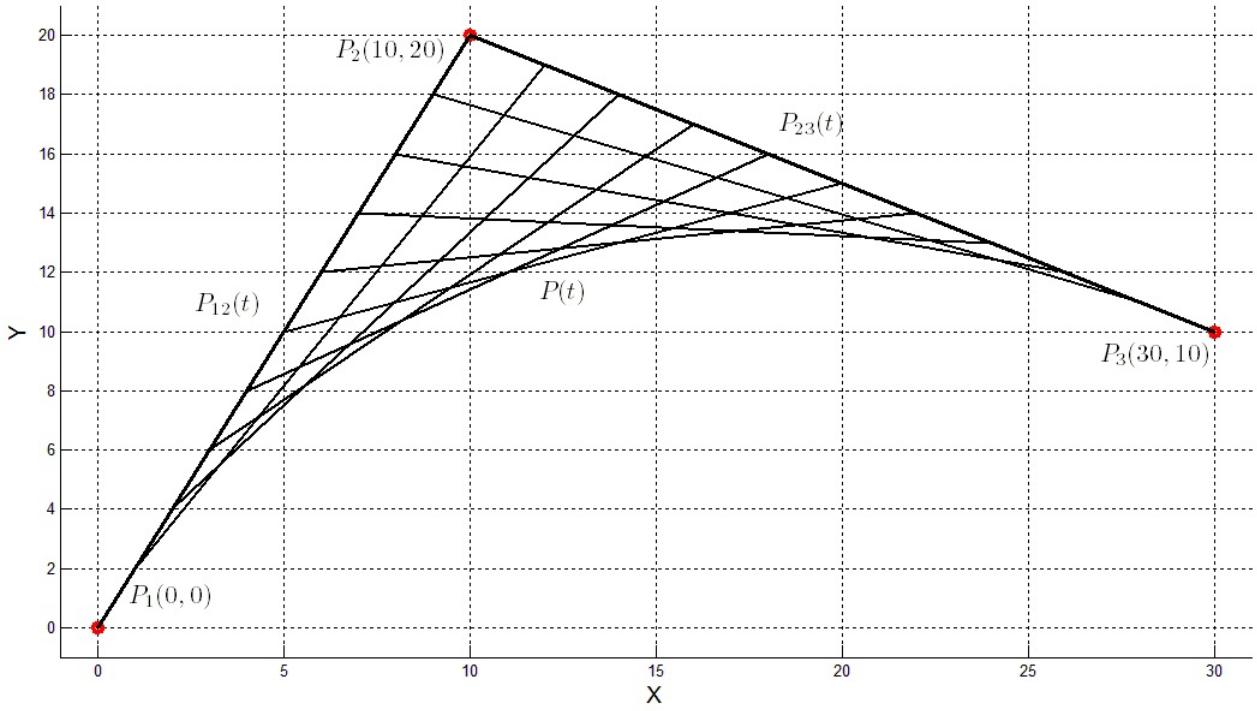


Figure 6.4: Multi-linear interpolation with de Casteljau construction in $\mathbb{R}^2$

Similarly a multi linear interpolating curve between points $Q_1$ and $Q_4$ with $Q_2$ and $Q_3$ as control points results in a cubic curve

$$P(t) = \sum_{i=0}^{3} \binom{3}{i} t^i (1-t)^{3-i} Q_{i+1}. \tag{6.13}$$

This expression involves Bernstein's polynomials and is called a Bezier interpolating curve, see [37]. The construction shown in Figure 6.5 is an instance of de Castaljau interpolation algorithm in which straight line segments are used to interpolate between points and gives exactly the same expression as (6.13). We can rewrite (6.13) in matrix notations as,

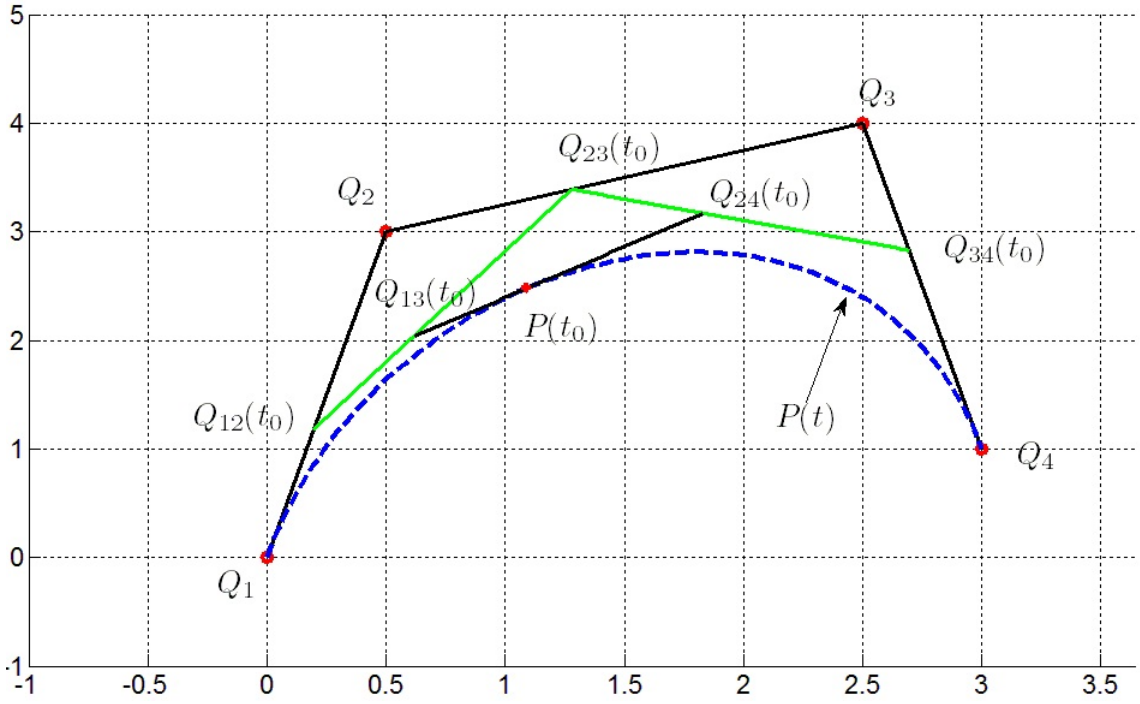


Figure 6.5: Cubic interpolation with de Casteljau construction in $\mathbb{R}^2$

$$P(t) = T(t)BQ = [t^3\ t^2\ t\ 1] \begin{bmatrix} -1 & 3 & -3 & 1 \\ 3 & -6 & 3 & 0 \\ -3 & 3 & 0 & 0 \\ 1 & 0 & 0 & 0 \end{bmatrix} \begin{bmatrix} Q_1 \\ Q_2 \\ Q_3 \\ Q_4 \end{bmatrix}. \tag{6.14}$$

By equating (6.7) and (6.14) we arrive at an interesting relationship between the set of control points ($Q := \{Q_1, \ldots, Q_4\}$) and the set of points and tangents at end points ($P := \{P_1, P_2, P_1^t, P_2^t\}$). The matrix $C$ relating the geometric quantities $P$ and $Q$, i.e. $P = CQ$, is given by

$$C = \begin{bmatrix} 1 & 0 & 0 & 0 \\ 0 & 0 & 0 & 1 \\ -3 & 3 & 0 & 0 \\ 0 & 0 & -3 & 3 \end{bmatrix}. \tag{6.15}$$

With the help of (6.15) it is possible to convert the boundary condition given in the form of tangent vectors to a set of control points. This approach works for a point set in $\mathbb{R}^n$. For further details refer to [37]. If the straight line segments are replaced by the geodesics (corresponding to the underlying Riemannian manifold) in the above construction, this algorithm extends to a point set in a Riemannian manifold. For example, in [1] a similar approach is used to interpolate between two points in $SE(3)$. It is easy to connect multiple segments with appropriate boundary conditions in form of a $C^2$ curve as done in case of open (6.9) and closed (6.10) spline interpolations. In Figure 6.1, we show an example of $C^2$ interpolating curve using de Casteljau algorithm. Since in $SE(3)$ we have closed form expressions for the exponential and log maps, it is easy to construct geodesics between two points in $SE(3)$.

## 6.3 Summary of Reconstruction Algorithm

We begin with a set $\mathcal{S} := \{s_0, s_1, \ldots, s_{n-1}\}$ of sample points of the curve $\mathcal{C} \subset \mathcal{M}$. We assume that $\mathcal{S}$ is a dense sample. Using the Riemannian metric defined on $\mathcal{M}$ we calculate distances, $d(s_i, s_j),\ i \neq j$, between sample points for $i, j = 1, 2, \ldots, n-1$. Using the minimum spanning tree algorithm we reorder the set of sample points. Suppose $\mathcal{S}_\sigma = \{s_{\sigma(0)}, s_{\sigma(1)}, \ldots, s_{\sigma(n-1)}\}$ is the reordered set where $\sigma$ is a permutation on the set of $n$ symbols. We interpolate $\mathcal{S}_\sigma$ using the de Casteljau interpolation scheme and produce a $C^2$ continuous curve.

# Chapter 7

# Examples of Curves Reconstructed in Riemannian Manifolds

## 7.1 Curves on a Sphere

We begin our simulations with examples of curves on a unit sphere. We show two curves with different densities required by the MST for correct reordering of the samples.

The curves after reordering the sample points are shown in Figure 7.1(a) and Figure 7.1(b).

## 7.2 Curves in $SE(2)$ : Application to Video Frame Sequencing

As an application of the curve reconstruction we take up a task of ordering the frames $\{F_i\}_{i=1,\ldots,N}$ of a video sequence. In Figure 7.2 there are sixteen frames of a video sequence. We use the rigid euclidean motion of an object in the frames as a clue for re-ordering the frames. Let us assume that the object under observation is masked by a rectangle and it is segmented out of the frames. We also assume that the motion of the object is the rigid body euclidean motion in $\mathbb{R}^2$. Further let the video frames from the sequence form a dense sample set of the motion curve. As discussed in section 4.5

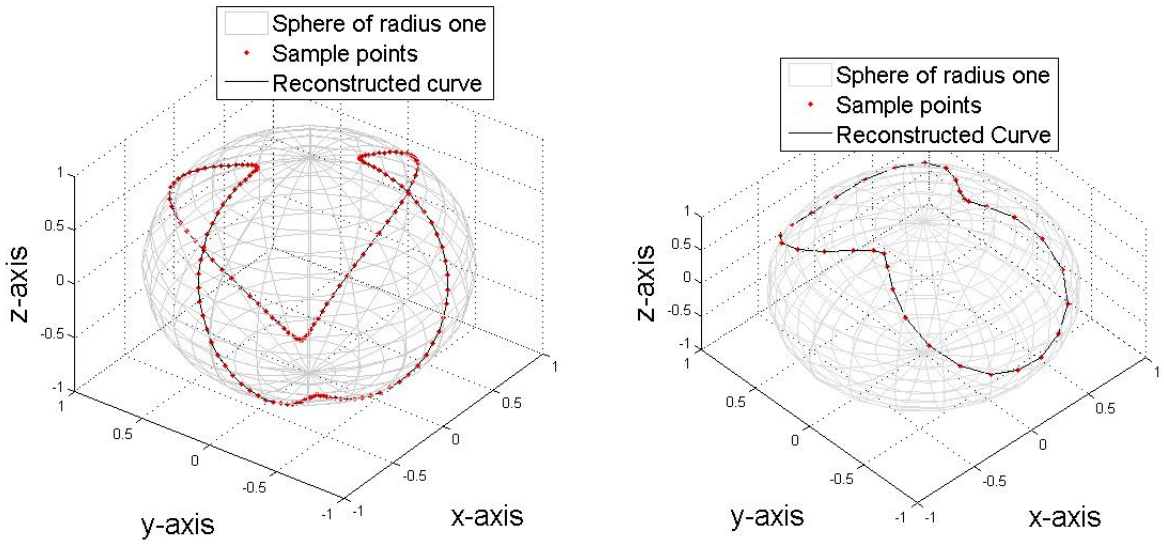


(a) (b)

Figure 7.1: Example curves on a unit sphere.

we calculate the distances between frames as the distance between elements of $SE(2)$. Although we do not focus on how to estimate the rotations we give a very primitive looking argument below to estimate the distances between two frames. It turns out that the estimates are good enough in this case to reconstruct the curve. But in general we use $[\theta, x, y]$ as the elements of $SE(2)$ and we assume that we have an oracle to give these frame coordinates to the algorithm.

The euclidean distance between the means found out from the relative positions of the rectangle is the first part of the distance metric. Next, we estimate the rotation angle of the object with respect to a fixed inertial frame. For this purpose, we first register the objects with their means. It is observed that if we overlap the registered rectangles, the area of the overlapping region provides a good estimate of the rotation angle. In fact, for $\theta > \arctan(\frac{b}{a})$, the overlapped area is $\frac{a^2}{\sin\theta}$, where $a$ is the shorter side of the rectangle, which clearly indicates as $\theta$ increase the overlapping area decreases up to $\theta = \pi/2$. For calculating the area we count the number of lattice points (pixels) inside the overlapping regions. Finally, the estimate for $\theta$ combined with the euclidean distance between means gives the $d^*(F_1, F_2)$. Using sequential search with known initial frame we re-order

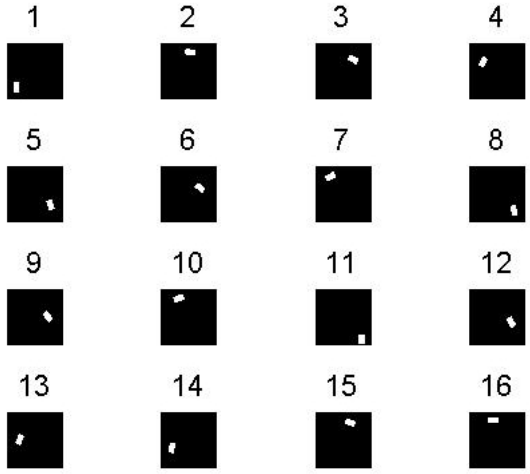


Figure 7.2: Unordered video frames

the frames see Figure 7.4. Even if we do not know the initial frame, MST computes the correct connections of the frames and gives a correct ordering up to end points.

Let us reconsider the distance metric on $SE(2)$ given in (4.5). If we scale the three axes properly, the problem of curve reconstruction in $SE(2)$ reduces to the problem of curve reconstruction in $\mathbb{R}^3$ and we may use all the non-uniform sampling schemes and voronoi diagram based reconstruction algorithms. As an example we have used NN-CRUST to reconstruct the curve above in the motion sequence and we get the correct ordering as expected.

## 7.3 Curves in $SE(3)$

In Figure 7.5 an unordered set of frames in $SE(3)$ is shown. We assume that the sample shown is dense.

By the distance metric defined in (4.17), we compute distances between all the frames. Finally we compute the MST for the complete weighted graph of frames with the computed distances as the edge weights.

Once the ordering is done we interpolate the sample with partial geodesic scheme. Results of

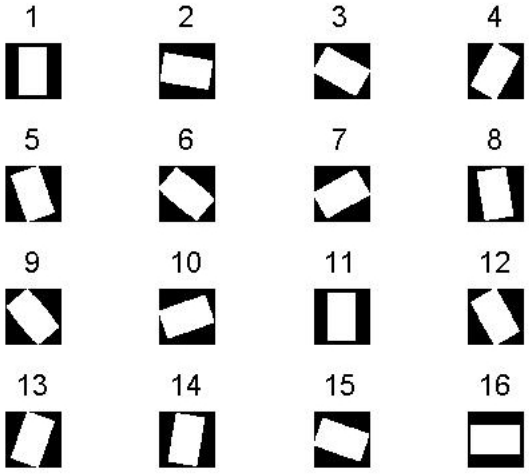


Figure 7.3: Mean cancellation and rotation estimation

interpolation with two different granularities is presented in Figure 7.6 and Figure 7.7.

## 7.4 Another Useful Manifold

Suppose for a planar object in motion, we include scaling with respect to the center of mass along with the rotation and translation. The resultant element will be of the following form

$$A = \begin{bmatrix} e^{\lambda}R & d \\ 0 & 1 \end{bmatrix}. \tag{7.1}$$

This element operates on the point of the object in plane. It scales($e^{\lambda}$) and rotates($R$) the object with respect to its center of mass and then translates($d$) the center of mass. With each such element we can associate a vector $[\lambda, \theta, d_x, d_y]$. The elements of the form given by (7.1), with standard matrix multiplication forms a Lie group. We can extend the notions of tangent space and exponential map to this lie group. As discussed previously in section 4.6 this group is a semi-direct product of elements of scaled rotations and translations. The tangent space elements at identity, Lie algebra

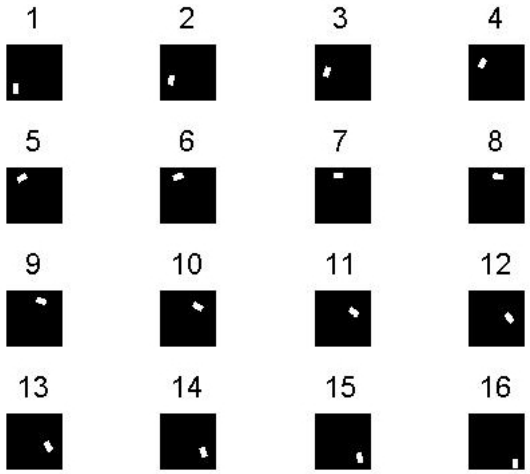


Figure 7.4: Ordered video frames

elements, for scaled rotations are given by

$$[a] = \lambda \begin{bmatrix} 1 & 0 \\ 0 & 1 \end{bmatrix} + \theta \begin{bmatrix} 0 & -1 \\ 1 & 0 \end{bmatrix} \tag{7.2}$$

And the usual matrix exponentiation gives

$$\exp[a] = e^{\lambda} \begin{bmatrix} \cos\theta & -\sin\theta \\ \sin\theta & \cos\theta \end{bmatrix}. \tag{7.3}$$

We can construct a left-invariant riemannian metric on this group. It can be shown that for two elements $A_1, A_2$ in this group

$$d(A_1, A_2) = \sqrt{\alpha((\lambda_1 - \lambda_2)^2 + (\theta_1 - \theta_2)^2) + \beta \parallel d_1 - d_2 \parallel} \tag{7.4}$$

is a valid distance metric. In Figure 7.8, a circular object under the action of this group is shown for various time steps. Assuming the curve is sampled densely, along with the distance measured by (7.4) we reconstruct the curve using MST. The successfully reconstructed curve, with the values

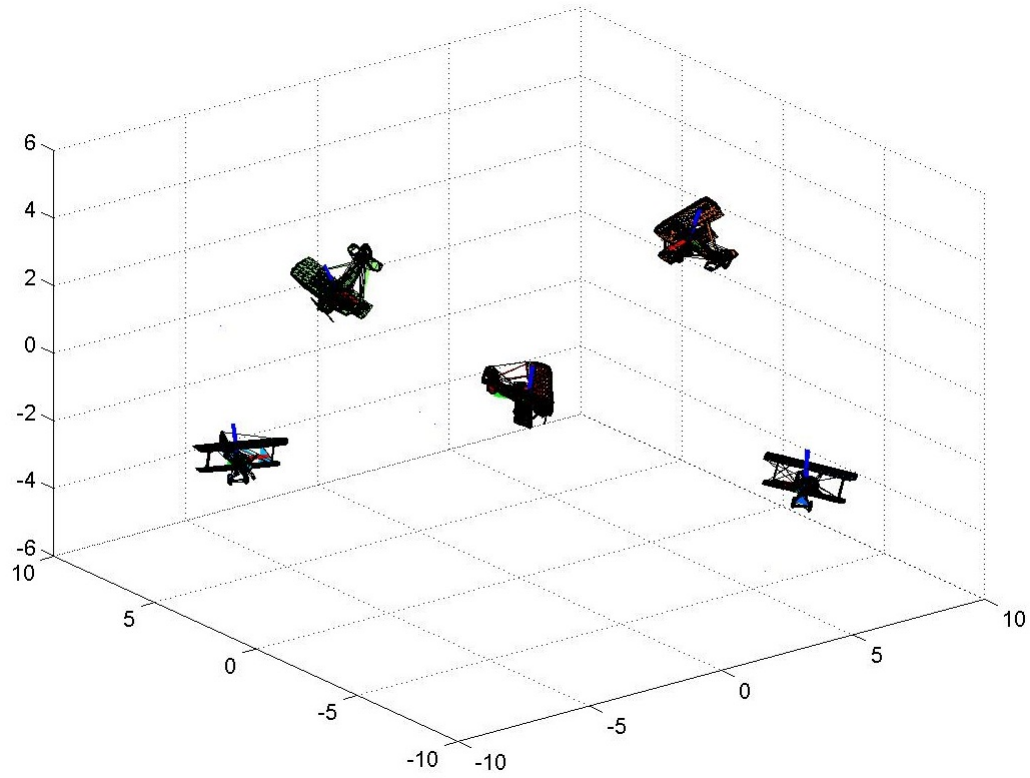


Figure 7.5: A sample $\mathcal{S}$ of a curve $\mathcal{C} \subset SE(3)$

$\alpha = 10$ and $\beta = 1$, is shown in Figure 7.9. Important fact to note here is that the curve presented here is not a closed curve. The algorithm is modified in this case to take care of the end points. In fact a simple nearest neighbor search will also do the job of reconstruction once we give the initial point.

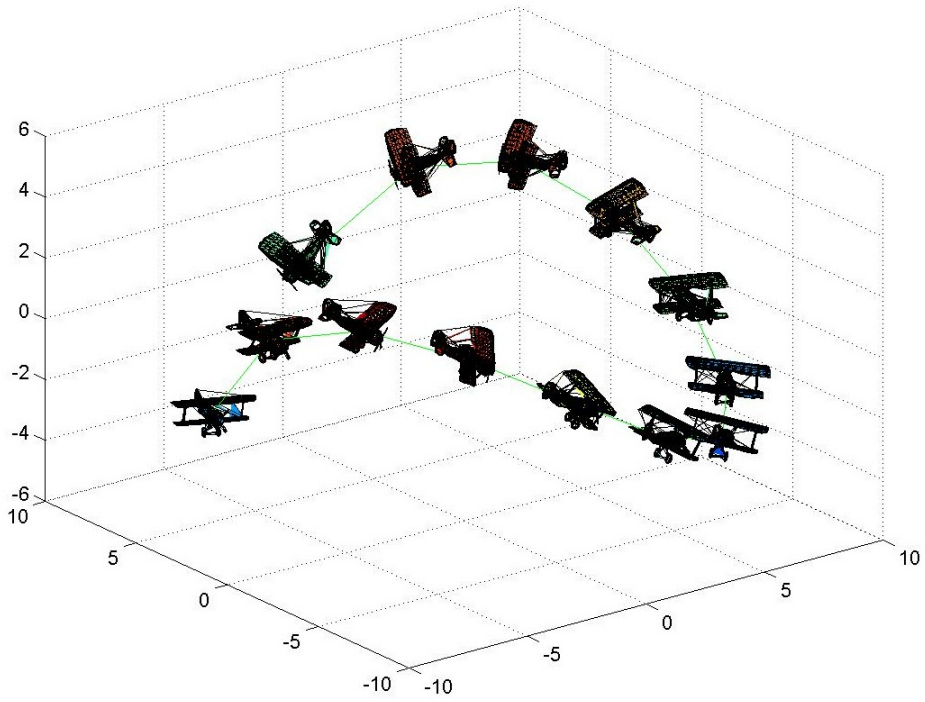


Figure 7.6: Reconstructed curve in $SE(3)$

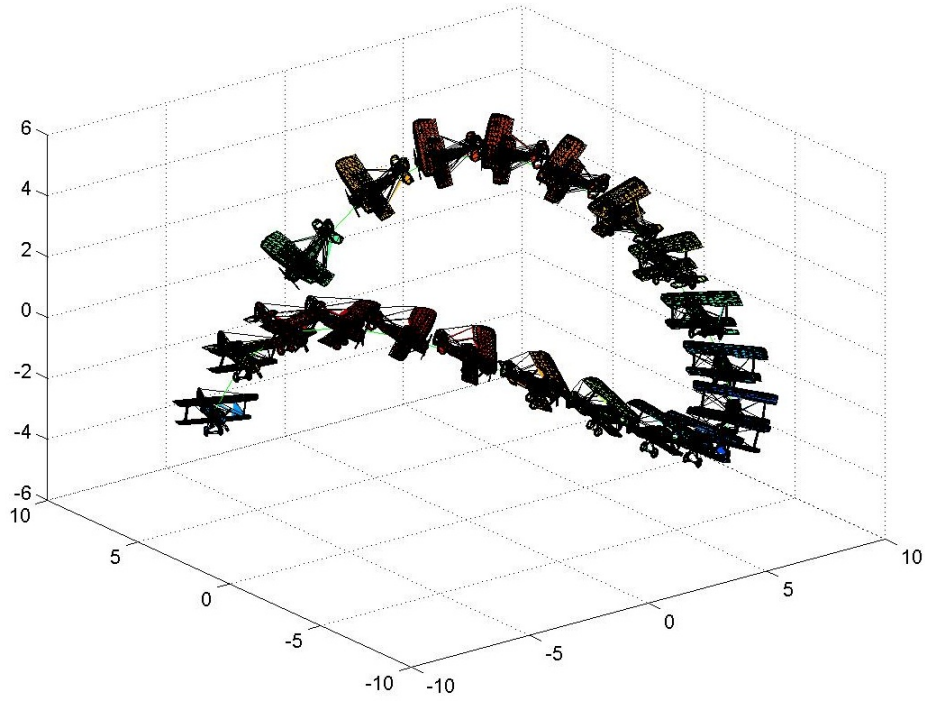


Figure 7.7: Reconstructed curve in $SE(3)$ with finer interpolation

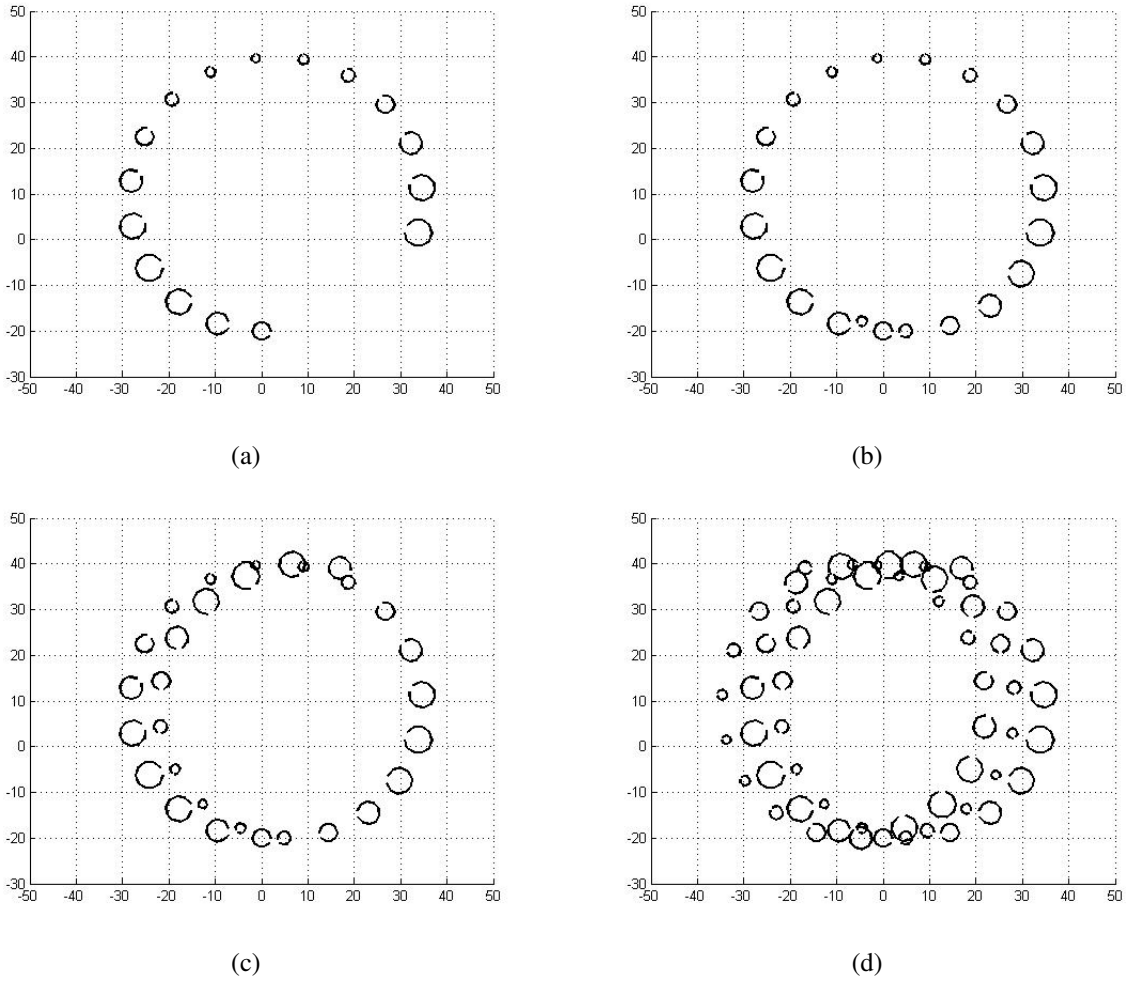

(a) (b)

(c) (d)

Figure 7.8: Various instances of a curve in $SE(2)$ with scaling.

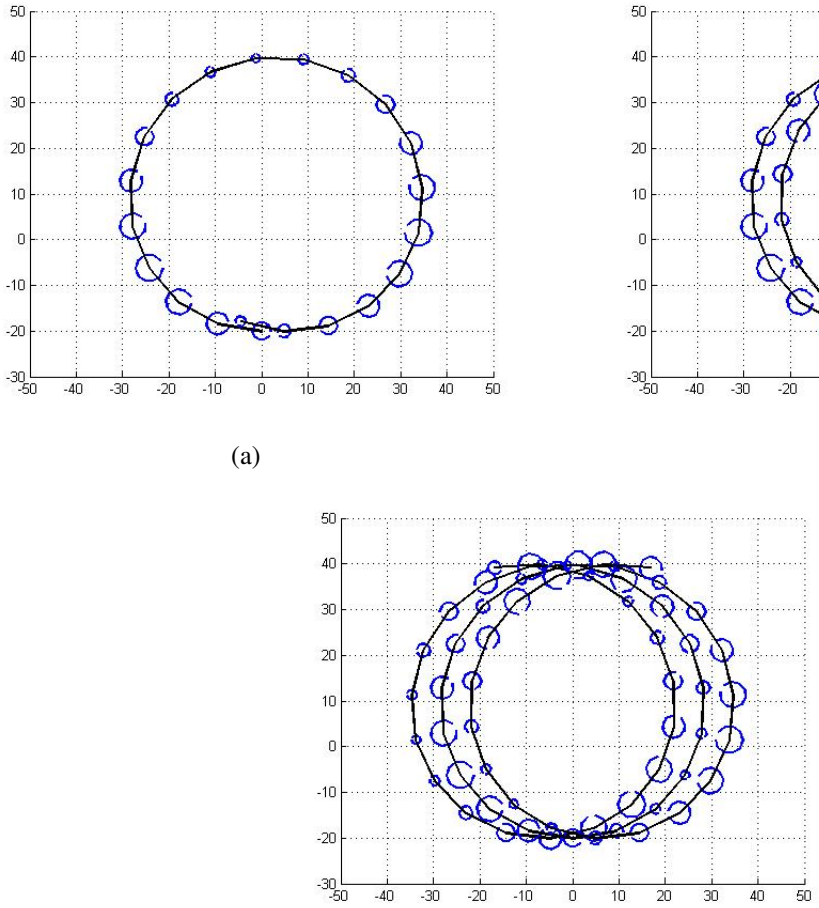


(a) (b)

(c)

Figure 7.9: Instances of the reconstructed curve in $SE(3)$ with scaling.

# Chapter 8

# Conclusion

In this thesis, we have extended the computational geometry based approach for curve reconstruction to curved spaces. This work can also be looked upon as a systematic study of the problem of curve reconstruction in Riemannian manifolds.

Some of the key steps involved in this extension process are as follows:

1. An example is identified in section 5.3 that shows the need of revising the Least Feature Size based sampling criterion while working on a Riemannian manifold.

2. With the help of a few observations made in section 5.3 we were able to show the effect of curvature of the underlying manifold on the sampling density for a given curve.

3. We gave an alternate proof of flatness of a curve segment inside the tubular neighborhood for curves in $\mathbb{R}^n$, which was further extended to curves in Riemannian manifolds in section 5.4.1.

4. We proved that the MST gives the correct re-ordering for a dense sample of a curve and worked out a conservative bound for the uniform sampling of the curve based on the injectivity radius of the manifold. In essence, the effect of local topological behavior of the

underlying manifold was clearly identified and resolved by working inside the injectivity radius (see Chapter 5 and Chapter 6).

5. We have presented a concise version of the above, including proofs and simulation results of successfully reconstructed curves in $SE(2)$ and $SE(3)$ in [40].

The following major results are believed to be original:

- In the following result for a plane curve we give a conservative bound on the value of $\varepsilon$ for which $N_\varepsilon(\mathcal{C})$ becomes a tubular neighborhood.

  **Proposition 5.4** *If $N_\varepsilon(\mathcal{C})$ is a tubular neighborhood of $\mathcal{C}$, then $\varepsilon < \frac{1}{k}$, where $k = \max\{k(p), p \in \mathcal{C}\}$ and $k(p)$ is the curvature of the curve at point $p$.*

- Based on the definition of tubular neighborhood and the medial axis we were able to demonstrate the denseness of a sample with sampling density $\varepsilon$.

  **Proposition 5.7** *For plane curves if $\varepsilon < \min_{p\in\mathcal{C}} f(p)$ then a uniform $\varepsilon$-sample $\mathcal{S}$ of curve $\mathcal{C}$ is a dense sample.*

- The curvature of the underlying Riemannian manifold plays a crucial role in defining the sampling density of a curve. We propose to work within the injectivity radius of the manifold to avoid cases similar to the example presented in section 5.3.

  **Proposition 5.8** *Let $\mathcal{C} \in \mathcal{M}$ be a smooth, simple and closed curve. If $\mathcal{S}$ is a uniform $\varepsilon$-sample of $\mathcal{C}$, then $\mathcal{S}$ is dense for $\varepsilon < \min\{\inf_{p\in\mathcal{C}} f(p), i(\mathcal{M})\}$.*

- We give an alternate proof of the following theorem for curves in the plane which is then extended to Riemannian manifolds.

  **Theorem 5.9** *Let $p$ and $q$ be two points on an arc $\mathcal{C} \subset \mathbb{R}^2$ such that $q$ is inside the tubular disk $B_\varepsilon(p)$ centered at $p$. Then the sub arc $pq$ of $\mathcal{C}$ is completely inside $B_{pq/2}(c)$, where $c$ is the mid-point of diameter $pq$.*

- Using the Gauss lemma, we extend the proof of the previous result and show that the curve segment inside a tubular disc does not wiggle too much in a Riemannian manifold.

  **Theorem 5.10** *Let $p$ and $q$ be two points on an arc $\mathcal{C} \subset \mathcal{M}$, where $\mathcal{M}$ is any Riemannian manifold, such that $q$ is inside the tubular disk $B_\varepsilon(p)$ centered at $p$. Then the sub arc $pq$ of $\mathcal{C}$ is completely inside $B_{pq/2}(c)$, where $c$ is the mid-point of diameter $pq$.*

- Putting pieces together we finally show that the MST correctly re-orders the dense sample of a curve in a Riemannian manifold.

  **Theorem 6.1** *If $\mathcal{S}$ is a dense sample of $\mathcal{C} \subset \mathcal{M}$, then the MST gives a correct re-ordering on $\mathcal{S}$ and hence a correct geodesic polygonal reconstruction of $\mathcal{C}$, where $\mathcal{C}$ is a smooth, closed and simple curve.*

In section 6.2, we describe an interpolation scheme based on the de Castaljau algorithm to interpolate between ordered sample points in a Riemannian manifold. Finally, we validate our proposed scheme with the help of few examples of curves in Riemannian manifolds. We have selected Riemannian manifolds which are widely used in engineering applications (a sphere, surfaces, $SE(3)$ and $SE(2)$ with scaling). We have also shown applications of combinatorial curve reconstruction for ordering motion frames in graphics and robotics.

John Nash proved in [31] that every Riemannian manifold can be isometrically embedded into some Euclidean space. Due to this result one might be tempted to think that reconstruction of curves in $\mathbb{R}^n$ directly implies reconstruction of curves in Riemannian manifolds. But, it is difficult to construct such an isometric embedding. This inadequacy of knowledge of the isometric embedding has prompted researchers to work in Riemannian manifolds intrinsically. To the best of our knowledge, no results have so far been reported in the direction, where the curve to be reconstructed is embedded in a curved space. Our work is an initial contribution in this direction. The motivation to work in this field is the growing applications of manifold methods in robotics, graphics and computer vision.

We believe that the results of non-uniform sampling for curves in $\mathbb{R}^n$ are transferable to the

curves in Riemannian manifolds with appropriate modifications. As an extension to this work we would like to work out necessary proofs and carry out simulations to support our belief. The effect of noise on the sampling density and the reconstruction algorithm, in the case of curved spaces, will be a challenging question. In future, we wish to work on the problem of curve reconstruction from a noisy sample on curved spaces.

# Appendix A

# Immersions and Embeddings

**Definition A.1.** Let $\mathcal{M}$ and $\mathcal{N}$ be differentiable manifolds. A differentiable mapping $\phi : \mathcal{M} \to \mathcal{N}$ is said to be an immersion if $d\phi_p : T_p\mathcal{M} \to T_{\phi(p)}\mathcal{N}$ is injective for all $p \in \mathcal{M}$ . If, moreover $\phi$ is injective or $\phi$ is a homeomorphism onto $\phi(\mathcal{M}) \subset \mathcal{N}$ we say that $\phi$ is an embedding.

**Definition A.2.** Let $(\mathcal{M}, g)$ and $(\mathcal{N}, h)$ be Riemannian manifolds. An isometric embedding is a smooth embedding $\phi : \mathcal{M} \to \mathcal{N}$ which preserves the metric in the sense that $g$ is equal to the pullback of $h$ by $\phi$, i.e. $g = \phi^* h$. Explicitly, for any two tangent vectors $v,\ w\ \in T_p(\mathcal{M})$ we have

$$g(v, w) = h(d\phi(v), d\phi(w))$$

.

**Theorem A.3.** *[31] Every compact $n$-dimensional Riemannian manifold $\mathcal{M}$ of class $C^k$ ($3 \leq k \leq \infty$ can be $C^k$ isometrically embedded in any small portion of a Euclidean space $\mathbb{R}^N$ where $N = \frac{n}{2}(3n + 11)$.*

*Every non-compact $n$-dimensional Riemannian manifold $\mathcal{M}$ of class $C^k$($3 \leq k < \infty$ can be $C^k$ isometrically embedded in any small portion of a Euclidean space $\mathbb{R}^N$ where $N = \frac{n}{2}(n + 1)(3n + 11)$.*

# Appendix B

# Euler-Lagrange Minimization

$$\min I(y)_{y\in C^(0,1)} = \int_0^1 F(y, y', x)dx \tag{B.1}$$

Given a functional $I : C^1(0,1) \to \mathbb{R}$, where $C^1(0,1)$ is the space of all real functions defined on $(0,1)$ with a continuous first derivative, to find a stationary point of this functional we must ensure that $\frac{dI(\tilde{y})}{d\alpha}|_{\alpha=0}$ vanishes for all variations $\eta(x)$ with boundary conditions $\eta(0) = \eta(1) = 0$ where $\tilde{y}(x) = y(x) + \alpha\eta(x)$.

$$\begin{aligned}
\frac{dI(\tilde{y})}{d\alpha} &= \int_0^1 \frac{dF}{d\tilde{y}}\frac{d\tilde{y}}{d\alpha} + \frac{dF}{d\tilde{y}'}\frac{d\tilde{y}'}{d\alpha}dx \\
&= \int_0^1 \left[\frac{dF}{d\tilde{y}}\eta(x) + \frac{dF}{d\tilde{y}'}\eta'(x)\right]dx \\
&= \int_0^1 \frac{dF}{d\tilde{y}}\eta(x)dx + \left[\frac{dF}{d\tilde{y}'}\eta(x)\right]_0^1 - \int_0^1 \frac{d}{dx}(\frac{dF}{d\tilde{y}'})\eta(x)dx
\end{aligned} \tag{B.2}$$

The second term in the equation vanishes since the variation $\eta(x)$ vanishes at the end points. Now substituting $\alpha = 0$ in the Equation B.2 and rearranging the terms we get,

$$\frac{dI(y)}{d\alpha}|_{\alpha=0} = \int_0^1 \left[\frac{dF}{dy} - \frac{d}{dx}\left(\frac{dF}{dy'}\right)\right]\eta(x)dx \;=\; 0 \tag{B.3}$$

We know from the result [21] that if $f(x)$ is continuous in $[0, 1]$, and if

$$\int_0^1 f(x)\eta(x)dx = 0$$

for every function $\eta(x) \in C(0, 1)$ such that $C(0) = C(1) = 0$, then $f(x) = 0$ for all $x \in [0, 1]$.

Hence, we get the Euler-Lagrange equation,

$$\frac{dF}{dy} - \frac{d}{dx}\left(\frac{dF}{dy'}\right) = 0 \tag{B.4}$$

# Appendix C

# Parallel transport and the area of a region enclosed by a curve on $S^2 \subset \mathbb{R}^3$

In this appendix, we will discuss the role of covariant derivative in differential geometry. Differential geometry studies the properties of spaces (differentiable manifolds) from an intrinsic point of view. In general it is not possible to have a global notion of direction from which we are able to determine when a direction (tangent vector) at a point is the same as a direction at another point. However we say that they have the same direction with respect to geodesic if they are parallel transports of each other. The notion of parallel transport can be extended to arbitrary curves. With this it is possible to talk about how a particular vector quantity changes along a curve intrinsically.

Let $\mathcal{M}$ be a differentiable manifold and $c : [0, 1] \to \mathcal{M}$ be a smooth curve. A vector field $V$ along the curve $c(t)$ in $\mathcal{M}$ is said to be parallel if the derivative $\frac{DV}{dt} = 0$, i.e. the derivative $c'(t = t_p)(V)|_{p\in\mathcal{M}} \perp T_p\mathcal{M}$, where $\frac{D}{dt}$ is the covariant derivative along curve $c(t)$.

In a plane, since Gaussian curvature at every point is zero, if we transport a vector keeping its angle with the tangent along a closed curve constant, then at the return to the starting point, the transported vector is same as the initial vector. However this is not true on curved surfaces.

Let $S^2 \subset \mathbb{R}^3$ be parametrized by $\mathrm{x}(u, v) : [0, \pi] \times [0, 2\pi] \to \mathbb{R}^3$, as shown in (4.7). Let a

curve $c(t) = \mathrm{x}(u(t), v(t))$ be defined by $u(t) = \frac{\pi}{4}$ and $v(t) = t, t \in [0, 2\pi]$ is a closed curve, $c(0) = c(2\pi)$. We see that $c'(t) = [0\ 1]^T$ in this case. Let $V = v^1 \mathrm{x}_u + v^2 \mathrm{x}_v$ be a parallel vector field along $c(t)$. And the initial vector to be transported is $V|_{t=0} = [1\ 0]^T$. Since,

$$\frac{DV}{dt} = 0,\ along\ c(t)$$

we have,

$$\frac{dv^1}{dt}\mathrm{x_u} + v^1 \nabla_{\mathrm{x}_v} \mathrm{x}_u + \frac{dv^2}{dt}\mathrm{x_v} + v^2 \nabla_{\mathrm{x}_v} \mathrm{x}_v = 0$$

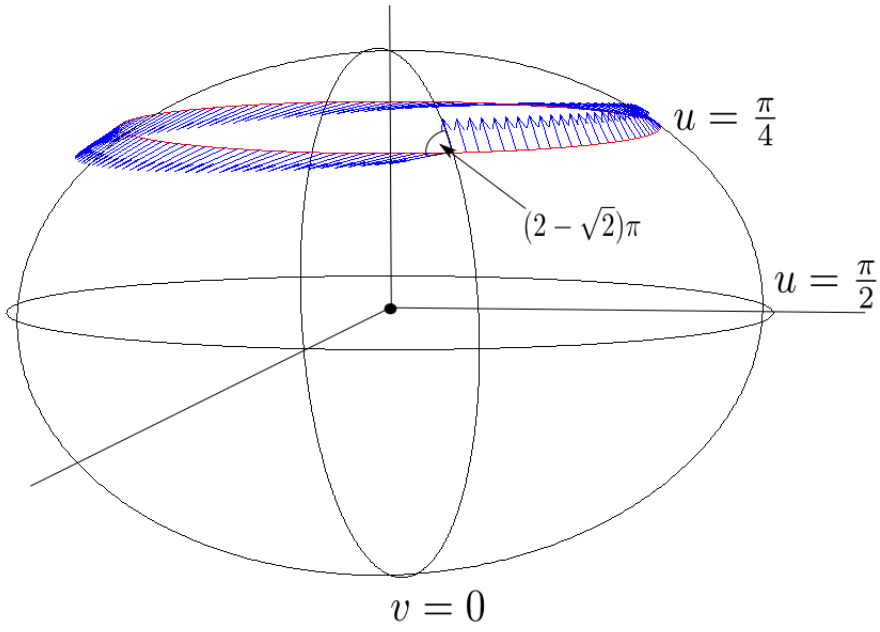


Figure C.1: Parallel transport of vector $[-1\ 0]^T$ along curve $c(t) = \mathrm{x}(u(t), v(t))$ where $u(t) = \pi/4,\ v(t) = t,\ t \in [0, 2\pi]$, a latitude.

We have the Riemannian metric $g_{ij}$ defined for $S^2$ as described in 4.8. Hence there exists a compatible, symmetric connection $\nabla$ on $S^2$ for which it can be shown that along $c(t)$

$$\nabla_{\mathrm{x}_v} \mathrm{x}_u = \mathrm{x}_v\ and\ \nabla_{\mathrm{x}_v} \mathrm{x}_v = \frac{1}{2}\mathrm{x}_u$$

Another way to compute covariant derivatives is to remove the normal component of the derivative from the directional derivatives.

$$\nabla_{\mathrm{x}_v}\mathrm{x}_u = \mathrm{x}_v\mathrm{x}_u - \langle \mathrm{x}_v\mathrm{x}_u, \hat{n}\rangle \hat{n}$$

which obviously agrees with the expressions derived from the defintion of connection. Now as $\mathrm{x}_u$ and $\mathrm{x}_v$ are independent vectors we have a system of first order ODE's as:

$$\begin{bmatrix} \frac{dv^1}{dt} \\ \frac{dv^2}{dt} \end{bmatrix} = \begin{bmatrix} 0 & \frac{1}{2} \\ -1 & 0 \end{bmatrix} \begin{bmatrix} v_1 \\ v_2 \end{bmatrix} \tag{C.1}$$

The solution to (C.1) gives the associated $v^1$ and $v^2$. Figure C shows the parallel transport of $[1\ 0]^T$ along $c(t)$ and corresponding $V$ is a parallel vector field.

As predicted, the vector on returning to its starting point has picked up an angle $(2-\sqrt{2})\pi$, which not surprisingly equals to the area of the region enclosed by the curve $c(t)$. This is in agreement with the Gauss-Bonnet theorem, see [22].

# Appendix D

# The exp and log map on $SE(3)$

*A* 1. Given $[\omega] \in so(3)$,

$$\exp[\omega] = I + \frac{\sin\|\omega\|}{\|\omega\|} \cdot [\omega] + \frac{1-\cos\|\omega\|}{\|\omega\|^2} \cdot [\omega]^2 \tag{D.1}$$

*A* 2. Let $(\omega, v) \in se(3)$. Then

$$\exp\begin{bmatrix} [\omega] & v \\ 0 & 0 \end{bmatrix} = \begin{bmatrix} \exp[\omega] & Av \\ 0 & 1 \end{bmatrix} \tag{D.2}$$

where

$$A = I + \frac{1-\cos\|\omega\|}{\|\omega\|^2} \cdot [\omega] + \frac{\|\omega\| - \sin\|\omega\|}{\|\omega\|^3} \cdot [\omega]^2$$

*A* 3. Given $\theta \in SO(3)$ such that $Tr(\theta) \neq -1$. Then

$$\log(\theta) = \frac{\phi}{2\sin\phi}(\theta - \theta^T) \tag{D.3}$$

where $\phi$ satisfies $1 + 2\cos\phi = Tr(\theta)$, $|\phi| < \pi$. Further more, $\|\log\theta\|^2 = \phi^2$.

*A* 4. Suppose $\theta \in SO(3)$ such that $Tr(\theta) \neq -1$, and let $b \in \mathbb{R}^3$. Then

$$\log \begin{bmatrix} \theta & b \\ 0 & 1 \end{bmatrix} = \begin{bmatrix} [\omega] & A^{-1}b \\ 0 & 0 \end{bmatrix} \tag{D.4}$$

where $[\omega] = \log \theta$, and

$$A^{-1} = I - \frac{1}{2} \cdot [\omega] + \frac{2 \sin \|\omega\| - \|\omega\|(1 + \cos \|\omega\|)}{2\|\omega\|^2 \sin \|\omega\|} \cdot [\omega]^2$$

*A* 5. Let $\theta_1, \theta_2 \in SO(3)$. Then the distance $L = d(\theta_1, \theta_2)$ induced by the standard bi-invariant metric on $SO(3)$ is

$$d(\theta_1, \theta_2) = \| \log(\theta_1^{-1}\theta_2)\| \tag{D.5}$$

where $\| \cdot \|$ denotes the standard Euclidean norm.

*A* 6. Let $X_1 = (\theta_1, b_1)$ and $X_2 = (\theta_2, b_2)$ be two points in $SE(3)$. Then the distance $L = d(X_1, X_2)$ induced by the scale dependent left-invariant metric on $SE(3)$ is

$$d(X_1, X_2) = \sqrt{c\| \log(\theta_1^{-1}\theta_2)\|^2 + d\|b_2 - b_1\|^2} \tag{D.6}$$

where $\| \cdot \|$ denotes the Euclidean norm.

# Appendix E

# Singular Value Decomposition(SVD)

Any linear transformation $A_{m\times n} : \mathbb{R}^n \rightarrow \mathbb{R}^m$ can be decomposed into $A = U\Sigma V^*$ form where $U_{m\times m}$ and $V_{n\times n}$ are orthogonal matrices, $UU^* = I_{m\times m}$ and $VV^* = I_{n\times n}$, and $\Sigma_{m\times n}$ is the singular value matrix with $\Sigma_{ii} = \sigma_i$, where $\sigma_i$'s are the singular values. The decomposition of the above form displays a suitable orthonormal basis for all the subspaces related to the matrix $A$ [43].

If A is of rank $r$ then we have the decomposition as follows:

$$A_{m\times n} = \left[\begin{array}{ccc|ccc} | & | & | & | & | & | \\ u_1 & \dots & u_r & u_{r+1} & \dots & u_m \\ | & | & | & | & | & | \end{array}\right] \left[\begin{array}{ccc|c} \sigma_1 & & 0 & \\ & \ddots & & 0_{r\times m-r} \\ 0 & & \sigma_r & \\ \hline & 0_{m-r\times r} & & 0_{m-r\times m-r} \end{array}\right] \left[\begin{array}{ccc} - & v_1 & - \\ - & \vdots & - \\ - & v_r & - \\ \hline - & v_{r+1} & - \\ - & \vdots & - \\ - & v_n & - \end{array}\right] \tag{E.1}$$

The geometric interpretation of this decomposition of a square matrix $A$ is easy to visualize. Consider a square matrix $A_{n\times n}$. $A$ maps the unit sphere $\mathcal{S}^{n-1} = \{x \in \mathbb{R}^n :\| x \|_2= 1\}$ to an ellipsoid with half-axes $\sigma_i u_i$.

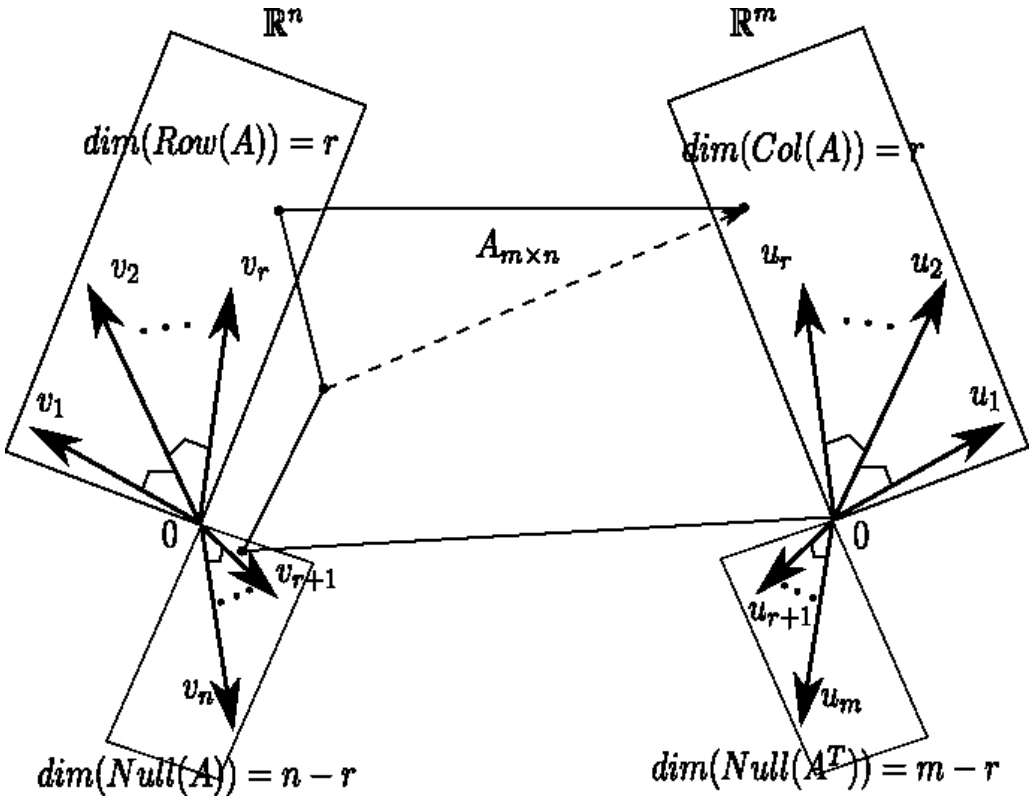


Figure E.1: Four subspaces related to a Matrix $A : \mathbb{R}^n \to \mathbb{R}^m$ of rank $r$ and hunt for orthogonal basis $\{v_1, v_2, \ldots, v_n\}$ and $\{u_1, u_2, \ldots, u_m\}$.

## E.1 Pseudo Inverse

The SVD can be used for computing the pseudo inverse of a matrix. The pseudo inverse of a matrix $A$ with decomposition $U\Sigma V^*$ is given by

$$A^\dagger = V^*\Sigma^\dagger U, \tag{E.2}$$

where $\Sigma^\dagger$ is formed by replacing every non zero diagonal entry of $\Sigma$ by its reciprocal and transposing the resultant matrix. Pseudo inverse is one way to solve the least squares problem $Ax = b$.

## E.2 Approximation of matrix $A_{3\times3}$ by a Rotation Matrix

Let an object be rotated, under the action of rotation matrix $R$, in $\mathbb{R}^3$. Suppose from the known correspondence of points between the point sets before and after rotation we estimate the transformation matrix $A$ using least squares. It may happen that due to discrete grid constraint we end up with a matrix which is not exactly the rotation matrix. Now we want to find out the rotation matrix which is closest to the estimated transformation matrix in some sense. Formally we want to minimize the Frobenius norm of the difference matrix $(R - A)$. The problem can be stated as follows:

$$\min_R \parallel R - A \parallel_F^2 \;\; subject\ to\ R^T R = I. \tag{E.3}$$

$$\begin{aligned} \parallel R - A \parallel_F^2 &= Trace((R-A)^T(R-A)) \\ &= 3 + Trace(A^T A) - 2Trace(R^T A) \end{aligned} \tag{E.4}$$

The minimization in (E.3) is reduced to minimizing the $Trace(R^T A)$ in (E.4). Substituting the SVD of $A = U\Sigma V^T$ in $Trace(R^T A)$,

$$\begin{aligned} Trace(R^T A) &= Trace(R^T U \Sigma V^T) \\ &= Trace(V^T R^T U \Sigma) \;=\; Trace(E\Sigma) \\ &= \sum_{i=1}^{3} e_{ii}\sigma_i \leq \sum_{i=1}^{3} \sigma_i \end{aligned} \tag{E.5}$$

This can be achieved if we set $R = UV^T$ which leads to $E = I_{3\times3}$.

# Bibliography


[1] C. Altafini, "The de casteljau algorithm on se(3)," in *Nonlinear control in the Year 2000*, ser. Lecture Notes in Control and Information Sciences, A. Isidori, F. Lamnabhi-Lagarrigue, and W. Respondek, Eds. Springer Berlin / Heidelberg, 2000, vol. 258, pp. 23–34, 10.1007/BFb0110205. [Online]. Available: http://dx.doi.org/10.1007/BFb0110205

[2] E. Althaus and K. Mehlhorn, "Polynomial time tsp-based curve reconstruction," *Proc 11th ACMSIAM Sympos Discrete Algorithms*, pp. 686–695, 2000.

[3] E. Althaus, K. Mehlhorn, S. Nher, and S. Schirra, "Experiments on curve reconstruction," in *In Proc. 2nd Workshop Algorithm Eng. Exper*, 2000, pp. 103–114.

[4] N. Amenta, M. Bern, and D. Eppstein, "The crust and the $\beta$-skeleton: Combinatorial curve reconstruction." *Graph. Models Image Process.*, no. 60, pp. 125–135, 1998.

[5] D. Attali, "R-regular shape reconstruction from unorganized points," *Proc 13th Annu ACM Sympos Comput Geom*, vol. 10, pp. 239–247, 1998.

[6] D. Avis and J. Horton, "Remarks on the sphere of influence graphs," *Ann New York Acad Sci*, vol. 440, pp. 323–327, 1982.

[7] C. Bajaj, I. Ihm, and J. Warren, "Higher-order interpolation and least squares approximation using implicit algebraic surfaces," *ACM Transactions on Graphics*, vol. 12, pp. 327–347, October 1993.

[8] P. J. Basser, S. Pajevic, C. Pierpaoli, J. Duda, and A. Aldroubi, "In vivo fibre tractography using dt-mri data," *Magnetic Resonance in Medicine*, 2000.

[9] S. Bougleux, G. Peyre, and L. Cohen, "Anisotropic geodesics for perceptual grouping and domain meshing," *ECCV2008*, vol. 5303, pp. 129–142, 2008. [Online]. Available: http://www.springerlink.com/index/t10k26241022w670.pdf

[10] J. W. Brandt and V. R. Algazi, "Continuous skeleton computation by voronoi diagram," *CVGIP Image Understanding*, vol. 55, no. 3, pp. 329–338, 1992. [Online]. Available: http://linkinghub.elsevier.com/retrieve/pii/1049966092900307

[11] T. H. Cormen, C. E. Leiserson, R. L. Rivest, and C. Stein, *Introduction to Algorithms*, T. H. Cormen, C. E. Leiserson, R. L. Rivest, and C. Stein, Eds. MIT Press, 2001, vol. 7, no. 9. [Online]. Available: http://www.jstor.org/stable/2583667?origin=crossref

[12] S. Dasgupta, C. Papadimitriou, and U. Vazirani, *Algorithms*. McGraw Hill, Boston, 2007.

[13] L. H. de Figueiredo and J. de Miranda Gomes, "Computational morphology of curves," *The Visual Computer*, no. 11, pp. 105–112, 1994.

[14] T. K. Dey, *Curve and Surface Reconstruction: Algorithms with Mathematical Analysis*, P. G. Ciarlet, A. Iserles, R. V. Kohn, and M. H. Wright, Eds. Cambridge, 2007.

[15] T. K. Dey and P. Kumar, "A simple provable algorithm for curve reconstruction," in *Proceedings of the tenth annual ACM-SIAM symposium on Discrete algorithms*, ser. SODA '99. Philadelphia, PA, USA: Society for Industrial and Applied Mathematics, 1999, pp. 893–894. [Online]. Available: http://portal.acm.org/citation.cfm?id=314500.315073

[16] T. K. Dey and W. Zhao, "Approximating the medial axis from the voronoi diagram with a convergence guarantee," *Algorithmica*, vol. 38, no. 1, pp. 179–200, 2003. [Online]. Available: http://www.springerlink.com/index/10.1007/s00453-003-1049-y

[17] M. P. do Carmo, *Riemannian Geometry*. Birkhauser, 1992.

[18] H. Edelsbrunner, "Shape reconstruction with delaunay complex," *LATIN'98 LNCS 1380: Theoretical Informatics*, pp. 119–132, 1998.

[19] H. Edelsbrunner, D. G. Kirkpatrick, and R. Seidel, "On the shape of a set of points in the plane," *IEEE Transactions on Information Theory*, vol. 29, no. 4, pp. 551–559, 1983. [Online]. Available: http://ieeexplore.ieee.org/lpdocs/epic03/wrapper.htm?arnumber=1056714

[20] D. Freedman, "Efficient simplicial reconstructions of manifolds from their samples," *IEEE Transaction on Pattern Analysis and Machine Intelligence*, vol. 24, no. 10, October 2002.

[21] I. M. Gelfand and S. V. Fomin, *Calculus of Variations*. Dover Publications, October 2000.

[22] A. Gray, E. Abbena, and S. Salamon, *Modern Differential Geometry of Curves and Surfaces with Mathematica*, ser. Studies in advanced mathematics. Chapman & Hall/CRC, 2006.

[23] M.-J. Kim, M.-S. Kim, and S. Y. Shin, "A c/sup 2/-continuous b-spline quaternion curve interpolating a given sequence of solid orientations," *Computer Animation*, vol. 0, p. 72, 1995.

[24] R. Kimmel and J. A. Sethian, "Computing geodesic paths on manifolds," in *Proc. of National Academy of Sciences, USA*, vol. 95, no. 15, 1998, pp. 8431–8435.

[25] D. G. Kirkpatrick, "Efficient computation of continuous skeletons," *Proc of the 20th Annual IEEE Symposium on Foundations of Computer Science*, pp. 18–27, 1979.

[26] D. G. Kirkpatrick and J. D. Radke, *A framework for computational morphology*. North-Holland, 1985, pp. 217–248.

[27] G. Leibon and D. Letscher, "Delaunay triangulations and voronoi diagrams for riemannian manifolds," in *Symposium on Computational Geometry*, 2000, pp. 341–349.

[28] J. Li and P.-w. Hao, "Smooth interpolation on homogeneous matrix groups for computer animation," *Journal of Zhejiang University - Science A*, vol. 7, pp. 1168–1177, 2006, 10.1631/jzus.2006.A1168. [Online]. Available: http://dx.doi.org/10.1631/jzus.2006.A1168

[29] A.-R. Mansouri, D. P. Mukherjee, and S. T. Acton, "Constraining active contour evolution via lie groups of transformation," *IEEE Transactions on Image Processing*, vol. 13, no. 6, pp. 853–863, 2004. [Online]. Available: http://viva.ee.virginia.edu/publications/04_Constraining.pdf

[30] M. Melkemi, "A-shapes of a finite point set," *Proc of 13th annual Symposium on Computational Geometry*, pp. 367–369, 1997.

[31] J. Nash, "The imbedding problem for riemannian manifolds," *The Annals of Mathematics*, vol. 63, no. 1, pp. pp. 20–63, 1956. [Online]. Available: http://www.jstor.org/stable/1969989

[32] J. O'Rourke, *Computational Geometry in C*, 2nd ed. Cambridge University Press, 1998.

[33] F. C. Park, "Distance metrics on the rigid-body motions with applications to mechanism design," *ASME Journal of Mechanism Design*, vol. 117, no. 1, pp. 48–54, 1995.

[34] F. C. Park and B. Ravani, "Smooth invariant interpolation of rotations," *ACM Transactions on Graphics*, vol. 16, no. 3, pp. 277–295, July 1997.

[35] I. Pesenson, "Variational splines on riemannian manifolds with applications to integral geometry," *Advances in Applied Mathematics*, vol. 33, no. 3, pp. 548 – 572, 2004. [Online]. Available: http://www.sciencedirect.com/science/article/pii/S0196885804000387

[36] T. Popiel and L. Noakes, "Bzier curves and interpolation in riemannian manifolds," *Journal of Approximation Theory*, vol. 148, no. 2, pp. 111 – 127, 2007. [Online]. Available: http://www.sciencedirect.com/science/article/pii/S0021904507000469

[37] D. Salomon, *Curves and Surfaces for Computer Graphics*. Berlin, Germany / Heidelberg, Germany / London, UK / etc.: Springer-Verlag, 2006.

[38] J. M. Selig, *Geometric Fundamentals of Robotics*, ser. Monographs in Computer Science. Springer, 2005.

[39] P. Shah, "Active contours in action," Master's thesis, DAIICT, Gandhinagar, 2005.

[40] P. Shah and S. Chatterji, "On the curve reconstruction in riemannian manifolds," *Journal of Mathematical Imaging and Vision*, pp. 1–14, 2012. [Online]. Available: http://dx.doi.org/10.1007/s10851-012-0344-0

[41] K. Shoemake, "Animating rotation with quaternion curves," *SIGGRAPH Comput. Graph.*, vol. 19, no. 3, pp. 245–254, 1985.

[42] M. Spivak, *A Comprehensive Introduction to Differential Geometry*. Publish or Perish, 1999, vol. 1, no. 4. [Online]. Available: http://www.jstor.org/stable/2319112?origin=crossref

[43] G. Strang, *Linear Algebra and Its Applications*, 3rd ed. Harcourth Brace Jovanovich, February 1988.

[44] A. Tatu, F. Lauze, S. Sommer, and M. Nielsen, "On restricting planar curve evolution to finite dimensional implicit subspaces with non-euclidean metric," *J. Math. Imaging Vis.*, vol. 38, pp. 226–240, November 2010. [Online]. Available: http://dx.doi.org/10.1007/s10851-010-0218-2

[45] G. Taubin, "Nonplanar curve and surface estimation in 3-space," May.

[46] ——, "Estimation of planar curves, surfaces and nonplanar space curves defined by implicit equations, with applications to edge and range image segmentation," *IEEE Transactions on Pattern Analysis and Machine Intelligence*, vol. 13, pp. 115–138, Nov. 1991.

[47] G. Taubin and R. Ronfard, "Implicit simplicial models for adaptive curve reconstruction," *IEEE Transactions on Pattern Analysis and Machine Intelligence*, vol. 18, pp. 321–325, March 1996.

[48] D. Terzopoulos and K. Fleischer, "Deformable models," *The Visual Computer*, vol. 4, pp. 306–311, 1988.

[49] Y. Wang, eshend Wang, and A. M. Bruckstein, "On variational curve smoothing and reconstruction," *Journal of Mathematical Imaging and Vision*, 2010.

[50] S. Willard, *General Topology*. Dover Publications, 2004.

[51] C. Xu and J. L. Prince, "Snakes, shapes, and gradient vector flow." *IEEE Transactions on Image Processing*, vol. 7, no. 3, pp. 359–369, 1998. [Online]. Available: http://www.ncbi.nlm.nih.gov/pubmed/18276256

[52] M. Zefran, V. Kumar, and C. Croke, "On the generation of smooth three-dimensional rigid body motions," *IEEE Transactions on Robotics and Automation*, 1995.